Response to Anonymous Referee #1

General Comment. The manuscript presents three case studies of the exchange of polluted air masses between an Alpine valley and the foreland (Po basin). The case studies are based on multi-site, multi-instrument field data complemented by numerical modelling. They cover three different seasons. The case studies nicely illustrate the complex transport phenomena that occur during the episodes which each last several days. Qualitative agreement is quite good, however, quantitative disagreement between model and observations leads to various hypotheses for the reasons, which require further study and improvements. The paper is carefully written, well-structured and nicely illustrated. Its content is very relevant in the context of the complex dynamical and chemical (transport) processes in and near mountainous terrain. I strongly encourage publication in ACP, pending the few minor corrections below.

We thank the reviewer for taking the time to revise our manuscript and for his/her pertinent comments. Our reply to these is given hereafter (the text in italics represents a citation of the revised manuscript and the figure references follow the updated numbering).

Referee's comment 1. The authors extensively use lidar backscatter (scattering ratio) for tracking the aerosol load of the valley atmosphere (Figs. 4a, 5, 10a, 11, 13a). This parameter is well correlated with relative humidity, which is strongly temperature dependent, but less so with absolute humidity SH (Fig. S8b). SH is a better indicator of air mass transport (and particulates) than RH, i.e. I would expect to see more variation in SH when Po basin air arrives to replace the valley air mass. This is visible for example in the afternoon on 28 May. Could you discuss the constancy of SH with the arrival of the Po valley air mass and its implications for the humidity profile in more detail?

Author's response 1. We thank the reviewer for this comment, which gave us the opportunity to study in more depth the measured and the model simulated SH fields, their difference and the relation of this difference to model inaccuracies in reproducing the wind fields. In fact, this further analysis showed that the model-based evolution of SH is strictly linked to the simulated wind regimes (as expected) and further revealed some inaccuracies of the model.

In fact, we found *differences between the simulated and measured daily cycle of specific humidity* (e.g., Fig. S15 for case study 1 as an example). *In particular, the measured SH usually increases during the first advection day as a result of the transport from source areas with more stagnating conditions, but stays rather constant for the rest of the episode. Conversely, COSMO yields larger dynamics, with SH maxima in the late afternoon and subsequent decrease.* This is likely due to the fact, that *COSMO overestimates the nighttime drainage winds (katabatic winds), as noticeable from Fig.S13* (the figure refers again to case study 1). *This might trigger enhanced cleansing of the lower atmospheric layers during the night as simulated by FARM, but undetected by the ALC.*

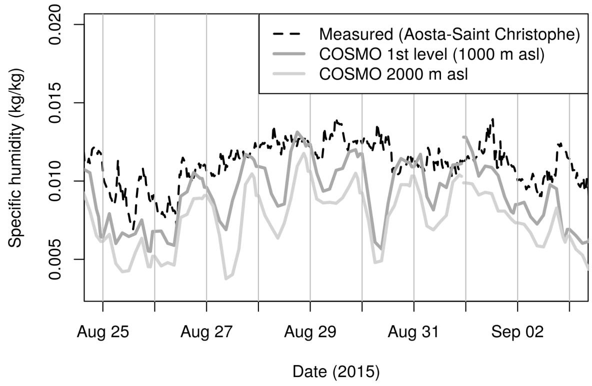

Figure S15: Comparison among specific humidity measured at Aosta–Saint Christophe and simulated by COSMO at two different altitudes (surface and 2000 m a.s.l.).

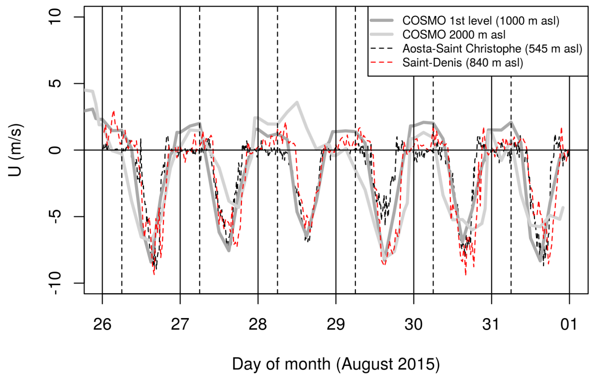

Figure S13: Zonal component of wind velocity during episode 1 (August 2015) from COSMO (1000 and 2000 m a.s.l.) and two surface stations (Aosta–Saint Christophe and Saint-Denis). Positive U represent wind from the west, negative U wind from the east.

Following the reviewer's suggestions, and our related analysis, Sections 4.1.2 and 4.4 were updated accordingly, as well as the conclusions.

As a final remark, please note that the sharp increase of SH in the afternoon of 28 May is due to rainfalls, as visible from the corresponding ALC panels and also mentioned in the text (former line 12, page 30).

RC2. Another aspect is the vertical extent of the scattering ratio in the late afternoons of case study 1 and 3. The wind field indicates strong winds in the lower few hundred meters above valley floor (up to ca. 1200 m), while higher up winds are rather weak or calm (at 2000 m). Yet the polluted air mass almost instantaneously reaches from 1000 to 2000 m upon arrival. With a wind shear from 10 m/s to 1 m/s over 1000 m can we expect quasi-simultaneous arrival of polluted air on all altitudes? Is this

front-like structure real or is it an effect of radiative cooling which increases RH and particle growth throughout the valley atmosphere? Or – alternatively – is this an artifact of the combination of real backscatter measurements with the modeled wind field?

AR2. We think that the impression of a "front-like" structure mentioned by the reviewer is partly due to the temporal extent of former Figs. 4 and 13, and the resulting "squeezing" of the daily ALC profiles. In fact, if we consider only one day at a time, e.g. 25 May 2017 (case 3, former Fig. 3 in the discussion paper, also reported here below), or 27 August 2015 (case 1, Fig. A here below), we observe a different, and more accurate picture of the phenomenon. These figures, also representative of a general behaviour noticeable during the advection events, show a more gradual growth of the layer characterised by large SR values. In particular, two distinct regions can be identified: a first one, where an initial increase of SR is visible (region 1, light-blue/green colour), and a second one, where the backscatter is rapidly enhanced (region 2, yellow colour). Based on the discussion in Sects. 4.4 and S7, we ascribe these regions to two different physical processes. Region 1 defines the spatio-temporal domain where advection of dry aerosol during the afternoon occurs. Real transport of aerosol is indeed confirmed at the surface, e.g., by an increase of the number of particles detected by the OPC during event days and an increase of mass concentration from the PM monitors, which operate in dry conditions and are thus not influenced by hygroscopic processes. This region (e.g., quantitatively defined by the SR=3 envelope) can be effectively fitted by a smooth curve as a function of time, as done using a sigmoid function in the companion paper (Diémoz et al., 2019, to be submitted to ACP). Conversely, region 2 refers to the domain where hygroscopic growth takes place during the evening/night, as soon as the sun sets and RH increases. Further investigations and parametrisations of this last phase would require the measurement of profiles of different meteorological variables as well as knowledge of the aerosol properties along the vertical, and will be the topic of future studies.

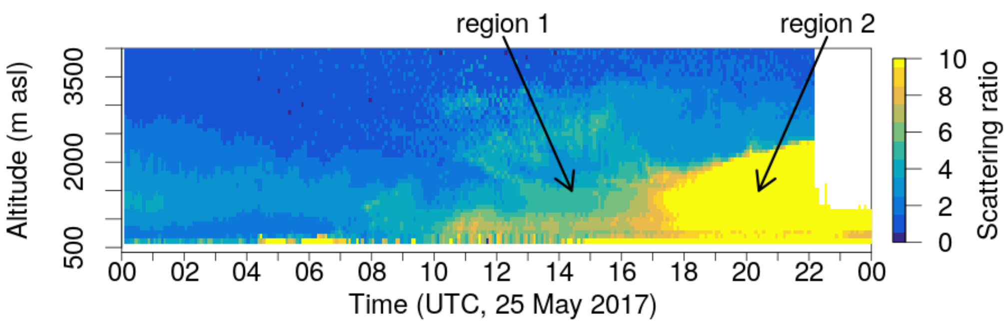

Figure 3 (discussion paper): ALC profile on 25 May 2017.

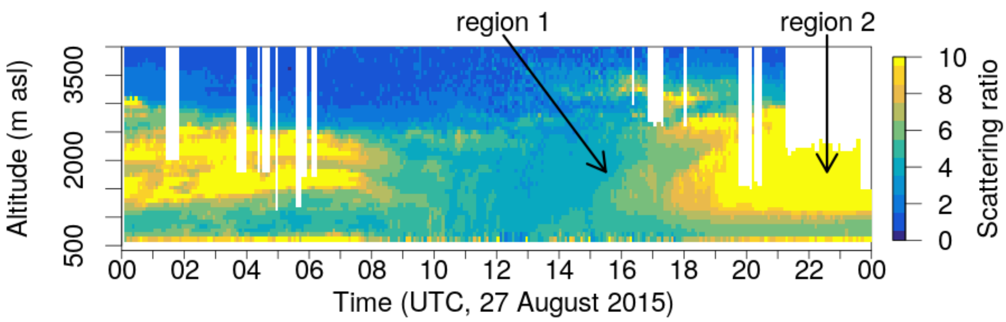

Figure A: ALC profile on 27 August 2015.

A second factor mentioned in the reviewer's comment is the wind profile. We think that some artifacts in the modelled wind fields by COSMO are triggered by *the smoothed valley orography used in the NWP model compared to the real one. This is displayed in Fig. S14, showing the difference of the Digital Elevation Model (DEM) used within COSMO and a more realistic DEM (10 m resolution): both valleys and mountain crests are clearly smoothed out by COSMO, with absolute differences well* > 500 *m (and up to 1000 m)* (Sect. 4.4 of the revised text). *This difference could [...] explain why the altitude of the entrainment zone (i.e., the boundary between the free atmosphere and the boundary layer where the thermally-driven circulation develops) is underestimated by COSMO compared to the height of the aerosol layer detected by the ALC.*

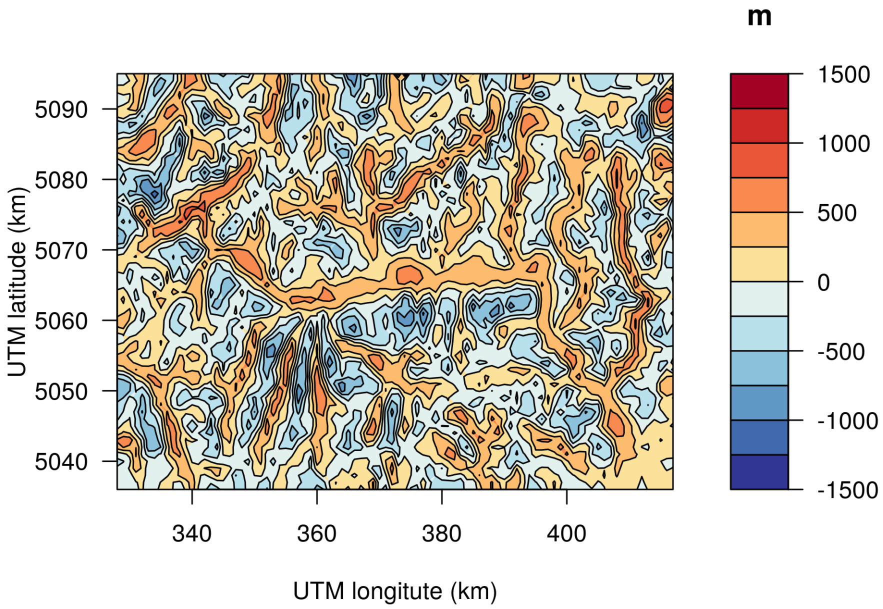

Figure S14: Difference between the (smoothed) Digital Elevation Model (DEM) used by COSMO-I2 (2.8 km resolution) and a higher-resolution DEM ("real topography", 10 m resolution).

RC3. The back-trajectories are good indicators of the regional origin of the polluted air. The graphical representation of all heights up to 4000 m hides, however, the details of the low-level (< 1500 **m) transport route of the air masses within the valley. I suggest to show additional afternoon graphs only for these low levels.**

AR3. We thank the reviewer for pointing this out. Following this and the other reviewer's comments, the back-trajectories figures were modified in this way: we plotted in separate panels trajectories ending at altitudes < 2000 and > 2500 m a.s.l. over Aosta–Saint Christophe. Also, following a remark from referee #4 (RC7) to further simplify the figures, we only show back-trajectories for specific times corresponding to the most significant variations of circulation patterns. Finally, according to referee #3 (RC15), for each time selected we added a bottom panel with the trajectory altitude along their journey. An example of the new plots now included in the paper is provided in Fig. 5.

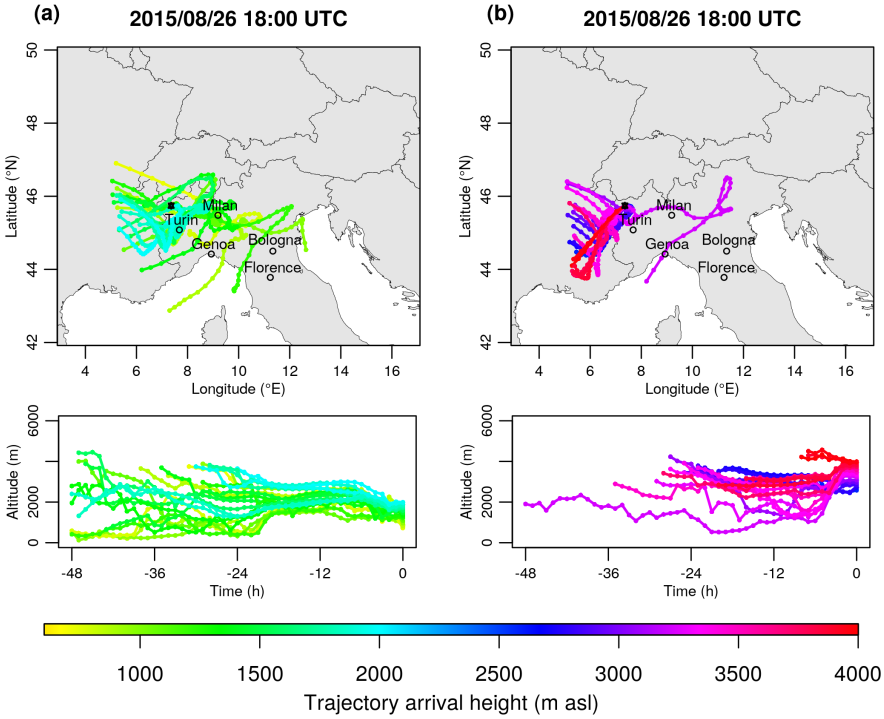

Figure 5: 48-hours back-trajectories ending at Aosta–Saint Christophe on 26 August 2015 at 18 UTC at altitudes lower than 2000 m a.s.l. (a) and higher than 2500 m a.s.l. (b). The trajectories are cut at the border of the COSMO model. The colour scale represents the back-trajectory arrival height. Corresponding altitudes of the backtrajectories vs time are reported in the bottom panels. The dots along each trajectory mark a 1-hour step and the black star indicates the trajectory arrival point (Aosta–Saint Christophe).

RC4. The COSMO-I2 model with 2.8 km grid resolution might still be too coarse for a detailed 3-d simulation of the valley atmosphere with its various mixing processes. With the valley width of 4 km at Aosta, two grid points fit into the valley cross-section at the floor. This may be insufficient for resolving the complex 3-d flow field of an Alpine valley, and may be another explanation of a part of the discrepancy between model and observations.

AR4. The reviewer raised a highly topical issue. We are aware of this problem and decided to integrate Sect. 4.4 with the following text:

As a final remark, we also mention that the 2.8 km grid resolution of the COSMO-I2 model might still be insufficient for resolving the complex 3-D flow field of an Alpine valley and is too coarse to reproduce the mountain atmosphere with its various mixing processes. Follow-up studies using next generation NWP models with increased resolution (1 km or lower) would be of great interest. On the other hand it should also be noticed that decreasing the grid spacing below the scale for which turbulence parametrisations have been developed, i.e. modelling the "grey zone" (or "terra incognita", e.g., Wyngaard, 2004), does not necessary lead to better performances. In this context, comparison of high-resolution simulations with our vertically-resolved dataset could represent a challenging future benchmark for this relevant topic of ongoing research.

RC5. P13L7 omit "the" – should read "covering central and southern Europe"

AR5. Done.

RC6. P22L4 Valley-mountain (and sea-land) breezes are ... (shift the bracket)

AR6. Done.

RC7. P27L20 hundreds

AR7. Done.

RC8. Fig. 7, caption I could not find the link to the video

AR8. We added the following link to the caption: `https://doi.org/10.5446/38391`.

RC9. Supplement: P11L15 replace "grow" with "growth"

AR9. Done.

RC10. Fig. S10 mention the PM10 units for all graphs, not only for a) and b). This can be done in the caption.

AR10. Done.

References

Diémoz, H., Gobbi, G. P., Magri, T., Pession, G., Pittavino, S., Tombolato, I. K. F., Campanelli, M., and Barnaba, F.: Transport of Po Valley aerosol pollution to the northwestern Alps. Part 2: long-term impact on air quality, submitted to Atmos. Chem. Phys., 2019.

Wyngaard, J. C.: Toward Numerical Modeling in the "Terra Incognita", J. Atmos. Sci., 61, 1816–1826, doi:

10.1175/1520-0469(2004)061<1816:TNMITT>2.0.CO;2, 2004.

Response to Anonymous Referee #2

General comment. The manuscript describes in detail the phenomenon of aerosol transport from the Po basin into the Aosta valley, investigated both by a fairly comprehensive instrumentation and from a modeling perspective. This effect is of universal importance for air quality dynamics in Alpine valleys. While the study does not reveal significant new findings about the phenomenon, it adds another valuable data set and discussion to the scientific literature. The manuscript is well structured and written coherently, the scientific questions are clearly set at the beginning and the analysis is focused on the their respective answers in the conclusions. Three case studies are investigated thoroughly with respect to available measurements and models. Besides some very minor comments below, I do not see any further obstacle on the way for publication in ACP.

We thank the reviewer for taking the time to revise our manuscript and for his/her pertinent comments. Our reply to these is given hereafter (the text in italics represents a citation of the revised manuscript and the figure references follow the updated numbering).

Referee's comment 1. p9, Fig. 4 and all subsequent figures showing heat maps. The blue-yellow-red color maps (diverging color maps) are not ideal for the sequential type data of e.g. backscatter ratios. Sequential color maps with monotonous increase in luminance would be a better alternative here.

Author's response 1. Following the reviewer suggestion, we now use a more appropriate colour map starting from Fig. 3 (new numbering) and for all subsequent figures. The new colormap (which is similar to the "Parula" one used in Matlab) is sequential, perceptually uniform, colorblind safe and print/photocopy safe.

RC2. p20, l12pp. If only daily averages from August 26 until August 31 are considered, as for the hourly data in Fig. 4, the increase is less pronounced.

AR2. The reviewer is right. Following this comment, and similar remarks from referee #3 (RC1 and 10) and referee #4 (RC6), we expanded (and homogenised) former panels 4, 10 and 13 (old numbering) to include the same number of days. At the same time, we also paid attention at introducing into the sequence a "clear" day in order to better show the effect of the advections. We thus opted to show one week of measurements in each of these figures, as a compromise between completeness and detail (e.g., of the wind velocity field). The new plots extend from 25 to 31 August 2015 (case 1), from 24 to 30 January 2017 (case 2) and from 24 to 30 May 2017 (case 3), respectively. This allows to better appreciate the difference between event- (clear) and non-event (polluted) days.

Finally, for each episode, the information on the respective seasonal average concentrations were added to the text to provide reference values. Also note that a rigorous assessment of the long-term impact of the phenomenon presented in this part 1 is indeed the purpose of our companion paper (Diémoz et al., 2019) based on a statistical analysis of the complete dataset (2015–2017).

RC3. p22, Fig. 9b. The red/blue contours are really difficult to distinguish, but I also acknowledge this might be a hard visualization task.

AR3. Thank you for your suggestion. We made the contour lines thicker now and the revised figure looks better (Fig. 8).

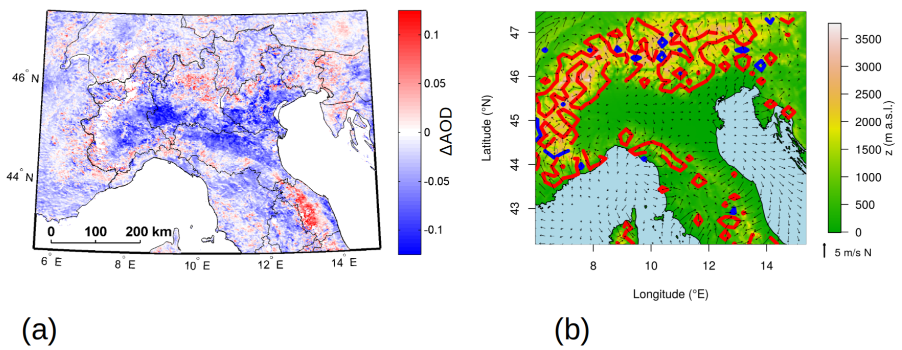

Figure 8: (a) Average difference between AOD estimated from Aqua and Terra satellites during days 27–31 August 2015 using the MAIAC algorithm. (b) Horizontal wind velocity from COSMO (arrows), vertical velocity (red/blue contours, $\pm 0.1\,\mathrm{m\,s^{-1}}$) over the same domain and the same hours as in Fig. (a).

RC4. p22, l5pp. The winter study seems a little more complex than the summer/spring studies. As the authors point out, the synoptic wind from the Po basin is mainly above the very stable PBL, so are the Aosta aerosols really all advected and mixed down to the surface?

AR4. First of all, we updated the introduction of this case study to highlight that indeed the winter episode is more complex than the other ones:

Although local emissions (e.g., residential heating and traffic, additionally worsened by the temperature inversion), might have also increased in this period, the influence of pollution transport from the Po basin is unambiguous. As a result of the advection, the PM concentrations measured in the Aosta Valley were found to be significant in the whole region (e.g., PM_{10} >100 $\mu g m^{-3}$ in Aosta–Downtown and Donnas), even at some remote measuring sites (e.g., PM_{10} ~70 $\mu g m^{-3}$ in Antey, Sect. 4.2.3, and remarkably higher *than the average concentrations in the same period (e.g., 33 $\mu g m^{-3}$ for PM_{10} and 23 $\mu g m^{-3}$ for $PM_{2.5}$ in Aosta–Downtown in 2015–2017).*

Then, to further support our analysis and data interpretation, we also changed former Fig. S5 in the Supplement. The new figure shows the vertical gradient of *pseudo-equivalent potential temperatures (e.g., Freney et al., 2011) at different altitudes [...], thus providing a rough indication of the vertical extent of the mixed layer.* For this second episode, *the arrival of a different air mass is revealed by the temperature/humidity sensors along the mountain slope. Pseudo-equivalent potential temperatures at different altitudes are shown in Fig. S5. As clearly noticeable, the spread among the series recorded at 550 m a.s.l. and the ones at higher altitudes remarkably, and quickly, decreases on 26 January, especially during the night, suggesting that the strong (and very shallow) temperature inversion weakens and mixing of the upper aerosol layers down to the surface is favoured.*

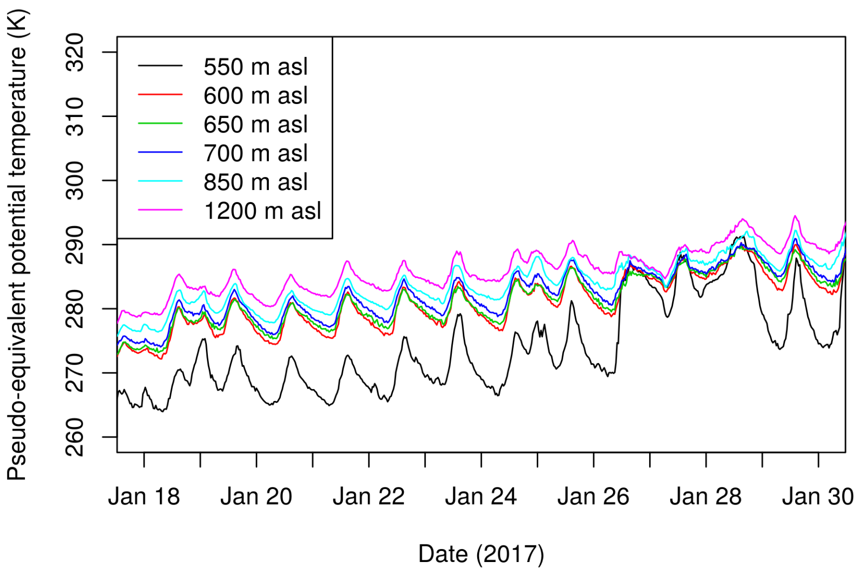

Figure S5: Profile of pseudo-equivalent potential temperature measured along the mountain slope on January 2017. A weakening of the temperature inversion, and a more mixed boundary layer, are clearly detected from 26 to 28 January, i.e. during the advection episode.

RC5. Maybe the contribution of local emissions is of more significant relevance here? Indeed, the daily cycles of measured PM10 surface concentration in Aosta seem to be influenced by local emissions (traffic, heating, etc.).

AR5. We agree that the daily cycle of measured PM_{10} may be partly influenced by local emissions during this episode as well as during other advection events. In this respect, in the companion paper, we indeed study the typical daily cycle of PM concentrations in different conditions (e.g., no aerosol layer detected by the ALC, aerosol layer arriving in the afternoon or leaving in the morning), based on statistical analyses of the long-term dataset. The PM daily cycles in these cases are represented in Fig. 10 (from companion paper). Although the overall daily tendency may vary as a function of the day type (e.g., increasing trend in case of a layer arriving in the afternoon, decreasing trend in case of a layer leaving in the morning), a common, typical feature of all plots is a double daily peak, resulting from both increased local emissions in the morning and late afternoon, and the evolution of the mixing layer height. The daily cycle of Polycyclic Aromatic Hydrocarbons (PAHs), detected at the same site, is also plotted. In fact, as demonstrated in “part 2” of the study (using Positive Matrix Factorisation), PAHs are related to (and are a good proxy of) the local emissions (e.g., traffic, combustion).

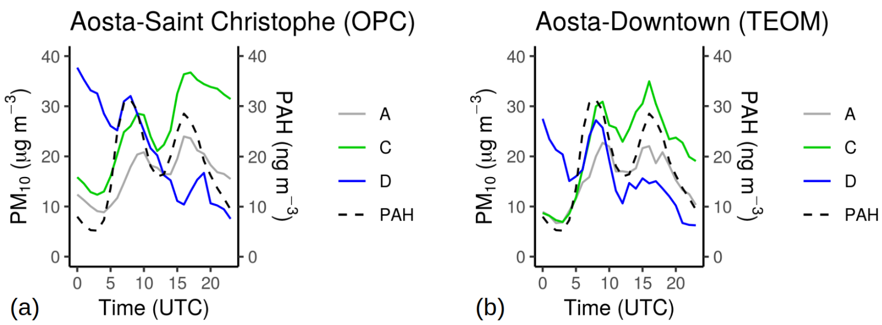

Figure 10 (companion paper): (a) Daily PM_{10} cycle sampled by the OPC in Aosta–Saint Christophe during non-event days (class A) and days with arriving and leaving aerosol layers (classes C and D), plotted together with the daily evolution of PAH as a proxy of the local sources (dotted line, right vertical axis, in $ng\,m^{-3}$). (b) Same as (a) using the TEOM in Aosta–Downtown.

During case study 2 (Fig. A), this typical daily cycle in Aosta–Downtown is visible in non-event days, i.e. Thursday 26 and Sunday 29 January 2017, but is missing during event days, i.e. on Friday 27 and Saturday 28 January, where the correlation between PM_{10} and PAHs is lost. We ascribe this behaviour to the advection of non-local, secondary aerosol from the Po Valley, such as ammonium nitrate. In fact, the chemical analyses show a remarkable increase of this compound, which we demonstrate (in the companion paper) to be a clear marker of the typical aerosol transported from the Po basin. This implies that local emissions are not the main effect modulating the PM_{10} concentrations in the winter case study.

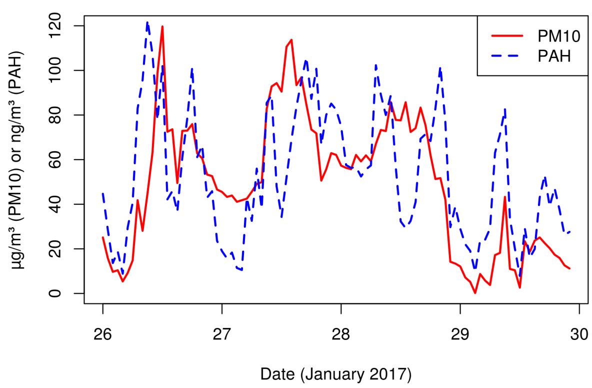

Figure A: PM_{10} and Polycyclic Aromatic Hydrocarbons (PAH) concentrations measured in Aosta–Downtown during case study 2.

RC6. However, I am no expert in atmospheric chemistry to evaluate the significance of the Nitrate and Ammonium percentages during Jan 27 and 28 in Aosta as an indication for air mass origin.

AR6. This topic will be thoroughly and rigorously discussed in the companion paper using the Positive Matrix Factorisation (PMF) technique coupled with the SR profiles from the ALC. There we demonstrate that nitrates (mostly in winter), sulfates (mostly in summer) and ammonium are indeed good markers of the advections from the Po basin. Also, locally-produced secondary aerosols are expected to be *minor contributors to* PM_{10}*, owing to missing sources of precursors in the Aosta Valley.*

RC7. p34, l17. Maybe the two cases for air quality degradation could be distinguished more clearly here, i.e. thermally driven winds in summer/spring and synoptic winds in winter in stable PBL conditions with no surface wind.

AR7. Right. This was mentioned in the revised conclusions:

We show that these advections are due to thermally-driven winds (especially in the warm period of the year, e.g. case studies 1 and 3) or synoptic flows (mainly in the cold season, e.g. case 2) from the east (Po basin) to the west. A more systematic analysis of the flow regimes and their impacts on transport based on comprehensive statistics are provided in the companion paper (Diémoz et al., 2019) exploiting the full 3-year record of ALC measurements.

RC8. p16, l11. ... in a few hours.

AR8. Done.

RC9. p34, l29. ... regime is established.

AR9. Done.

References

Diémoz, H., Gobbi, G. P., Magri, T., Pession, G., Pittavino, S., Tombolato, I. K. F., Campanelli, M., and Barnaba, F.: Transport of Po Valley aerosol pollution to the northwestern Alps. Part 2: long-term impact on air quality, submitted to Atmos. Chem. Phys., 2019.

Freney, E. J., Sellegri, K., Canonaco, F., Boulon, J., Hervo, M., Weigel, R., Pichon, J. M., Colomb, A., Prévôt, A. S. H., and Laj, P.: Seasonal variations in aerosol particle composition at the puy-de-Dôme research station in France, Atmos. Chem. Phys., 11, 13 047–13 059, doi:10.5194/acp-11-13047-2011, 2011.

Response to Anonymous Referee #3

The paper analyses 3 cases of transport from the Po Valley to NW Alps with several in-situ (4 sites in Aosta and in pristine environment) and REM instruments from ground and space. All these measurements are extensively documented in the paper and in the supplement, allowing to have a broad view of the pollution events. After having validated the meteorological model COSMO, a chemical transport model (FARM) is evaluated. This paper is a clear documentation of middle range pollution events affecting the Alps and the evaluation of model's performances under these conditions is very interesting.

We thank the reviewer for taking the time to revise our manuscript and for his/her pertinent comments. Our reply to these is given hereafter (the text in italics represents a citation of the revised manuscript and the figure references follow the updated numbering).

Referee's comment 1. Figures do not always allow to verify the descriptions or conclusions of the study. For example, higher aerosol concentrations are measured during the case studies (Fig. 4e, Fig. 8, Fig. 13e Fig. S8, ...), but the figures do allow to be sure that the increase in aerosol load is really specific and cannot be attributed to usual/local fluctuations. In other words, it is not possible to see the differences between the period of the case studies and the period without influence from the Po Valley. I do understand that figures similar to Fig. 4 cannot display longer period of time, but another solution should be found! The time period covered by Fig. 12 is fine.

Author's response 1. Following this comment, and similar remarks from referee #2 (RC2) and referee #4 (RC6), we expanded (and homogenised) former panels 4, 10 and 13 (old numbering) to include the same number of days. At the same time, we also paid attention at introducing into the sequence a "clear" day in order to better show the effect of the advections. We thus opted to show one week of measurements in each of these figures, as a compromise between completeness and detail (e.g., of the wind velocity field). The new plots extend from 25 to 31 August 2015 (case 1), from 24 to 30 January 2017 (case 2) and from 24 to 30 May 2017 (case 3), respectively. This allows to better appreciate the difference between event- (clear) and non-event (polluted) days.

Moreover, for each episode, the information on the respective seasonal average concentrations were added to the text to provide reference values. Also note that a rigorous assessment of the long-term impact of the phenomenon presented in this part 1 is indeed the purpose of our companion paper (Diémoz et al., 2019) based on a statistical analysis of the complete dataset (2015–2017).

RC2. FARM leads to too low PM10 concentration in summer and in spring, but seems to work better (even if it does not reproduce the diurnal cycle correctly) in winter (case study 2). Is there an explanation for this difference between summer and winter?

AR2. We recognise that the results of case study 2 could give the mistaken impression that FARM works better in winter. However, this episode is not representative of a more general behaviour, as thoroughly explained in our companion paper. The latter specifically address the long-term evaluation of the phenomenon described in this "part 1" of the study. We anticipate here Fig. 17 of the companion paper, showing that the discrepancies between simulated and observed PM_{10} concentrations at the surface are larger in winter compared to the other seasons. This is to ascribe to an underestimation of the PM_{10} emission sources from outside the boundaries of the domain (in the second row, the comparison looks better if this external contribution is multiplied by a factor W=4).

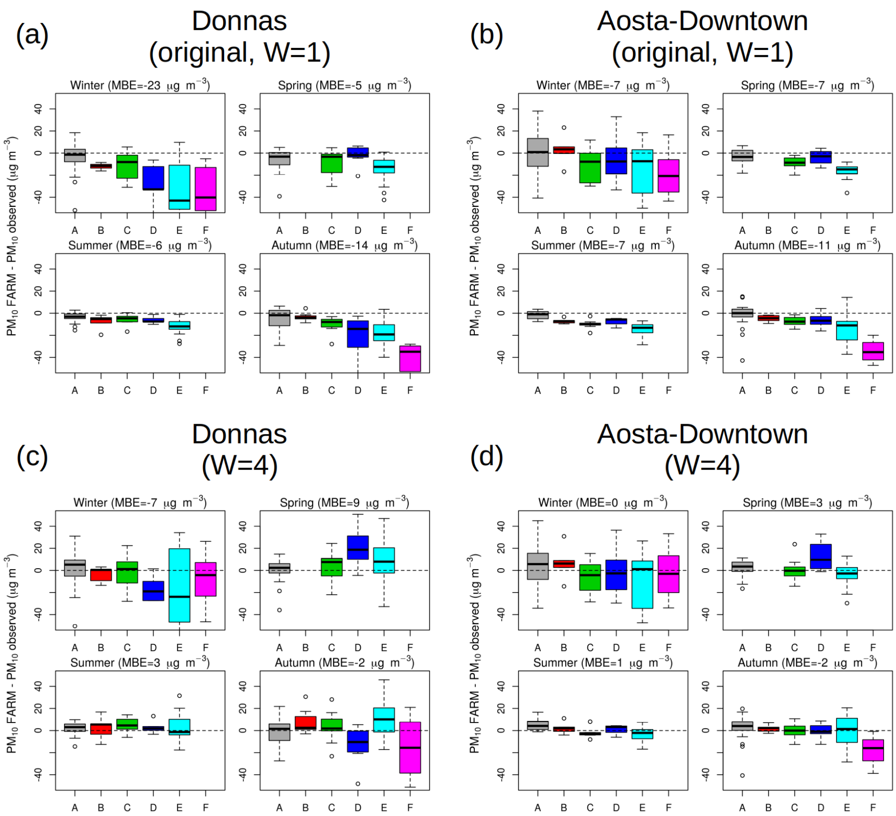

Figure 17 (companion paper): Differences between simulated and observed PM_{10} concentrations at the surface. The mean bias error (MBE) for each case is reported in the plot titles. First row: FARM simulations as currently performed in ARPA for the Donnas (a) and Aosta–Downtown (b) stations. Second row: the PM_{10} concentrations from outside the boundaries of the domain were multiplied by a factor W=4.

Section 4.4 of the revised manuscript was slightly modified to anticipate this issue: *The emission inventory used within FARM likely underestimates the real emissions, as also reported in other cases, and for different models, in the scientific literature (e.g., EMEP, 2016; Uchino et al., 2017). In particular, the boundary conditions could not be accurate enough for our aims owing to the abrupt change of the national emission inventory grid resolution (12 km) to the local scale (1 km). This issue can affect the comparison between the model (dry* PM_{10}*) and surface measurements, especially in winter, as discussed more extensively in the companion paper (Diémoz et al., 2019).*

RC3. Why FARM regularly has time shift in its estimation (for example in Fig. 13 for case study 3)? Fig. S10 shows that modification of the PM concentration from the boundary conditions and the modification of the hygroscopic growth have no impact on the time of the aerosol increase.

AR3. The reviewer raised an important issue, also mentioned by referee #4 (RC11). We therefore further investigated this aspect, added a figure (S13 in the Supplementary) and updated Sect. 4.4 to include a discussion of this phenomenon:

As already mentioned in the description of the three cases, the model: a) underestimates the PM mass both in the layer aloft and at the surface, and b) anticipates the peak concentrations compared to the profiles from the ALC. A variety of (possibly concurrent) reasons can explain the observed underestimation [...] The previous considerations, however, fail at comprehensively explaining the time shifts sometimes noticeable between the model and the measurements, i.e. anticipation of the advection arrival time (even in "dry" conditions in the afternoon on the first day of each sequence) and of the layer disappearance in the morning (where hygroscopicity may have an important role). Although an accurate assessment would require a more sophisticated set of instruments to characterise the vertical profile of the wind velocity, here we formulate some hypotheses:

1. *the NWP model likely anticipates and overestimates the easterly thermally-driven winds in the first hours of the afternoon. This is noticeable, for example, in Fig. S13, where the zonal component of the wind from both COSMO and the surface measurements for case study 1 (August 2015) is plotted, and, on a longer statistical basis, in Fig. S1(b,c), showing that the model has the tendency to see easterly winds more often and with higher intensity compared to the observations. A possible reason for that is the smoothed valley orography used in the NWP model compared to the real one. This is displayed in Fig. S14, showing the difference of the Digital Elevation Model (DEM) used within COSMO and a more realistic DEM (10 m resolution): both valleys and mountain crests are clearly smoothed out by COSMO, with absolute differences well* > 500 *m (and up to 1000 m). This difference could additionally explain why the altitude of the entrainment zone (i.e., the boundary between the free atmosphere and the boundary layer where the thermally-driven circulation develops) is underestimated by COSMO compared to the height of the aerosol layer detected by the ALC;*
2. *COSMO overestimates the nighttime drainage winds (katabatic winds), as noticeable, again, from Fig. S13 for case study 1. This might trigger enhanced cleansing of the lower atmospheric layers during the night as simulated by FARM (see, e.g., the supplementary video file,* `https://doi.org/10.5446/38391`*), but undetected by the ALC. An overestimation of the drainage winds would also explain the differences between the simulated and measured daily cycle of specific humidity [...]*

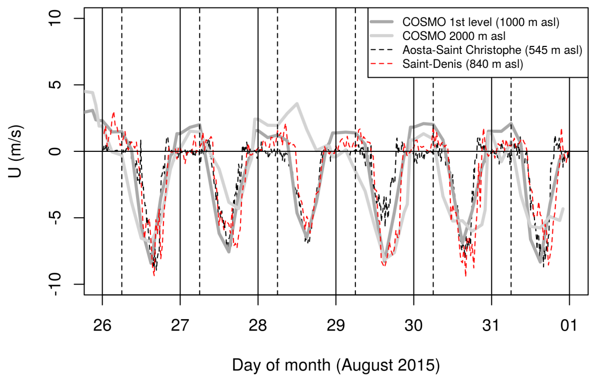

Figure S13: Zonal component of wind velocity during episode 1 (August 2015) from COSMO (1000 and 2000 m a.s.l.) and two surface stations (Aosta–Saint Christophe and Saint-Denis). Positive U represent wind from the west, negative U wind from the east.

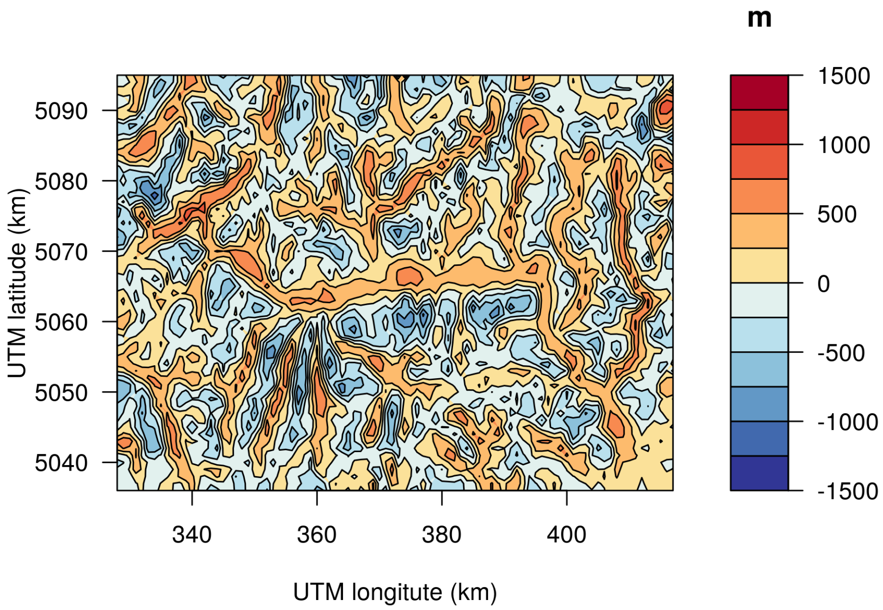

Figure S14: Difference between the (smoothed) Digital Elevation Model (DEM) used by COSMO-I2 (2.8 km resolution) and a higher-resolution DEM ("real topography", 10 m resolution).

Conclusions were also updated to underline this issue:

Our investigation allowed an evaluation of the FARM model. Notably, FARM could reproduce the observed arrival of elevated aerosol layers and it correctly attributed them to sources external to the Aosta Valley. However, absolute values of PM concentrations and the timing of the advections were poorly reproduced, with underestimations of aerosol concentrations and time anticipations compared to the measurements. On the basis of a sensitivity study, the former issue may be partly attributed to both water uptake by highly-hygroscopic particles, not fully taken into account in the model, and deficiencies in the emission inventories, especially owing to the coarse resolution of the national one (12 km). As for the timing discrepancies, suboptimal performances of the NWP model to simulate daytime (thermally-driven) and *nighttime (katabatic) winds are the most likely sources of error. Despite these limitations, FARM brought insights on the phenomenology addressed, supporting the observations and helping to interpret them. On the other hand, the observation-based results of this work could drive the improvement of the emission inventories, thus enhancing the reliability of the CTM (e.g., Diémoz et al., 2019). In turn, this could allow extending the findings of this work to a wider domain, not covered (or not fully covered) by observations.*

RC4. P. 1 line 14: "and hygroscopic": the begin of the sentence is a comparison, so that the meaning of this last 2 words is not obvious.

AR4. Thank you for pointing this out. The sentences now reads: *Results also indicate that the aerosol advected from the Po Valley is hygroscopic, smaller in size and less light-absorbing compared to the aerosol type locally-emitted in the northwestern Italian Alps.*

RC5. P. 1–2, lines 22–1: for clarity purpose I would add a TO: "likely owing to deficiencies in the emission inventory and TO particle water uptake not fully taken into account"

AR5. Done.

RC6. Figure 4d + p. 19 lines 2–7: 1) "PM concentration from non-local sources is represented by the coloured background and the effect of local sources by the contour line, at logarithmic steps;" The logarithmic steps are hardly visible on Fig. 4d (I had to discover that they exist on Fig. 10 to find them on Fig. 4). Could you perhaps use a color scheme with a legend? Without this, it is not evident that the non-local sources exceed the local ones.

AR6. To address this problem highlighted by the referee, we modified the figures in the following way: a) we made the lines thicker; b) we used different line styles (rather than an additional colour legend) and reported the corresponding concentrations in a new legend. An example is provided below, in Fig. 9 (panel d).

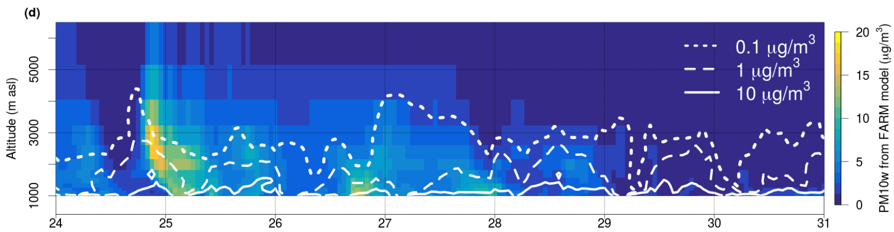

Figure 9 (panel d): Case study of 24–30 January 2017. (d) Mass concentration (PM_{10w}) from FARM. PM concentration from non-local sources is represented by the coloured background and the effect of local sources by the contour line, at logarithmic steps (dotted: 0.1 $\mu g\,m^{-3}$; dashed: 1 $\mu g\,m^{-3}$; continuous, near the surface: 10 $\mu g\,m^{-3}$).

RC7. P. 16 line 11: delete the "," after "scattering ratio" + give some indication on the altitude of the described layer.

AR7. Done, the sentence was modified as follows: *The appearance of the PBL layer is clearly noticeable on 26 August as an increase in the backscatter coefficient up to an altitude of 3 km a.s.l., with scattering ratios SR*$\simeq 4$ *at midday (light-blue area in the figure) almost doubling (SR*> 8*, orange-yellow) in a few hours.*

RC8. P. 16 lines 12-19: I do not really understand your description: from the end of 26th of September, the lowest layer measured by ALC already shows a SR of about 6, so that the "lower levels, with potential consequences on the surface air quality" are already impacted before sunrise on the 27th of September. Your description does not really describes why the SR decrease in the middle of the days. Is the aerosol rich layer entering the ML and contributes then to higher aerosol load in this ML (not observed in Fig. 4a), is it dispersed to higher altitude due to the thermal convection or dispersed horizontally? Please clarify.

AR8. We believe that the reviewer is referring here to the case of August 26-27 (not September). Indeed, we clearly stated in the text that *a thick aerosol layer is detected by the ALC over the Aosta–Saint Christophe observatory from the afternoon of 26 August*, thus well before the sunrise of August 27, and further specified that *the appearance of the PBL layer is clearly noticeable on 26 August as an increase in the backscatter coefficient up to an altitude of 3 km a.s.l., with scattering ratios SR*$\simeq 4$ *at midday (light-blue area in the figure) almost doubling (SR*> 8*, orange-yellow) in a few hours.*

With respect to the missing explanation of the SR decrease in the middle of the day, this was because the interpretation of this ALC-observed behaviour was left to the following paragraphs. However, following the referee's comment, we modified the relevant sentence as follows:

On 27 August, the ALC backscatter is then observed to decrease in the central part of the day and to increase again in the afternoon. This behaviour keeps very regular for almost a week, with the aerosol-rich layer extending from ground up to 3–3.5 km. As further discussed in the next paragraphs, we anticipate here that the main factor driving this cycle is likely an enhanced hygroscopic growth of aerosol advected from the Po Valley from the afternoon to the early morning, this effect also leading to formation of low clouds within the aerosol layer at night (screened out as white areas in the figure). In fact, the transition from aerosol to the cloud phase is very sharp, as also noticeable from the sudden increase of more than 40 Wm^{-2} *of the downward infrared irradiance monitored at the same site.*

RC9. P. 19: is it possible that the observed shift (from some hours to 1/4 of a day) of the maximum concentration between FARM and ALC can be due to an overestimation of the local effects in comparison to the non-local ones?

AR9. Local effects can indeed impact on the daily evolution of the concentrations. However, we believe that the shift observed in this case is mainly triggered by suboptimal simulations of the wind fields by the NWP model, as explained at point AR3 of the present document.

RC10. Figure 8 and p. 6 lines 18–20 + p. 20 lines 13–15: the measured PM2.5 and PM10 during the case study are similar to the annual mean concentration (p.6). An increase of PM2.5 and PM10 is clearly visible from the 26th of August to the beginning of September (at least at Aosta), but the readers cannot be sure that this does not correspond to a usual fluctuations of the aerosol load. Similarly, it is not really visible that FARM predicts an increase of the PM10 concentration at Aosta during the case study.

AR10. Following this comment, we modified the relevant sentence as follows: *An increase in daily concentrations (up to maximum values of 10* $\mu g m^{-3}$ *for* $PM_{2.5}$ *and 16–22* $\mu g m^{-3}$ *for* PM_{10}*) can be clearly noticed at both sites, leading to concentrations slightly higher than average for the same period (7* $\mu g m^{-3}$ *for* $PM_{2.5}$ *in Aosta–Downtown and 12* $\mu g m^{-3}$ *for* PM_{10} *at both sites, considering the 2015–2017 series). The statistical significance of such PM increases during these transport episodes, compared to the natural variability of the aerosol load in non-advection conditions, is assessed in the companion paper using the full long-term dataset.*

Moreover, as already mentioned in AR1, the seasonal average concentrations were added to the text to provide reference values.

RC11. Fig. 4e + page 20 lines 8–9: the PM10 daily cycle does not correspond to the Po Valley air masses transport seen by the ALC. The given explanation relates to the mass losses occurring in TEOM due to secondary aerosol volatility. Is it expected that this volatility should be different between nighttime and daytime (i.e. larger during the night) in order to explain the different diurnal cycles?

AR11. This is an important remark. We therefore decided to update the manuscript to discuss this issue in further detail.

Section 3.1.5: *Two Tapered Element Oscillating Microbalance (TEOM) 1400a monitors (Patashnick and Rupprecht, 1991) are used for continuous measurements of* PM_{10} *hourly concentrations at the stations of Aosta–Downtown and La Thuile. These instruments are not compensated for mass loss of semi-volatile compounds (Green et al., 2009) and could be insensitive to specific compounds, such as ammonium nitrate (e.g., Charron et al., 2004), which leads to underestimations, especially in the cold season, compared to the SM200. Conversely, overestimations by the TEOM compared to daily averages from the SM200 reference instrument are found in summer and are not fully understood at present. Therefore, TEOM monitors are only employed here for qualitative estimates of short-term variations of the aerosol burden while daily-averaged concentrations will be only taken from the SM200 instruments.*

Section 4.1.3: *To evaluate the impacts on surface air quality parameters during the episode, hourly* PM_{10} *concentrations at the surface as measured in Aosta–Downtown and simulated by FARM in Aosta–Saint Christophe are presented in Fig.3e (*PM_{10} *monitoring at La Thuile was not yet operational, at that time). Apart two spikes (80* $\mu g m^{-3}$*) on 25 and 26 August (presumably of local origin), the concentrations measured in Aosta–Downtown by the TEOM show a slight increase after the arrival of the layer, but without sudden jumps. Also, PM concentrations are generally higher during daytime compared to the night, according to the expected cycle of the summertime local sources (e.g., traffic, resuspension, etc.). This features, however, can be connected to the fact that mass loss occurs in TEOM due to secondary aerosol volatility, as better discussed in the companion paper by comparing the daily* PM_{10} *cycle from this instrument and the Fidas OPC in Aosta–Saint Christophe. Moreover, this volatility could be different between nighttime and daytime, which would also contribute to the observed daily behaviour. Besides, FARM estimates at the surface are again lower than measurements (-60%, on average). Daily* PM_{10} *concentrations observed by Opsis SM200 instruments during the case study in Aosta–Downtown and Donnas are shown in Fig. 7, which includes the whole episode (correlation index with TEOM measurements* $\rho = 0.84$*).*

RC12. Fig. S5 is cited before Fig. S4

AR12. Corrected, thank you.

RC13. P. 25 line 2: it has however to be mentioned (and perhaps explained) that the wind direction at Saint-Denis (Fig. S4e), after turning to the east during the afternoon of the 26th of January, turns again to west on the 27th in the morning and stay globally at west during the rest of the case study.

AR13. To better show the different flow regimes during this episode, we made some integrations to the analysis. First, wind direction was plotted in Fig. S4 only for cases when wind speeds exceeds 1 $m\,s^{-1}$ to exclude calm wind conditions. Secondly, we further considered the wind measurements in Donnas, where the wind regime change is much clearer, owing to the weaker temperature inversion. Table 1 (used instruments) was modified accordingly.

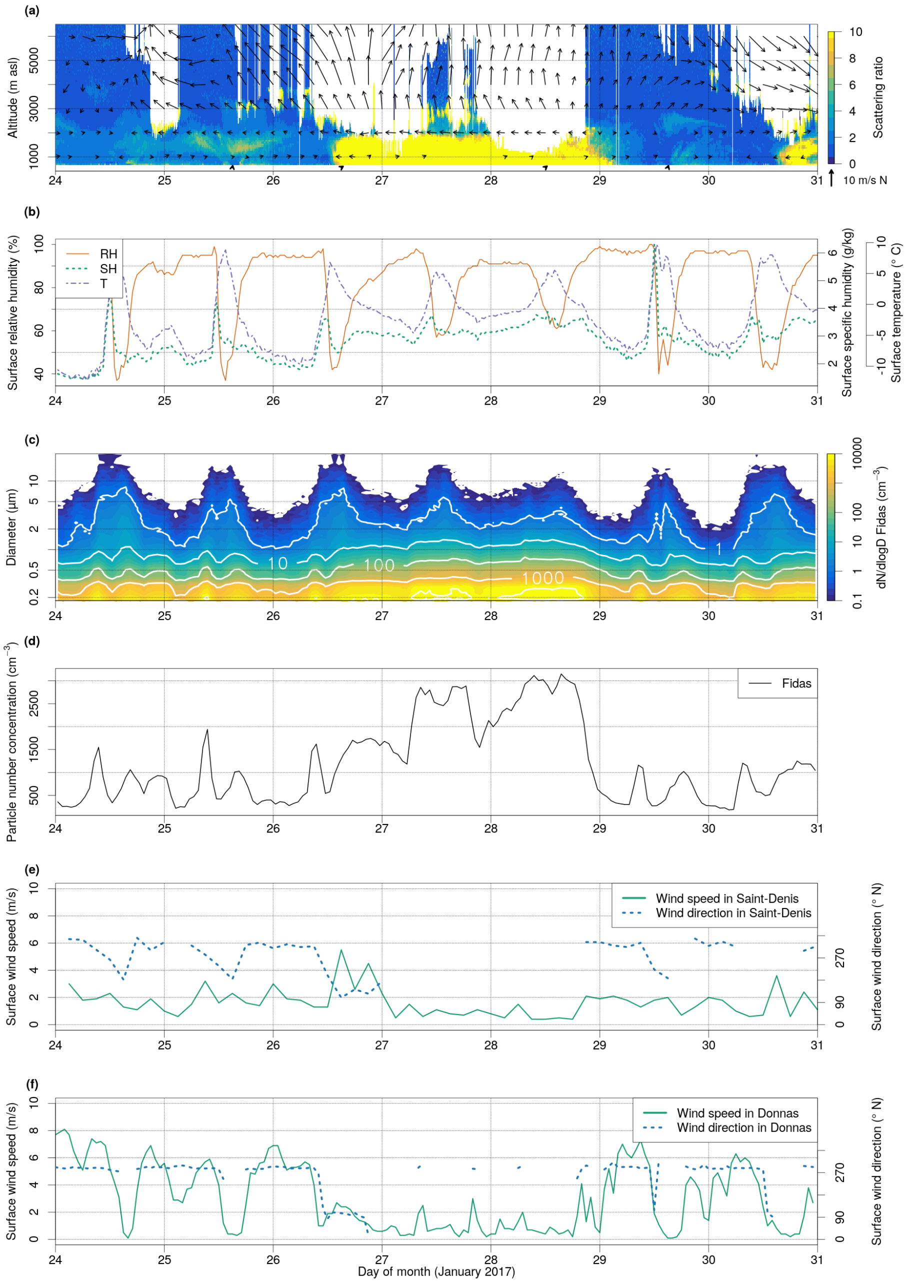

Figure S4: Case study of 26–29 January 2017. (a) Same as in Fig. 9 in the main paper; (b) Surface relative humidity, specific humidity and temperature measured at the Aosta–Saint Christophe weather station; (c) Particle number distribution from the Palas optical counter; (d) Particle number concentration (sum of all channels) from the Palas optical counter; (e) Wind speed and direction at the Saint-Denis station (800 m a.s.l); (f) Wind speed and direction at the Donnas station (316 m a.s.l). No data from the photometer are available for the selected period, since the instrument was not operating.

Given these changes, Sect. 4.2.2 now reads:

The wind field over Aosta–Saint Christophe, depicted in Fig. 9a, presents a very different pattern compared to the first case addressed (Fig. 3a). Firstly, calm wind is measured for the whole period at the bottom of the valley. This is due to a shallow temperature inversion in the lower atmospheric layers in the main valley. Conversely, at the Saint-Denis station, located above the inversion layer, and at the Donnas station, where the temperature inversion is weaker, the wind pattern is more representative of the wider circulation: for example, the average wind speed in Saint-Denis is about 4 $m\,s^{-1}$ *on 26 January afternoon (Fig. S4e) and* *the wind clearly turns from west (morning) to east (afternoon), simultaneously with the appearance of the layer. The same wind change is detected in Donnas on the same day (Fig. S4f), with easterly wind speeds* $> 1\ ms^{-1}$ *for several hours in the afternoon. As a further difference with the first case, the forecasted wind at 1000–2000 m a.s.l. does not show any change in direction typical of the thermal winds. For example, at 2000 m a.s.l. the circulation is continuous, and vigorous (up to 6* ms^{-1}*), from the afternoon of 26 to the beginning of 29 January. Indeed, this winter case study interestingly shows that thermally-driven winds are not the only mechanism, especially in winter, driving the advection of air masses from the Po Valley to the Alps. Rather, the synoptical circulation can push the air masses towards the Alpine valleys, as in this case. In fact, the flow clearly reveals its southern origin at elevations above the mountain crest (e.g., 3000 m a.s.l.), where the wind is not channelled within the main valley. At that altitude, the wind speed is even greater than 20* ms^{-1}*. Finally, on 29 January, the measurements in Saint-Denis (gradual increase of the speed of westerly wind) and in Donnas (even stronger wind, again from the west), and COSMO simulations (wind reversal at 1000–2000 m a.s.l) correlate with the disappearance of the layer better than observations performed at the bottom of the valley (calm wind). [...]*

RC14. P. 25 lines 10–12: the increase of the wind speed at Saint-Denis on the 29th is not very large (about 2 m/s on the 26th in the morning, increase to 4 m/s on the 26th in the afternoon, about 1 m/s until the end of the 28th, then 2 m/s), so that the correlation with the disappearance of the layer is not really explicit.

AR14. Please, refer to AR13.

RC15. Fig. S6 + p. 25 lines 13–15: the described transition (for the lowest levels I suppose) is quite difficult to see: too much backtrajectories, the lowest ones being represented under the highest ones. A figure allowing to see not only the trajectories but also the change of the altitude over the Po Valley (lines 15–29) would perhaps be more interesting).

AR15. Following this comment, and the ones by referee #1 (RC3) and #4 (RC7), we modified the back-trajectory figures in the following way: a) we plotted in separate panels trajectories ending at altitudes < 2000 and > 2500 m a.s.l. over Aosta–Saint Christophe; b) to further simplify the figures, we only show back-trajectories for specific times corresponding to the most significant variations of circulation patterns; c) for each time selected we added a bottom panel with the trajectory altitude along their journey. An example of the new plots now included in the paper is provided in Fig. 5.

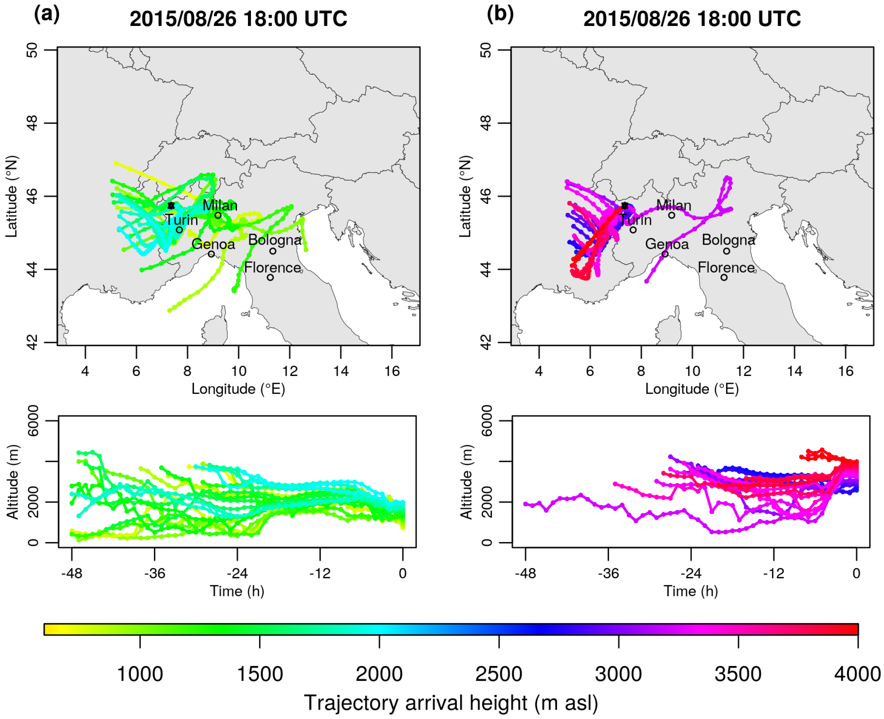

Figure 5: 48-hours back-trajectories ending at Aosta–Saint Christophe on 26 August 2015 at 18 UTC at altitudes lower than 2000 m a.s.l. (a) and higher than 2500 m a.s.l. (b). The trajectories are cut at the border of the COSMO model. The colour scale represents the back-trajectory arrival height. Corresponding altitudes of the backtrajectories vs time are reported in the bottom panels. The dots along each trajectory mark a 1-hour step and the black star indicates the trajectory arrival point (Aosta–Saint Christophe).

RC16. Fig. S4d: the particle number concentration increase during the case study is clearly visible. It is however not possible to determine if this is a peculiar or a normal event occurring regularly during winter.

AR16. As explained in AR1, the duration of the phenomenon represented in the figure was extended to one week in order to include more "non-event" days and better show the effect of the advections on the "standard" conditions in Aosta. The text in Sect. 4.2.3 was also updated in the following way: *The instrument reveals a notable increase in the number concentration for particles smaller than 0.5* µm *(Fig. S4c) in coincidence to the arrival of the aerosol layer. The total number concentration (Fig. S4d) gradually increases from few hundreds particles cm*$^{-3}$ *up to 3000 particles cm*$^{-3}$ *and decreases again on 29 January (the average value in winter 2016–2017 in conditions of local pollution being 650 particles cm*$^{-3}$*).*

RC17. Fig. S9 is cited before fig. S8.

AR17. Corrected.

RC18. P. 32–33, lines 31–6:The hygroscopic growth of the aerosol can clearly be a cause of the discrepancy between FARM and ALC, even if FARM is also not able to reproduce PM measurements and their diurnal cycles. The difference of the measured size fraction (TSP for ALC and PM10 for FARM does however not seem to be really relevant since: 1) Aerosol from the Po Valley are described as small ones in the paper, see for ex. Case study 2, where the increase in PM10 is similar to the one of PM2.5 (Fig. 12), 2) the size distribution measured by the OPC and sun photometer peak in the accumulation mode and do not show big particles.

AR18. The referee is right, we modified the relevant sentence as follows:

A variety of (possibly concurrent) reasons can explain the observed underestimation, mainly related to:

1. *inaccuracies in retrieving the PM concentration from the ALC backscatter. As mentioned, ALC measures aerosol backscatter, so that specific tools were developed (Dionisi et al., 2018) and are used here to associate a PM value to it. Still, the expected error associated to these estimates is of the order of 30–40%. In addition, the ALC retrieval is based on functional relationships derived assuming maximum RH of 95%. Higher FARM-ALC discrepancies can be expected when RH>DRH, and particularly at RH>95%;*
2. *inaccuracies in the CTM simulations [...]*

RC19. P. 33 lines 7–13: How good is the estimation of the PBL height in the CTM simulations? Could a bad estimation of the PBL height be also a source of inaccuracies?

AR19. This could be a further, interesting evaluation of the model output to be performed by comparing the mixing layer height (Hmix) of the model pre-processor (SURFPRO) to the ALC measurements. In fact, these instruments are generally quite powerful in showing the temporal evolution of the mixing layer using the aerosol as tracer (e.g., Angelini et al., 2009). According to this comment/suggestion we modified Sect. 4.4 as follows:

Finally, some underestimation of PM values could also be due to overestimation of the FARM simulated PBL height. An evaluation of this kind of effect is in principle possible by comparing the simulations with the ALC-derived PBL height (e.g., Angelini et al., 2009; Haeffelin et al., 2012). However, this should be performed only selecting non-advection conditions, i.e., those in which the ceilometer signal is only affected by local aerosols and is thus able to follow the daily evolution of the local PBL using local particles as tracers. This kind of investigation was, however, beyond the scope of the present work. Challenges and recent efforts to define a PBL in mountainous areas ("Mountain Boundary Layer", MBL) and discrepancies between the MBL and the aerosol layer are more extensively described by Lehner and Rotach (2018).

RC20. P. 34 line 30–32: as explained previously, I do not see any evidence of a residual layer sinking towards the surface in this study.

AR20. Following the referee's comment, all references about sinking residual layers were removed from the text.

References

Angelini, F., Barnaba, F., Landi, T. C., Caporaso, L., and Gobbi, G. P.: Study of atmospheric aerosols and mixing layer by LIDAR, Radiat. Prot. Dosim., 137, 275–279, doi:10.1093/rpd/ncp219, 2009.

Charron, A., Harrison, R. M., Moorcroft, S., and Booker, J.: Quantitative interpretation of divergence between PM10 and PM2.5 mass measurement by TEOM and gravimetric (Partisol) instruments, Atmos. Environ., 38, 415 – 423, doi:10.1016/j.atmosenv.2003.09.072, 2004.

Diémoz, H., Gobbi, G. P., Magri, T., Pession, G., Pittavino, S., Tombolato, I. K. F., Campanelli, M., and Barnaba, F.: Transport of Po Valley aerosol pollution to the northwestern Alps. Part 2: long-term impact on air quality, submitted to Atmos. Chem. Phys., 2019.

Dionisi, D., Barnaba, F., Diémoz, H., Di Liberto, L., and Gobbi, G. P.: A multiwavelength numerical model in support of quantitative retrievals of aerosol properties from automated lidar ceilometers and test applications for AOT and PM_{10} estimation, Atmos. Meas. Tech., 11, 6013–6042, doi: 10.5194/amt-11-6013-2018, 2018.

EMEP: Transboundary particulate matter, photo-oxidants, acidifying and eutrophying components, Tech. rep., MSC-W, CCC and CEIP, 2016.

Green, D. C., Fuller, G. W., and Baker, T.: Development and validation of the volatile correction model for PM10 – An empirical method for adjusting TEOM measurements for their loss of volatile particulate matter, Atmos. Environ., 43, 2132 – 2141, doi:10.1016/j.atmosenv.2009.01.024, 2009.

Haeffelin, M., Angelini, F., Morille, Y., Martucci, G., Frey, S., Gobbi, G. P., Lolli, S., O'Dowd, C. D., Sauvage, L., Xueref-Rémy, I., Wastine, B., and Feist, D. G.: Evaluation of Mixing-Height Retrievals from Automatic Profiling Lidars and Ceilometers in View of Future Integrated Networks in Europe, Bound.-Lay. Meteorol., 143, 49–75, doi:10.1007/s10546-011-9643-z, 2012.

Lehner, M. and Rotach, M. W.: Current Challenges in Understanding and Predicting Transport and Exchange in the Atmosphere over Mountainous Terrain, Atmosphere, 9, doi:10.3390/atmos9070276, 2018.

Patashnick, H. and Rupprecht, E. G.: Continuous PM-10 Measurements Using the Tapered Element Oscillating Microbalance, J. Air Waste Manage., 41, 1079–1083, doi:10.1080/10473289.1991.10466903, 1991.

Uchino, O., Sakai, T., Izumi, T., Nagai, T., Morino, I., Yamazaki, A., Deushi, M., Yumimoto, K., Maki, T., Tanaka, T. Y., Akaho, T., Okumura, H., Arai, K., Nakatsuru, T., Matsunaga, T., and Yokota, T.: Lidar detection of high concentrations of ozone and aerosol transported from northeastern Asia over Saga, Japan, Atmos. Chem. Phys., 17, 1865–1879, doi:10.5194/acp-17-1865-2017, 2017.

Response to Anonymous Referee #4

General comments: The paper analyzes the impact of pollutants transport from the Po Valley to the air quality on the Alpine region. Three selected cases studies of transport over the Aosta Valley are selected among a 3 years period and analyzed in detail by means of a wide- ranging set of observations and numerical simulations. Moreover, the observational data are used to evaluate the performances of the FARM chemical transport model. These results provide an interesting and comprehensive description of the complex phenomena of mountain-valley exchange and deserve therefore to be published.

We thank the reviewer for taking the time to revise our manuscript and for his/her pertinent comments. Our reply to these is given hereafter (the text in italics represents a citation of the revised manuscript and the figure references follow the updated numbering).

Referee's comment 1. Even if the paper is well written, though, the large amount of data presented in both the main paper and the support material makes the manuscript dispersive and fragmented. I would suggest to further select the figures that are useful to support their message and eliminate redundancies. For example, I invite the authors to carefully evaluate if the section 4.1.5 is bringing any relevant information: the analysis seems not fully convincing, is limited to a single case and the information that intends to bring is already conveyed by the FARM model. Similarly, some figures can be just substituted by a short mention in the text (I would reconsider the relevance of fig. 3, S2c, S4e, S5, S12).

Author's response 1. We understand the referee's objection. At the same time, we believe that the evaluation of the spatial extent of the phenomenon under investigation is important for its understanding. In this respect, Sect. 4.1.5 is the only one in which the phenomenon, which is carefully evaluated locally (Aosta region) with a large set of in situ and ground based measurements, is **observed** (not simulated) over the wider Northern Italy domain using space-based data. We therefore believe that this section, although with some limitations, is an important **observation-based** support to the FARM **model** results. For this reason, we would prefer to keep it.

We are also aware that the manuscript has a high number of figures to show results and support the relevant discussion, including several points raised by the reviewers. That's why we made the choice to leave additional, supporting material out of the main text (Supplement). We believe this choice still allows a straightforward reading of the main text, while providing additional details to those readers interested in more specific aspects of the study.

Still, following the reviewer's advice, we removed Fig. 3 from the text as most information was already available in Fig. 4a.

RC2. Page 2, line 19–22: Basing on the results of the FARM comparison I would rather highlight that the paper aimed at an evaluation of the model and then mentioning that, despite its limitations, it still brought insights on the cases, supporting the observations. Similarly, I would rephrase the paragraph in the conclusions, accordingly (Page 35, line 14 onward)

AR2. Both the abstract and the conclusions were rephrased following the reviewer's advice.

Abstract: *Results show that the simulations are important to the understanding of the phenomenon under investigation. However, in quantitative terms, modelled PM_{10} concentrations are 4–5 times lower than the ones retrieved from the ALC and maxima are anticipated in time by 6–7 hours. Underestimated concentrations are likely mainly due to deficiencies in the emission inventory and to water uptake of the advected particle not fully reproduced by FARM, while timing mismatches are likely an effect of suboptimal simulation of up-valley and down-valley winds by COSMO.*

Conclusions: *Our investigation allowed an evaluation of the FARM model. Notably, FARM could reproduce the observed arrival of elevated aerosol layers and it correctly attributed them to sources external to the Aosta Valley. However, absolute values of PM concentrations and the timing of the advections were poorly reproduced, with underestimations of aerosol concentrations and time anticipations compared to the measurements. On the basis of a sensitivity study, the former issue may be partly attributed to both water uptake by highly-hygroscopic particles, not fully taken into account in the model, and deficiencies in the emission inventories, especially owing to the coarse resolution of the national one (12 km). As for the timing discrepancies, suboptimal performances of the NWP model to simulate daytime (thermally-driven) and nighttime (katabatic) winds are the most likely sources of error. Despite these limitations, FARM brought insights on the phenomenology addressed, supporting the observations and helping to interpret them. On the other hand, the observation-based results of this work could drive the improvement of the emission inventories, thus enhancing the reliability of the CTM (e.g., Diémoz et al., 2019). In turn, this could allow extending the findings of this work to a wider domain, not covered (or not fully covered) by observations.*

RC3. Page 4, line 3: Do you really mean that is the partition between local and non-local sources that help to assess the impact of air pollutants on health, climate and ecosystem?

AR3. No, we meant to say that in order to set up mitigation actions to limit the impact of air pollutants on health, climate and ecosystems it is first necessary to understand where these are originated. Thank you for pointing out that the sentence was misleading, we rephrased it as follows:

Over the impacted areas, a correct partitioning between local and non-local sources is therefore necessary to 1) correctly interpret the exceedances of air quality limits; 2) develop joint efforts and large-scale mitigation strategies (WMO, 2012) to reduce the frequency and impact of pollution episodes on citizen health (Straif et al., 2013; WHO, 2016; Zhang et al., 2017), climate (Clerici and Mélin, 2008; Lau et al., 2010; Zeng et al., 2015) and ecosystems (Carslaw et al., 2010; Bourgeois et al., 2018; Burkhardt et al., 2018).

RC4. Page 14, line 21. "Therefore, to reduce errors in trajectories with increasing running time, we limit the computation to this duration". The sentence between commas, in this context, is misleading. Rewrite as "Therefore, we limit the computation to this duration"

AR4. Done.

RC5. Page 18, Figure 6. It would be more meaningful to show the trajectories at 18:00 UTC for this case, since at this time you observe the start of the intense layer arrival and the trajectories are also showing a larger impact from the Po Valley.

AR5. The figure (Fig. 5, with the new numbering) was modified according to the referee's comment. It is shown here below (cf. also AR7 for further updates to the figure):

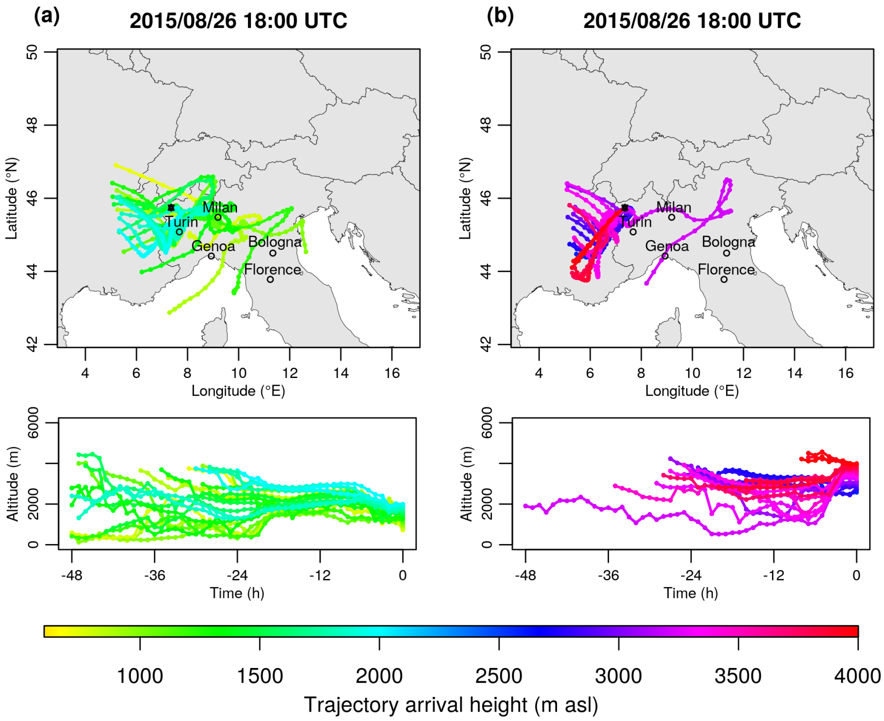

Figure 5: 48-hours back-trajectories ending at Aosta–Saint Christophe on 26 August 2015 at 18 UTC at altitudes lower than 2000 m a.s.l. (a) and higher than 2500 m a.s.l. (b). The trajectories are cut at the border of the COSMO model. The colour scale represents the back-trajectory arrival height. Corresponding altitudes of the backtrajectories vs time are reported in the bottom panels. The dots along each trajectory mark a 1-hour step and the black star indicates the trajectory arrival point (Aosta–Saint Christophe).

RC6. Page 16, line 14: Mention here that you see these surface impacts in your measurements (Fig. 8). Also, what will happen if you average the hourly measurements of TEOM on a daily interval? Will it be consistent with the results of figure 8? Please note that the time interval shown in figure 4 seems to be, compared to figure 8, in the middle of the event (Starting from 26 August and ending at the end of 3 September), so that is not possible to identify any difference with the previous or following phase.

AR6. The discussion about the TEOM has been refined in the updated manuscript, also following the comment by referee #3 (RC11).

Section 3.1.5: *Two Tapered Element Oscillating Microbalance (TEOM) 1400a monitors (Patashnick and Rupprecht, 1991) are used for continuous measurements of PM_{10} hourly concentrations at the stations of Aosta–Downtown and La Thuile. These instruments are not compensated for mass loss of semi-volatile compounds (Green et al., 2009) and could be insensitive to specific compounds, such as ammonium nitrate (e.g., Charron et al., 2004), which leads to underestimations, especially in the cold season, compared to the SM200. Conversely, overestimations by the TEOM compared to daily averages from the SM200 reference instrument are found in summer and are not fully understood at present. Therefore, TEOM monitors are only employed here for qualitative estimates of short-term variations of the aerosol burden while daily-averaged concentrations will be only taken from the SM200 instruments.*

Section 4.1.3: *To evaluate the impacts on surface air quality parameters during the episode, hourly PM_{10} concentrations at the surface as measured in Aosta–Downtown and simulated by FARM in Aosta–Saint Christophe are presented in Fig.3e (PM_{10} monitoring at La Thuile was not yet operational, at that time). Apart two spikes (80 $\mu g m^{-3}$) on 25 and 26 August (presumably of local origin), the concentrations measured in Aosta–Downtown by the TEOM show a slight increase after the arrival of the layer, but without sudden jumps. Also, PM concentrations are generally higher during daytime compared to the night, according to the expected cycle of the summertime local sources (e.g., traffic, resuspension, etc.). This features, however, can be connected to the fact that mass loss occurs in TEOM due to secondary aerosol volatility, as better discussed in the companion paper by comparing the daily PM_{10} cycle from this instrument and the Fidas OPC in Aosta–Saint Christophe. Moreover, this volatility could be different between nighttime and daytime, which would also contribute to the observed daily behaviour. Besides, FARM estimates at the surface are again lower than measurements (-60%, on average). Daily PM_{10} concentrations observed by Opsis SM200 instruments during the case study in Aosta–Downtown and Donnas are shown in Fig. 7, which includes the whole episode (correlation index with TEOM measurements $\rho = 0.84$).*

Regarding the second comment by the referee about the time interval shown in former Fig. 4, we followed the reviewer's suggestion and similar remarks from referee #2 (RC2) and referee #3 (RC1 and RC10). Thus, we expanded (and homogenised) former panels 4, 10 and 13 (old numbering) to include the same number of days. At the same time, we also paid attention at introducing into the sequence a “clear” day in order to better show the effect of the advections. We thus opted to show one week of measurements in each of these figures, as a compromise between completeness and detail (e.g., of the wind velocity field). The new plots extend from 25 to 31 August 2015 (case 1), from 24 to 30 January 2017 (case 2) and from 24 to 30 May 2017 (case 3), respectively. This allows to better appreciate the difference between event- (clear) and non-event (polluted) days.

Moreover, for each episode, the information on the respective seasonal average concentrations were added to the text to provide reference values. Also note that a rigorous assessment of the long-term impact of the phenomenon presented in this part 1 is indeed the purpose of our companion paper (Diémoz et al., 2019) based on a statistical analysis of the complete dataset (2015–2017).

RC7. Page 17, line 33: Do you mean here that the transport from the Po Valley persists at every hour along the following days? Indeed, considering the evolution of the layer as seen from the measurements, it would be useful to show which is the typical transport during the whole event at different hours, for example adding the average position of the trajectories (or the PDF of the position in case of large variability) on the considered period. If the authors want to still keep the trajectory of the first day of the episode as a reference for the layer arrival, I would suggest, to avoid burden the paper with additional plots, showing just the synoptic hours instead of a 3-hour time step; it should still be enough to demonstrate the transport evolution. This would also allow comparing the first and third transport type with the mean transport behaviour of the second case study, when the layer persists for the whole duration of the event.

AR7. The sentence at line 33 was modified as follows: *The analysis of the corresponding back-trajectories confirms that transport of polluted air masses from the Po basin also occurs in the afternoons of the other days of this episode, until the flux changes again to a north-western configuration (Fig. S3c and f).*

Following the comment by the reviewer (and similar remarks from referees #1 (RC3) and #3 (RC15)), the back-trajectories figures were modified in this way: we plotted in separate panels trajectories ending at altitudes < 2000 and > 2500 m a.s.l. over Aosta–Saint Christophe. Also, to further simplify the figures, we only show back-trajectories for specific times corresponding to the most significant variations of circulation patterns. Finally, according to referee #3 (RC15), for each time selected we added a bottom panel with the trajectory altitude along their journey. An example of the new plots is provided in Fig. 5, see AR5.

RC8. Page 21, line 15: Can you add some reference for the typical Angstrom exponent for the Aosta valley in comparison?

AR8. Done, we added the following sentence: *These values should be compared to the lower Ångström exponents typically measured in the Aosta Valley, i.e. ~1.1 on average (Diémoz et al., 2014, 2019).*

RC9. Page 25, line 18 (but same for page 30, line 6): How do you estimate this residence time, is it an average of the time spent by each trajectory over the Po Valley at all levels? From the shown figure (even if it is difficult to distinguish), the transport, including the part outside the PBL, seems faster (around 20 hours or even less). Can you be more specific?

AR9. This was simply computed considering that each dots along each trajectory mark a 1-hour step (as stated in caption of Fig. 5). Given this comment we clarified this point in the text as follows: *The trajectory altitude tends to decrease in the afternoon reaching the elevations of the polluted boundary layer (Fig. S6b), thus leading to effective aerosol transport to the Aosta Valley. In fact, considering that each dot in Fig. S6b represents a 1-hour step, we estimate a mean air masses residence time in the Po Valley PBL of 30–35 hours before arriving over the observing site. Finally, trajectories turn westerly on 29 January, in agreement with the removal of the layer over Aosta (Fig. S6c and f).*

RC10. Page 25, line 33–35: How do you justify these affirmations?

AR10. The sentence was partially rephrased: *Taking into consideration these different daily evolution patterns and the sources included in the emission inventory, the most likely reasons for the differences between the model and the measurements at the surface appear to be an underestimation of the residential heating (actually switched on all day during these very cold days) and an overestimation of the traffic road contribution, together with an overestimation of the mixing layer height growth at midday by the NWP model.*

RC11. Page 32, line 29: It would be interesting to see this comparison indeed since, from figure S1, it seems that the model has the tendency to see easterly winds more often and with higher intensity

respect to the observations. Is this comparison limited just to the surface measurements? May it be that there are problems in the higher layers (where most of the pollution layer transport is coming from)? For example, in the case study 2, when the winds were weaker both at the ground and at higher layers, the time evolution of the FARM simulation of Figure 10d was in better agreement with the observations. Is also interesting to note that the time evolution of the vertical distribution of PM10 from FARM is in better agreement (especially the local contribution) with the surface TEOM measurements rather than with the elevated layers observations.

AR11. The reviewer raised some important issues, also mentioned by referee #3 (RC3). We therefore decided to better investigate the capability of COSMO in reproducing the measured wind fields (unfortunately, our instrumentation allows validation only at the surface) and we updated Sect. 4.4 accordingly:

As already mentioned in the description of the three cases, the model [...] anticipates the peak concentrations compared to the profiles from the ALC [...], i.e. [it shows] anticipation of the advection arrival time (even in "dry" conditions in the afternoon on the first day of each sequence) and of the layer disappearance in the morning (where hygroscopicity may have an important role). Although an accurate assessment would require a more sophisticated set of instruments to characterise the vertical profile of the wind velocity, here we formulate some hypotheses:

1. *the NWP model likely anticipates and overestimates the easterly thermally-driven winds in the first hours of the afternoon. This is noticeable, for example, in Fig. S13, where the zonal component of the wind from both COSMO and the surface measurements for case study 1 (August 2015) is plotted, and, on a longer statistical basis, in Fig. S1(b,c), showing that the model has the tendency to see easterly winds more often and with higher intensity compared to the observations. A possible reason for that is the smoothed valley orography used in the NWP model compared to the real one. This is displayed in Fig. S14, showing the difference of the Digital Elevation Model (DEM) used within COSMO and a more realistic DEM (10 m resolution): both valleys and mountain crests are clearly smoothed out by COSMO, with absolute differences well* > 500 *m (and up to 1000 m). This difference could additionally explain why the altitude of the entrainment zone (i.e., the boundary between the free atmosphere and the boundary layer where the thermally-driven circulation develops) is underestimated by COSMO compared to the height of the aerosol layer detected by the ALC;*
2. *COSMO overestimates the nighttime drainage winds (katabatic winds), as noticeable, again, from Fig. S13 for case study 1. This might trigger enhanced cleansing of the lower atmospheric layers during the night as simulated by FARM (see, e.g., the supplementary video file, `https://doi.org/10.5446/38391`), but undetected by the ALC. An overestimation of the drainage winds would also explain the differences between the simulated and measured daily cycle of specific humidity [...]*

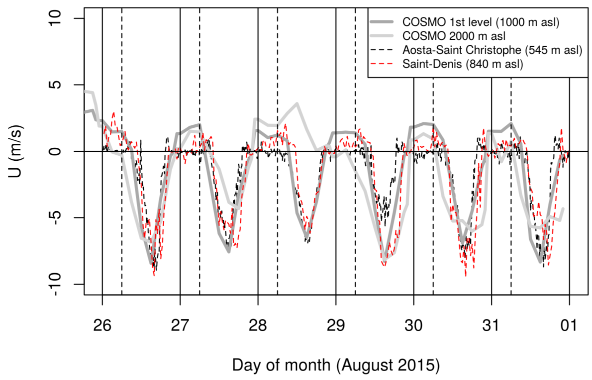

Figure S13: Zonal component of wind velocity during episode 1 (August 2015) from COSMO (1000 and 2000 m a.s.l.) and two surface stations (Aosta–Saint Christophe and Saint-Denis). Positive *U* represent wind from the west, negative *U* wind from the east.

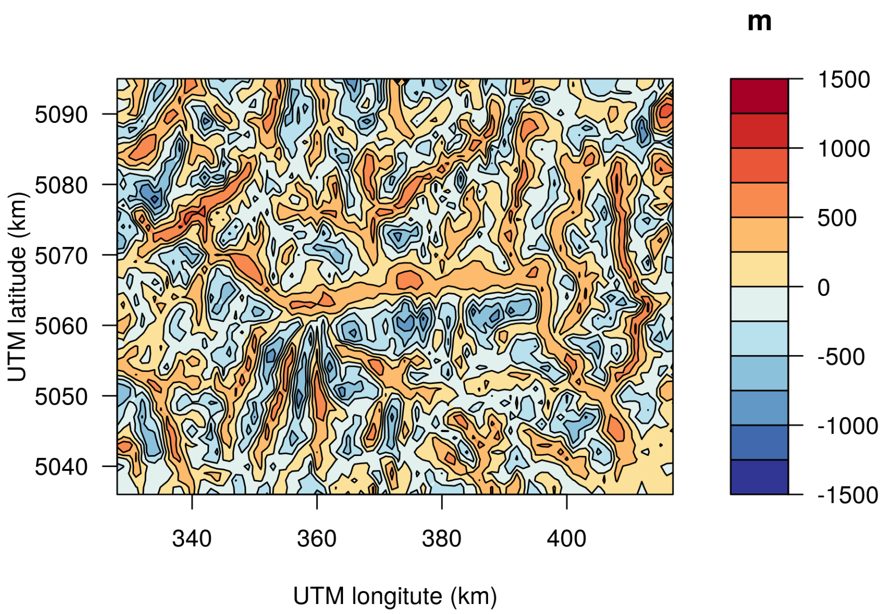

Figure S14: Difference between the (smoothed) Digital Elevation Model (DEM) used by COSMO-I2 (2.8 km resolution) and a higher-resolution DEM ("real topography", 10 m resolution).

Conclusions were also updated to underline this issue, as already mentioned in AR2: *As for the timing discrepancies, suboptimal performances of the NWP model to simulate daytime (thermally-driven) and nighttime (katabatic) winds are the most likely sources of error.*

Finally, please note that an in-depth examination of FARM capabilities to reproduce the observed PM concentrations for event and non-event days was done in the companion paper based on the long-term dataset (2015–2017). We anticipate here Fig. 17 (companion paper), showing that the discrepancies between simulated and observed PM_{10} concentrations at the surface are minimum in cases of non-event days, which agrees with the referee's remark.

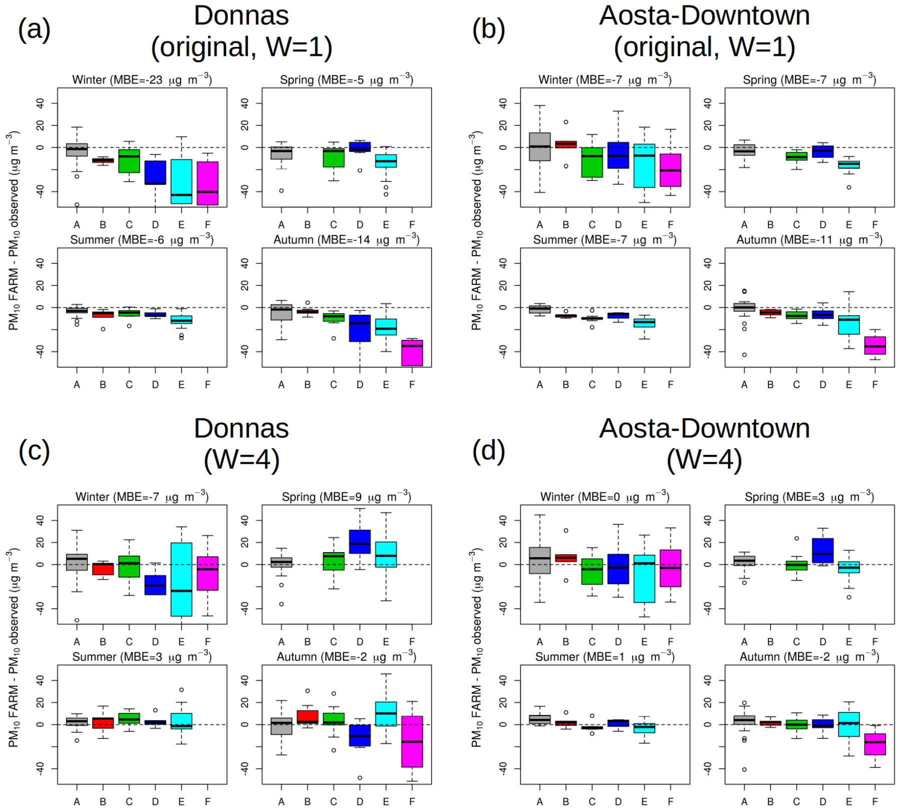

Figure 17 (companion paper): Differences between simulated and observed PM_{10} concentrations at the surface. The mean bias error (MBE) for each case is reported in the plot titles. First row: FARM simulations as currently performed in ARPA for the Donnas (a) and Aosta–Downtown (b) stations. Second row: the PM_{10} concentrations from outside the boundaries of the domain were multiplied by a factor W=4.

RC12. Page 4, line 10: "will be quantified in a companion ..."

AR12. Done.

RC13. Page 4, line 28: For easier reading, specify which valley are you talking about. In the same paragraph, you are referring to both the Po valley and the Alpine valleys.

AR13. Done. The sentence now reads: *[...] the heaviest burden of particles did not come from the largest urban settlement in the Aosta Valley, but rather from outside the region, namely from the Po basin.*

RC14. Figure 2: The dashed lines are not needed.

AR14. Removed.

RC15. Page 9, line 21: "... altitude of the extinction coefficient."

AR15. Done.

RC16. Page 21, line 22: Refer also to the figure S8.

AR16. Reference to the figure was added.

RC17. Page 34, line 6: Add a ":" after "(see Introduction)"

AR17. Done.

RC18. Page 35, line 19: "... these issues may be partly attributed to ..."

AR18. Done.

References

Bourgeois, I., Savarino, J., Caillon, N., Angot, H., Barbero, A., Delbart, F., Voisin, D., and Clément, J.-C.: Tracing the Fate of Atmospheric Nitrate in a Subalpine Watershed Using Δ17O, Environ. Sci. Tech., 52, 5561–5570, doi:10.1021/acs.est.7b02395, 2018.

Burkhardt, J., Zinsmeister, D., Grantz, D. A., Vidic, S., Sutton, M. A., Hunsche, M., and Pariyar, S.: Camouflaged as degraded wax: hygroscopic aerosols contribute to leaf desiccation, tree mortality, and forest decline, Environ. Res. Lett., 13, 085 001, doi:10.1088/1748-9326/aad346, 2018.

Carslaw, K. S., Boucher, O., Spracklen, D. V., Mann, G. W., Rae, J. G. L., Woodward, S., and Kulmala, M.: A review of natural aerosol interactions and feedbacks within the Earth system, Atmos. Chem. Phys., 10, 1701–1737, doi:10.5194/acp-10-1701-2010, 2010.

Charron, A., Harrison, R. M., Moorcroft, S., and Booker, J.: Quantitative interpretation of divergence between PM10 and PM2.5 mass measurement by TEOM and gravimetric (Partisol) instruments, Atmos. Environ., 38, 415 – 423, doi:10.1016/j.atmosenv.2003.09.072, 2004.

Clerici, M. and Mélin, F.: Aerosol direct radiative effect in the Po Valley region derived from AERONET measurements, Atmos. Chem. Phys., 8, 4925–4946, doi:10.5194/acp-8-4925-2008, 2008.

Diémoz, H., Campanelli, M., and Estellés, V.: One Year of Measurements with a POM-02 Sky Radiometer at an Alpine EuroSkyRad Station, J. Meteorol. Soc. Jpn., 92A, 1–16, doi:10.2151/jmsj.2014-A01, 2014.

Diémoz, H., Gobbi, G. P., Magri, T., Pession, G., Pittavino, S., Tombolato, I. K. F., Campanelli, M., and Barnaba, F.: Transport of Po Valley aerosol pollution to the northwestern Alps. Part 2: long-term impact on air quality, submitted to Atmos. Chem. Phys., 2019.

Green, D. C., Fuller, G. W., and Baker, T.: Development and validation of the volatile correction model for PM10 – An empirical method for adjusting TEOM measurements for their loss of volatile particulate matter, Atmos. Environ., 43, 2132 – 2141, doi:10.1016/j.atmosenv.2009.01.024, 2009.

Lau, W. K., Kim, M.-K., Kim, K.-M., and Lee, W.-S.: Enhanced surface warming and accelerated snow melt in the Himalayas and Tibetan Plateau induced by absorbing aerosols, Environ. Res. Lett., 5, 025 204, doi:10.1088/1748-9326/5/2/025204, 2010.

Patashnick, H. and Rupprecht, E. G.: Continuous PM-10 Measurements Using the Tapered Element Oscillating Microbalance, J. Air Waste Manage., 41, 1079–1083, doi:10.1080/10473289.1991.10466903, 1991.

Straif, K., Cohen, A., and Samet, J., eds.: Air pollution and cancer, WHO Press, World Health Organization, 2013.

WHO: Ambient air pollution: a global assessment of exposure and burden of disease, Tech. rep., 2016.

WMO: WMO/IGAC Impacts of megacities on air pollution and climate, Tech. rep., World Meteorological Organization, URL https://library.wmo.int/pmb_ged/gaw_205.pdf, 2012.

Zeng, Z., Chen, A., Ciais, P., Li, Y., Li, L. Z. X., Vautard, R., Zhou, L., Yang, H., Huang, M., and Piao, S.: Regional air pollution brightening reverses the greenhouse gases induced warming-elevation relationship, Geophys. Res. Lett., 42, 4563–4572, doi:10.1002/2015GL064410, 2015.

Zhang, Q., Jiang, X., Tong, D., Davis, S. J., Zhao, H., Geng, G., Feng, T., Zheng, B., Lu, Z., Streets, D. G., Ni, R., Brauer, M., van Donkelaar, A., Martin, R. V., Huo, H., Liu, Z., Pan, D., Kan, H., Yan, Y., Lin, J., He, K., and Guan, D.: Transboundary health impacts of transported global air pollution and international trade, Nature, 543, 705–709, doi:10.1038/nature21712, 2017.

Transport of Po Valley aerosol pollution to the northwestern Alps. Part 1: phenomenology

Henri Diémoz[1], Francesca Barnaba[2], Tiziana Magri[1], Giordano Pession[1], Davide Dionisi[2], Sara Pittavino[1], Ivan K. F. Tombolato[1], Monica Campanelli[2], Lara Sofia Della Ceca[3], Maxime Hervo[4], Luca Di Liberto[2], Luca Ferrero[5], and Gian Paolo Gobbi[2]

[1]ARPA Valle d'Aosta, Saint-Christophe, Italy
[2]Institute of Atmospheric Science and Climate, CNR, Rome, Italy
[3]Instituto de Física Rosario, Rosario, Argentina
[4]MeteoSwiss, Payerne, Switzerland
[5]GEMMA and POLARIS research centres, Department of Earth and Environmental Sciences, University of Milano-Bicocca, Italy

Correspondence to: Henri Diémoz (h.diemoz@arpa.vda.it)

Abstract.

Mountainous regions are often considered pristine environments, however they can be affected by pollutants emitted in more populated and industrialised areas, transported by regional winds. Based on experimental evidence, further supported by modelling tools, we demonstrate and quantify here the impact of air masses transported from the Po Valley, a European atmospheric pollution hotspot, to the northwestern Alps. This is achieved through a detailed investigation of the phenomenology of near-range (few hundreds km), trans-regional transport, exploiting synergies of multi-sensor observations mainly focussed on particulate matter. The explored dataset includes vertically-resolved data from atmospheric profiling techniques (Automated LiDAR-Ceilometers, ALC), vertically-integrated aerosol properties from ground (sun photometer) and space, and in situ measurements (PM_{10} and $\mathrm{PM}_{2.5}$, relevant chemical analyses, and aerosol size distribution). During the frequent advection episodes from the Po basin, all the physical quantities observed by the instrumental setup are found to significantly increase: the scattering ratio from ALC reaches values >30, ~~AOD~~ Aerosol Optical Depth (AOD) triplicates, surface PM_{10} reaches concentrations $> 100\ \mu\mathrm{g\,m}^{-3}$ even in rural areas, contributions to PM_{10} by secondary inorganic compounds such as nitrate, ammonium and sulfate increase up to 28%, 8% and 17%~~of the total mass~~, respectively. Results also indicate that the ~~advected aerosol is~~ aerosol advected from the Po Valley is hygroscopic, smaller in size and less light-absorbing compared to the aerosol type locally-emitted in the northwestern Italian Alps~~, and hygroscopic~~. In this work, the phenomenon is exemplified through detailed analysis and discussion of three case studies, selected for their clarity and relevance within the wider dataset, the latter being fully exploited in a companion paper quantifying the impact of this phenomenology over the ~~long- term~~ long-term (Diémoz et al., 2019). For the three case studies investigated, a high-resolution numerical weather prediction model (COSMO) and a lagrangian tool (LAGRANTO) are employed to understand the meteorological mechanisms favouring the transport and to demonstrate the Po Valley origin of the air masses. In addition, a chemical transport model (FARM) is used to further support the observations and to partition the contributions of local and non-local sources. Results show that the simulations are ~~not able to adequately reproduce the measurements (with~~ important to the understanding of the phenomenon under investigation.

However, in quantitative terms, modelled PM_{10} concentrations are 4–5 times lower than the ones retrieved from the ALC ~~, and maxima anticipated~~ and maxima are anticipated in time by 6–7 hours~~), likely owing~~. Underestimated concentrations are likely mainly due to deficiencies in the emission inventory and ~~particle water uptake not fully taken into account~~to water uptake of the advected particles not fully reproduced by FARM, while timing mismatches are likely an effect of suboptimal simulation of up-valley and down-valley winds by COSMO. The advected aerosol is shown to remarkably degrade the air quality of the Alpine region, with potential negative effects on human health, climate and ecosystems, as well as on the touristic development of the investigated area. The findings of the present study could also help design mitigation strategies at the ~~trans–regional~~ trans-regional scale in the Po basin, and suggest an observations-based approach to evaluate the outcome of their implementation.

1 Introduction

In mountainous regions, mutual exchanges between the valley atmosphere and the nearby plains have been recognised and studied for more than a century (e.g., Thyer, 1966, and references therein). Notably, daytime up-valley (nighttime down-valley) flows systematically develop as a result of faster heating (cooling) of mountain valleys compared to the foreland (Rampanelli et al., 2004; Serafin and Zardi, 2010; Schmidli, 2013; Wagner et al., 2014), and hence manifest on a very regular basis, especially during fair-weather days (nights) with weak synoptic circulation (Borghi and Giuliacci, 1980; Tampieri et al., 1981). The plain-to-mountain circulation regime conveys mass, heat and moisture within the planetary boundary layer (PBL), thus contributing to horizontal mixing on the mesoscale (Weissmann et al., 2005). Additionally, air parcels can be lifted by convection above the ridges and transported to the free troposphere, which favours air mass exchange in the vertical direction (Henne et al., 2004; Gohm et al., 2009; Schnitzhofer et al., 2009; Lang et al., 2015).

Thermally-driven wind systems are observed in mountainous regions throughout the world (e.g., Cong et al., 2015; Collaud Coen et al., 2018; Dhungel et al., 2018). The European Alps have been the ideal scenario for such kind of studies, owing to their rugged shape forming hundreds of main and tributary valleys, and large surrounding plains with strong emission sources, the most significant being in the Po basin. Indeed, this vast region, which includes a large portion of northern Italy, is one of the most densely populated (more than 20 millions of people and a population density of 414 inhabitants per km^2 (WMO, 2012)), industrialised, and thus polluted areas in Europe (Chu et al., 2003; Van Donkelaar et al., 2010; Fuzzi et al., 2015; EMEP, 2016). The valley morphology exacerbates the air quality. In fact, heavy emissions from productive activities as well as from vehicular traffic and residential heating are often trapped within the Po basin due to its characteristic topography strongly limiting the dispersion of pollutants, with the Alpine chain and the Apennines enclosing the plain on its northern, western and southern sides. As a consequence, the Po basin is one of the EU hotspots suffering from premature mortality associated to atmospheric pollution (EEA, 2015). In spite of the improvements in the last decades (e.g., Bigi and Ghermandi, 2016), the air quality in the Po Valley is still far from the standards established by the European Commission (EU Commission, 2008) and exceedances of these standards are expected to continue in the next years (Belis et al., 2017; Caserini et al., 2017; EEA, 2017; Guariso and Volta, 2017).

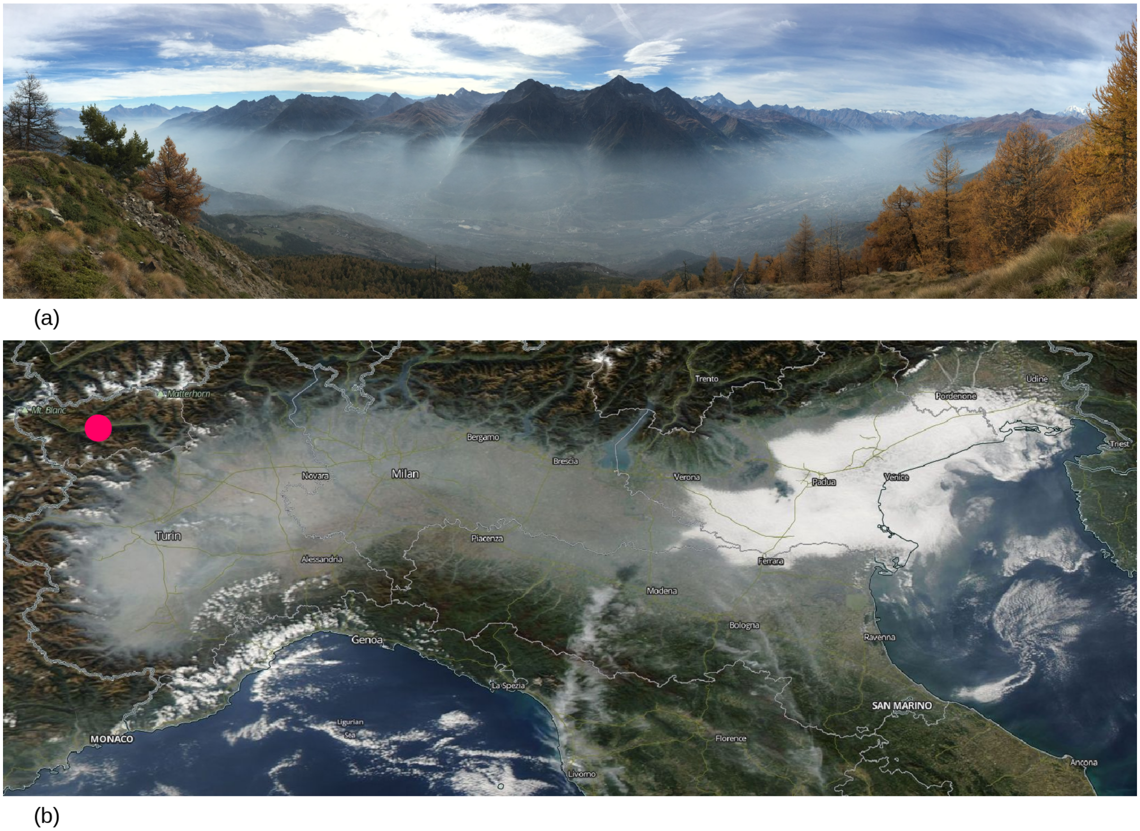

Figure 1. (a) Panoramic view of the main valley over the Aosta–Saint Christophe station during a pollution advection event. The picture was taken from Croce di Fana (2200 m a.s.l, Quart village, 6 km north-east of Aosta–Saint Christophe) on 21 October 2017. On that day, the advected layer of aerosol – visible in the picture as a hazy layer – reached an altitude of about 2000 m a.s.l. Photo kindly provided by C. Cometto. (b) Image of the Po Valley from the MODIS Aqua radiometer (corrected reflectance, true colour) only few days before the picture in the first panel was taken (18 October, https://worldview.earthdata.nasa.gov). The satellite view clearly shows that the hazy, aerosol-rich layer from the Po basin is starting to pour out into the Alpine valleys. The pink marker identifies the Aosta–Saint Christophe site.

Both theoretical studies and experimental campaigns demonstrated that transboundary transport of several kind of pollutants from the Po basin affects pre-Alpine areas (Dosio et al., 2002; Neftel et al., 2002; Mélin and Zibordi, 2005), the Italian Alpine valleys (Nyeki et al., 2002; Larsen et al., 2012; Ferrero et al., 2014), other Italian regions (Cristofanelli et al., 2009; Carbone et al., 2014; Moroni et al., 2015) and even neighbouring countries (e.g., Wotawa et al., 2000; Finardi et al., 2014). Over the impacted areas, a correct partitioning between local and non-local sources is therefore necessary to 1) correctly interpret the exceedances of air quality limits; 2) develop joint efforts and large-scale mitigation strategies (WMO, 2012) to reduce the frequency and impact of pollution episodes ~~(an example is the recently signed "antismog" agreement for the improvement of air quality in the Po basin, Italian Ministry of the Environment (2018)); 3) assess the impact of air pollutants~~ on citizen health (Straif et al., 2013; WHO, 2016; Zhang et al., 2017), climate (Clerici and Mélin, 2008; Lau et al., 2010; Zeng et al., 2015) and ecosystems (Carslaw et al., 2010; Bourgeois et al., 2018; Burkhardt et al., 2018). As an additional important aspect, in mountainous regions, pollution layers undermine the visual quality of the landscape (e.g., Fig. 1a) and thus touristic attractiveness, with obvious economics implications (de Freitas, 2003).

In the present study, we aim at illustrating and deeply investigating the phenomenology of aerosol transport events to the northwestern Alpine region through a detailed analysis and discussion of specifically-selected case studies. The impacts of this phenomenon over the long-term ~~are then~~ will be quantified in a companion paper (Diémoz et al., 2019). ~~This research exploits a multi-technique approach, combining a large set of measurements (at surface level, column integrated and vertically-resolved) with modelling tools such as chemical transport models (CTM).~~

In fact, several previous field campaigns investigated the atmospheric composition and transport mechanisms in the eastern and central part of the Po Valley (Nyeki et al., 2002; Barnaba et al., 2007; Ferrero et al., 2010; Larsen et al., 2012; Decesari et al., 2014; Khan et al., 2016; Rosati et al., 2016; Cugerone et al., 2018), but very few studies are available on the westernmost side of the basin (Anfossi et al., 1988; Mercalli et al., 2003; Manara et al., 2018). Earlier evidences of possible advections of pollutants from the Po basin to the northwestern Alps were collected in the framework of two intensive, 4-days-long campaigns performed between 2000 and 2001 (Agnesod et al., 2003). At that time, an equipped aircraft flew during anticyclonic conditions with weak synoptic circulation, in order to assess the effects of the local winds on the air quality in the Alpine valleys close to Mont Blanc (in Italy, France and Switzerland). The experiment was focussed on ozone measurements and its precursors, however aerosol concentrations were additionally measured. Capping inversions limiting the development of the mixing layer, vertical transport of pollutants along the valley slopes, and the ozone-polluted residual layer aloft (entrained into the mixing layer during the next day) were the most interesting phenomena explored by that study. Advections from the Po Valley with thermally-driven flows were hypothesised to be the main factor contributing to the high ozone concentrations found in the elevated layers. Although this result was supported by measurements of carbon monoxide, ambient particulate matter (PM) and relative humidity, the short duration of the campaign could not allow to exclude other effects. More recently, Diémoz et al. (2014a) analysed a one-year-long time series of columnar aerosol optical properties measured by a sun/sky photometer in the same area and found that the heaviest burden of particles did not come from ~~urban settlements within the valley~~the largest urban settlement in the Aosta Valley, but rather from outside the ~~valley, namely~~ region, namely from the Po basin.

~~Overall, this work attempts~~ The present research exploits a multi-technique approach, combining a large set of measurements with modelling tools, in order to answer the following scientific questions still lacking a comprehensive understanding:

1. What is the origin of the aerosol layers detected in the northwestern Alps?
2. What conditions are favourable to the aerosol flow into the valley?
3. How do the advected aerosol layers evolve in both altitude and time?
4. What is the impact of the transported aerosol on PM surface concentrations and chemical composition?
5. Are the current chemical transport models able to reproduce and explain the observations at the ground and along the vertical profile?

Though referred to the location object of the study, these questions are of more general interest, as several regions of the world are characterized by basin valleys surrounded by mountains. Hence, the role of pollution advections, their vertical behaviour and the final impact at ground-level is a matter of global interest (De Wekker et al., 2018; Lehner and Rotach, 2018; Serafin et al., 2018).

The paper is organised as follows: the investigated area is presented in Sect. 2, while Sect. 3 describes both the experimental (3.1) and the modelling (3.2) approach used. Results (Sect. 4) are presented by addressing specific case studies to exemplify the advection of polluted, aerosol-rich air masses and comparing them to the simulations. Conclusions are drawn in Sect. 5.

2 Investigated area and experimental sites

This study is mainly focussed on the Aosta Valley, the smallest Italian administrative region (130000 inhabitants, Fig. 2). It is about 80 km by 40 km wide, and is located in the northwestern side of the Alps, not far from the two major urban settlements and industrial areas of the Po Valley, i.e. Turin (80 km) and Milan (150 km). The region is characterised by a complex topography, typical of the Alpine valleys. Its surface elevation varies from 300 to 4800 m a.s.l. (average altitude > 2000 m a.s.l.), with several tributary valleys starting from the main valley. The latter connects Mt. Blanc (at the border with France, Fig. 2b) to the Piedmont region through a 90 km-long directrix, approximately divisible into three segments with NW-SE, W-E and NW-SE directions. This main valley is narrower at both ends (with minimum width of few hundreds meters) and widens in correspondence of the Aosta city, the largest urban settlement of the region (about 35000 inhabitants). The complex topography triggers several meteorological phenomena typical of mountain valleys, such as wind channelling along the main valley, thermally-driven winds from the plain to the mountains (and vice versa), rain-shadow (foehn) winds and temperature inversions. The latter are very frequent during wintertime, occurring about 50% of the time (Vuillermoz et al., 2013). Not surprisingly, these dynamics strongly affect the dispersion of pollutants and the air quality in the lowest atmospheric layers.

Data from several measuring sites in the Aosta Valley are used in this work (Fig. 2b). Most of the instruments employed (Sect. 3.1) are operated at the two observatories run by the regional Environment Protection Agency (ARPA) in Aosta: Aosta–Saint Christophe, and Aosta–Downtown. The Aosta–Saint Christophe station (WIGOS ID 0-380-5-1, 45.7°N, 7.4°E, 560 m

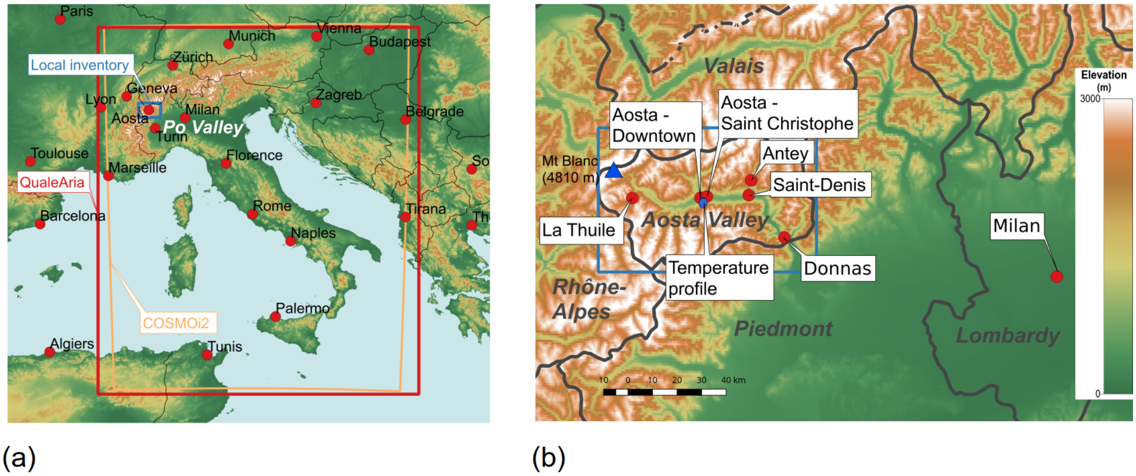

Figure 2. (a) Elevation map of Italy, showing the position of the investigated Alpine region and the geographical domains of: 1) the Numerical Weather Prediction model (COSMO-I2, orange box), 2) the national emission inventory (QualeAria, red box) and 3) the local inventory of the Aosta Valley (blue box). (b) Zoom over the Aosta Valley and northwestern Italy, with location of the measurement stations. The blue box corresponds to the geographic domain of the local inventory as in panel (a). The elevation (colour) scale is common to both figures.

a.s.l.) is located in a large floor with a wide field of view, at the bottom of the main valley, about 2.5 km east of Aosta–Downtown. The site is in a semi-rural context, partially influenced by vehicular traffic and anthropogenic activities from the city, such as domestic heating and industry. The experimental setup at this site includes an Automated LiDAR-Ceilometer (ALC) for the operational monitoring of the aerosol profile (Dionisi et al., 2018), a POM-02 sun photometer for the retrieval of column aerosol properties and water vapour (Diémoz et al., 2014a; Campanelli et al., 2018), and a Fidas 200s Optical Particle Counter for the surface aerosol size distribution, in addition to instruments measuring solar radiation and trace gases (Diémoz et al., 2011, 2014b; Siani et al., 2013, 2018; Federico et al., 2017). Aosta–Downtown (580 m a.s.l.) is a urban background site. This station is equipped with samplers for continuous monitoring of atmospheric pollution, mainly coming from car traffic, domestic heating and a steel mill located south of the city. To provide an idea of the aerosol load in Aosta–Downtown, the annual averages of $\mathrm{PM_{10}}$ and $\mathrm{PM_{2.5}}$ concentrations calculated for the last three years of measurements (2015–2017) range between 18–21 $\mu\mathrm{g\,m^{-3}}$ and 11–12 $\mu\mathrm{g\,m^{-3}}$, respectively. Despite these low average concentrations, daily $\mathrm{PM_{10}}$ exceedance episodes with maxima up to about 100 $\mu\mathrm{g\,m^{-3}}$ can be observed, their occurrence strongly depending on the encountered meteorological conditions (5 exceedance episodes in 2016, 13 in 2015 and 17 in 2017). Thus, there is the need to unravel their behaviour and the role played by regional transport from most polluted areas. Additional measurements used here were performed at the more elevated sites of La Thuile (1640 m a.s.l.), Saint-Denis (840 m a.s.l.) and Antey (1040 m a.s.l.), and at Donnas, a low-altitude site (316 m a.s.l., Fig. 2b) close to the border with the Piedmont region, at the entrance of the Aosta Valley. La Thuile is a remote mountain site in a tributary valley hosting a meteorological and air quality station managed by ARPA. Similarly, a weather station is operated in the village of Saint-Denis by the regional meteorological bureau. Antey is a further small village in a tributary valley where an ARPA mobile laboratory was temporary operated. Finally, the Donnas station is located in a rural area, only partially influenced by traffic and agricultural local activities, such as burning of agricultural residuals. However, due to its proximity to the Po basin, it is expected to be heavily influenced by pollution from the plain.

As the vertical dimension is important in this investigation, we also used measurements from an ALC operating in Milan (Fig. 2), this being representative of the contrasting conditions within the Po Valley. The system is located on the U9-building (45.5 °N, 9.2 °E, 132 m a.s.l.) of the University of Milano-Bicocca, in an urban background area northeast of the city centre. A full description of the site and measurements is reported in Ferrero et al. (2018).

3 Methods

3.1 Measurements

The experimental setup used in this work includes vertically-resolved measurements from ALCs (Sect. 3.1.1), vertically-integrated (columnar) aerosol measurements from both ground (Sect. 3.1.2) and space (Sect. 3.1.3), and in situ measurements of aerosol concentration and composition (Sects. 3.1.4–3.1.5), complemented by ancillary gas-phase pollutants and meteorological measurements (Sect. 3.1.6). Table 1 summarises the instruments used throughout this study in their respective measuring stations.

3.1.1 Automated LiDAR Ceilometers

Vertical profiles of air constituents are particularly useful in identifying transport of pollutants of non-local origin. However, the profiling capability of the Italian regional Environment Protection Agencies is still scarce. Over the Po basin, continuous monitoring of the atmospheric composition along the vertical profile is lacking and information at different altitudes is mostly available for short periods and during specific, dedicated field campaigns (e.g., Barnaba et al., 2007; Osborne et al., 2007; Raut and Chazette, 2009; Barnaba et al., 2010; Ferrero et al., 2014; Curci et al., 2015; Rosati et al., 2016; Bucci et al., 2018).

Light detection and ranging (LiDAR) instruments permit to resolve the vertical distribution of particles. The recent technological and data-processing advances (Wiegner and Geiß, 2012), and commercialisation, of simple LiDAR systems with operational capabilities allow to use this kind of system in monitoring (24/7) mode and in wide networks. In the present study, we employ two commercially-available ALCs (CHM15k-Nimbus, manufactured by Lufft GmbH, and formely by Jenoptik ESW), which have been operating since 2015 at the Aosta–Saint Christophe observatory and in Milan. Both ALCs are part of the Italian Alice-net (http://www.alice-net.eu/) and the European E-PROFILE (https://ceilometer.e-profile.eu/profileview) networks. They allow for continuous vertical profiling of the radiation emitted by a single-wavelength (1064 nm) pulsed laser (Nd:YAG; 6.5–7 kHz; 8 $\mu\mathrm{J\,pulse^{-1}}$) and backscattered by the atmosphere. At the operating wavelength, the backscatter is mainly dominated by aerosols and clouds in the atmosphere, whereas interference by water vapour has been estimated to be negligible (Wiegner and Gasteiger, 2015). The systems enable a typical temporal resolution of 15 s (integration time) and a vertical resolution of 15 m, up to 15 km above the ground. Main limitations of the instruments are: 1) need for corrections in

Table 1. Observation sites, measurements and instruments employed in this study.

Station	Elevation (m a.s.l.)	Measurement	Instrument	Data availability
Aosta–Saint Christophe (ARPA observatory)	560	Vertical profile of attenuated backscatter and derived products	CHM15k-Nimbus ceilometer	2015–now
		Aerosol columnar properties	POM-02 sun/sky radiometer	2012–now[a]
		Surface particle size distribution	Fidas 200s optical particle counter	2016–now
Aosta–Saint Christophe (weather station)	545	Standard meteorological parameters	Siap and Micros	1974–now
Aosta–Downtown	580	PM_{10} hourly concentration	TEOM 1400a	1997–now
		PM_{10} and $PM_{2.5}$ daily concentrations	Opsis SM200	2011–now
		Water-soluble anion/cation analyses on PM_{10} samples	Dionex Ion Chromatography System	2017–now
		EC/OC analyses on PM_{10} samples	Sunset thermo-optical analyser	2017–now[b]
		NO and NO2	Horiba APNA-370	1995–now
		Standard meteorological parameters	Vaisala WA15	1995–now
South mountain slope	550–1200	Temperature and RH profile	HOBO H8 Pro (10 thermometers)	2006–now
La Thuile	1640	PM_{10} hourly concentration	TEOM 1400a	2015–now
		NO and NO2	Teledyne API200E	1997–now
Saint-Denis	840	Standard meteorological parameters	Siap and Micros	2002–now
Antey	1040	PM_{10} daily concentration	Opsis SM200	2017
Donnas	316	PM_{10} daily concentration	Opsis SM200	2010–now
		NO and NO2	Teledyne API200E	1995–now
		Standard meteorological parameters	Micros	1994–now
Milan	132	Vertical profile of attenuated backscatter and derived products	CHM15k-Nimbus ceilometer	2015–now
		Standard meteorological parameters	Vaisala WXT5	2012–now

[a] Underwent major maintenance in the second half of 2016 and January 2017.

[b] Available 4 days every 10.

the lowermost levels, and 2) blind view above thick clouds. 1) In the lowermost levels, the field of view ($0.45\ \mathrm{mrad}$) of the receiver is only partially overlapped to the laser beam (90% overlap is achieved at about $700\ \mathrm{m}$), therefore, an overlapping-correction function is needed to correct the signal. This was provided by the manufacturer. 2) Thick clouds cause saturation in the detector signal (an avalanche photodiode operated in photocounting mode), followed by complete signal extinction. Thus, the attenuated backscatter above the cloud ceiling is not considered (nor plotted) in this study. The ALC firmwares used so far (versions 0.730–0.743 for Aosta–Saint Christophe and 0.730 for Milan) provide the background-, overlap- and range-corrected attenuated backscatter (RCS) in terms of instrumental raw counts, i.e.

$$\mathrm{RCS}(z,t) = \frac{(P(z,t) - B(t))\, z^2}{O(z)} \tag{1}$$

where $P(z,t)$ is the signal intensity (raw counts) backscattered from a specific distance (z) and measured at ground, $B(t)$ the time-varying background baseline and $O(z)$ the overlap function. To express the backscatter coefficient in SI units and make the results comparable with other similar instruments, a calibration factor (C_L) must be assessed, so that

$$\frac{\mathrm{RCS}(z,t)}{C_L} = \beta_{att}(z,t) = \beta_T(z,t)\, \mathrm{e}^{-2\int_{z_{min}}^{z} \alpha_T(z',t)\mathrm{d}z'} \tag{2}$$

where β_{att} is the attenuated backscatter coefficient, β_T is the total (particles and molecules) backscatter coefficient and α_T is the total extinction coefficient. C_L is determined during clear-sky time windows of at least 3 hours at night, i.e. when the background radiation is low, by the method (Rayleigh technique) described hereafter. First, the backscatter and extinction profiles are calculated by the Klett-Fernald backward algorithm (Fernald, 1984; Klett, 1985), then C_L is determined by inverting Eq. 2. Once a series of calibration factors has been estimated, the total (α_T, β_T) and particle (α_p, β_p) extinction and backscatter coefficients are computed for all times and sky conditions using a forward Klett method as described by Wiegner and Geiß (2012).

Usually, the above-mentioned solving techniques are based on an *a-priori* or independent estimate of the lidar ratio (LR, i.e. the ratio α_p/β_p) as a further constraint. In our case, LR is not fixed a-priori, but rather obtained using specific functional relationships linking α_p to β_p. Dionisi et al. (2018) demonstrated that this approach, previously proposed and tested on the signal inversion of research-type elastic LiDARs (e.g., Barnaba and Gobbi, 2001, 2004), provides better retrievals of α_p and β_p also from ALCs than using an a-priori, fixed LR. More specifically, an iterative data inversion scheme is adopted: at the first iteration, LR is set to an initial value of $38\ \mathrm{sr}$ (average value from the functional relationships) and a first retrieval of the backscatter coefficient β_p is calculated; starting from the second iteration, the calculated backscatter coefficient and the functional relationships are used to determine an altitude-dependent lidar ratio. The loop continues until convergence of the column-integrated backscatter is reached. The good agreement between the ALC-derived and the sun photometer-measured aerosol optical depth (AOD, i.e. the integral over altitude of the ~~the~~ extinction coefficient) is employed as a validation of the quality of the inversion results (Sects. 4.1.4 and 4.3.5) using these functional relationships, at least in daytime conditions (see also Dionisi et al. (2018) and ~~Fig. S2d, Sect. S4, and Fig. S8e, Sect. S6,~~ Figs. S2d and S9e in the Supplementary material).

For ease of comparison with pristine (aerosol-free) conditions, and with most LiDAR-based studies, ALCs measurements are provided in this study in terms of scattering ratio (SR, e.g. Zuev et al., 2017), i.e.

$$\mathrm{SR} = \frac{\beta_T}{\beta_m} = \frac{\beta_p + \beta_m}{\beta_m} \tag{3}$$

~~Example of particle backscatter profile, in terms of scattering ratio (SR), from the ALC in a typical advection day (25 May 2017, cf. Fig. 12). Areas above the detected cloud ceiling, where the backscatter from the ALC is not reliable, are plotted in white. Noisy measurements (e.g. interference by solar radiation in the middle of the day) are filtered on the basis of a spatial and temporal variability criterion (the standard deviation for each bin not exceeding 20% of the mean value). The Aosta–Saint Christophe ALC is located at an altitude of 560 m a.s.l.~~

where β_m is the molecular backscatter coefficient. In case of pure molecular scattering (no aerosol in the atmosphere), $\mathrm{SR} = 1$, while SR increases with increasing aerosol load. Finally, the high-resolution data from the ALC are downscaled to 75 m averages over the vertical and 5 min averages over time to increase the signal-to-noise ratio. ~~An~~ A first example of the output from the Aosta–Saint Christophe ALC, in terms of scattering ratio, ~~is depicted~~ can be found in Fig. ~~??. The~~ 3a. This image refers to a typical ~~advection day (25 May 2017~~sequence of days (August 2015), characterised by a ~~relatively clean atmosphere during the morning and a sudden~~ recurrent increase of the particle backscatter during the afternoon, up to an altitude of more than ~~2000~~ 2000–3000 m a.s.l. (the altitude of the surface being 560 m a.s.l in Aosta–Saint Christophe). As we will demonstrate here, this afternoon increase is due to the coupled effect of transport of polluted air masses from the Po basin and aerosol hygroscopic growth (see Sect. 4). Several analogous episodes were recorded in the ALC record since its installation in Aosta–Saint Christophe. The observation of this recurrent phenomenon was, in fact, the driving motivation for the present research.

In the study, we also convert the ALC-derived backscatter into aerosol volume following Dionisi et al. (2018), thus allowing a direct comparison to more standard air quality metrics (e.g. PM_{10}, this is done using a particle density ρ =1.3 $\mathrm{g\,cm^{-3}}$ independently estimated for the present study by an optical particle counter co-located with the ALC). The expected uncertainties in the retrieval of the aerosol backscatter and extinction coefficients, and of the aerosol volume range between 30 and 40% (Dionisi et al., 2018).

3.1.2 Sun photometer

A POM-02 sun/sky radiometer operates at the Aosta–Saint Christophe observatory since 2012. The radiometer is part of the European ESR-SKYNET network (http://www.euroskyrad.net/). The irradiances collected by the POM-02 at 11 wavelengths (315–2200 nm) are inverted to retrieve the aerosol optical properties using both the direct-sun (SUNRAD.pack algorithm to provide the AOD every 1 min, Estellés et al. (2012)) and the almucantar geometries (SKYRAD.pack software version 4.2 to retrieve a complete set of optical and microphysical columnar properties every 10 min, Nakajima et al. (1996)). The instrument is calibrated in-situ with the improved Langley technique, described by Campanelli et al. (2007) in more detail, and was successfully compared to other reference instruments during a recent international campaign (Kazadzis et al., 2018). The AOD (τ) from the POM-02 is interpolated to the ALC wavelength (1064 nm) using the Ångström (1929) relationship, i.e.

$$\tau = b\lambda^{-a} \tag{4}$$

where λ is the wavelength expressed in $\mathrm{\mu m}$ and a and b are the Ångström parameters from the regression. Finally, the Cloud Screening of Sky Radiometer data (CSSR) algorithm by Khatri and Takamura (2009), making use of the short-wave irradiance measurements by a co-located pyranometer, is applied to the POM-02 series to minimise the residual interference by clouds and to ensure the maximum measurement quality.

3.1.3 Space-based observations from MODIS

In this study, we also used satellite data to explore if and how the "local" phenomenon observed in Aosta is detectable over a regional scale. To this purpose, we used AOD data from the Moderate Resolution Imaging Spectroradiometer (MODIS) instrument. The MODIS instrument flies onboard the two NASA platforms Terra and Aqua, following a sun synchronous orbit with overpass time between 10.00 and 13.00, and 13.00 and 16.00 (local time), respectively. Since the MODIS instrument planning phase, specific retrievals have been set up to provide the AOD over ocean and land globally on a daily base at 10 km resolution (Kaufman and Tanré, 1998). Constant improvements to the AOD inversion algorithms currently allow to provide a 3 km-resolved standard AOD product (Remer et al., 2013). While such spatial resolutions have been extensively exploited for many regional-scale, aerosol-related studies, these are yet not sufficient for applications requiring more spatial detail, as in space-based evaluations of air quality within urban areas (e.g., Chudnovsky et al., 2014; Della Ceca et al., 2018) or in conditions of high AOD spatial variability as over mountain regions (e.g., Emili et al., 2011). For our purpose, we therefore used high-resolution (1 km) AOD data obtained inverting MODIS data with the recently developed algorithm MAIAC (Multi-Angle Implementation of Atmospheric Correction). Full details of this algorithm are thoroughly described in Lyapustin et al. (2011, 2012).

3.1.4 Optical Particle Counter

A Fidas®200s (Pletscher et al., 2016) optical particle counter operates at the ARPA observatory in Aosta–Saint Christophe. The spectrometer is based on the analysis of scattered light at 90° originating from a polychromatic light source (LED). These conditions ensure an accurate calibration curve without ambiguities within the Mie range and allow to retrieve high-resolution spectra (size measurements between 0.18 and 18 $\mathrm{\mu m}$, 32 channels/decade). Due to the peculiar T-aperture optics of the spectrometer and the simultaneous measurement of signal duration, border zone errors are eliminated. Once the particle size distribution is measured, the instrument algorithm is able to derive the mass concentration for several cutoff diameters (including $\mathrm{PM_{10}}$, i.e. ambient particulate with a diameter of 10 $\mathrm{\mu m}$ or less). Though not a direct mass measurement, the PM concentration derived by the instrument obtained the certificate of equivalence to the gravimetric method by TÜV Rheinland Energy GmbH on the basis of a laboratory and a field test. Moreover, to prevent any site-specific bias, an additional $\mathrm{PM_{10}}$

comparison with the gravimetric technique was organised at Aosta–Saint Christophe and provided satisfactory results (29 days; slope 1.08 ± 0.04; intercept $-3.8 \pm 1.4\ \mu g\,m^{-3}$; $R^2 = 0.96$).

3.1.5 PM concentration and composition

Daily averages of PM concentration are recorded by four Opsis SM200 Particulate Monitor instruments, two in Aosta–Downtown (PM_{10} and $PM_{2.5}$ inlets, with sampling fluxes of 1 $m^3\,h^{-1}$ and 2.3 $m^3\,h^{-1}$, respectively), one installed inside a mobile laboratory, which was parked in Antey (PM_{10}, 1 $m^3\,h^{-1}$), and one in Donnas (PM_{10}, 1 $m^3\,h^{-1}$). Moreover, two Tapered Element Oscillating Microbalance (TEOM) 1400a monitors (Patashnick and Rupprecht, 1991) are used for continuous measurements of PM_{10} hourly concentrations at the stations of Aosta–Downtown and La Thuile. These instruments are not compensated for mass loss of semi-volatile compounds (Green et al., 2009) ~~, therefore they~~ and could be insensitive to specific compounds, such as ammonium nitrate (e.g., Charron et al., 2004), which leads to underestimations, especially in the cold season, compared to the SM200. Conversely, overestimations by the TEOM compared to daily averages from the SM200 reference instrument are found in summer and are not fully understood at present. Therefore, TEOM monitors are only employed here for qualitative estimates of short-term variations of the aerosol burden ~~and could be insensitive to specific compounds, such as ammonium nitrate (e.g., Charron et al., 2004)~~while daily-averaged concentrations will be only taken from the SM200 instruments.

Sampling in Aosta–Downtown is complemented with chemical speciation analyses. We employed a Dionex Ion Chromatography System (AQUION/ICS-1000 modules) for water-soluble anion/cation chemical analyses on daily PM_{10} samples collected on PTFE-coated glass fiber filters by the Opsis SM200. The experimental setup is based on the CEN/TR 16269:2011 guideline and enables the determination of mass concentrations of the following water-soluble ionic compounds: Cl^-, NO_3^-, SO_4^{2-}, Na^+, NH_4^+, K^+, Mg^{2+}, Ca^{2+}. Samples collected on quartz fibre filters by a co-located Micro-PNS automatic low-volume sampling system (10 μm cutoff diameter, 2.3 $m^3\,h^{-1}$) are analysed alternatively for elemental/organic carbon (EC/OC, 4/10 days) and for metals (6/10 days, not used in the present study, but discussed by Diémoz et al. (2019)). The carbonaceous aerosol mass is determined with a Sunset Laboratory Inc. instrument (Birch and Cary, 1996) on portions of 1 cm^2 punches using a thermal-optical transmission (TOT) method with transmission correction for the split point and following the EUSAAR-2 protocol (Cavalli et al., 2010), according to the EN 16909:2017.

3.1.6 Gas-phase pollutants and meteorological ancillary data

Standard gas-phase pollutants subject to European regulations are routinely monitored at Aosta–Downtown, La Thuile and Donnas in the frame of the activities of the air quality network. Meteorological parameters, such as temperature, pressure, relative humidity (RH) and surface wind velocity are collected at the stations of Aosta–Saint Christophe~~and~~, Saint-Denis and Donnas. Moreover, 10 temperature and relative humidity sensors (Hobo H8 Pro) are installed along the north-facing mountain slope south of Aosta, at elevations ranging from 550 to 1200 m a.s.l. This set of measurements, representing a vertical profile of surface ~~temperatures, provides~~ temperature and RH, gives useful information about the thermal inversions in the main valley.

For example, pseudo-equivalent potential temperatures (e.g., Freney et al., 2011) at different altitudes can be easily calculated from this dataset, thus providing a rough indication of the vertical extent of the mixed layer (Sect. 4.2.2).

3.2 Models

Models are used to interpret and complement the observations. A numerical weather prediction model (COSMO, Consortium for Small-scale Modeling, www.cosmo-model.org, Sect. 3.2.1) is employed to drive a chemical transport model (FARM, Flexible Air quality Regional Model, Sect. 3.2.2) and a lagrangian model (LAGRANTO) to retrieve the trajectories of air masses arriving at the experimental site (Sect. 3.2.3).

3.2.1 Numerical Weather Prediction model

COSMO is a non-hydrostatic, fully compressible atmospheric prediction model working on the meso-β and meso-γ scales. A detailed description of the model can be found elsewhere (e.g., Baldauf et al. (2011)). The COSMO data are operationally disseminated by the meteorological operative centre – air force meteorological service (COMET) in two different configurations: a lower-resolution (7 km horizontal grid and 45 levels vertical grid, 72 hours integration) version (COSMO-ME), covering ~~the~~ central and southern Europe, and a nudged, higher-resolution (2.8 km, 65 vertical levels, ~~4~~ 2 runs/day), called COSMO-I2 (or COSMO-IT), covering Italy (Fig. 2). Owing to the complex topography of the Aosta Valley and the consequent need to resolve the atmospheric circulation at very small spatial scales, the COSMO-I2 variant is employed in this work.

As an example of the good agreement between COSMO and surface measurements, the average daily cycle of the wind speed and direction from both data sources is exhibited in Fig. S1 ~~, Sect. S1~~ in the Supplement. The figure clearly shows the regular development of the plain-mountain winds in the afternoon. The influence of the east-west directrix of the main valley along which the wind is channelled is well represented in both measurements and simulations.

3.2.2 Chemical Transport model

FARM (v4.7, Gariazzo et al., 2007; Silibello et al., 2008; Cesaroni et al., 2013; Calori et al., 2014) is a three-dimensional Eulerian model for simulating the transport, chemical conversion and deposition of atmospheric pollutants. The FARM source code has been inherited from the Sulfur Transport and dEposition Model (STEM), extensively tested and used since the eighties.

FARM can be easily interfaced to most available diagnostic or prognostic NWP models. A turbulence and deposition preprocessor (SURFace-atmosphere interface PROcessor, SURFPRO) computes the 3-D fields of turbulence scaling parameters, eddy diffusivities and deposition velocities for each species based on an input gridded land-use field and the results of the NWP model (Sokhi et al., 2003). Pollutants emission from both area and point sources can be simulated by FARM including plume rise calculations. Transformation of chemical species by gas-phase chemistry (more than 200 reactions using the SAPRC-99 chemical scheme as in Carter (2000)), dry removal of pollutants depending on local meteorology and land-use, and wet removal are considered. The AERO3_NEW module, coupled with the gas-phase chemical model and treating primary and secondary particle dynamics and their interactions with gas-phase species, is implemented for the calculation of the aerosol concentration fields, thus accounting for nucleation, condensational growth and coagulation (Binkowski, 1999). The aerosol size distribution is parametrised using three modes simulated independently: the Aitken mode (D < 0.1 μm), the accumulation mode (0.1 μm $<$ D $<$ 2.5 μm) and the coarse mode (D $>$ 2.5 μm). $PM_{2.5}$ is defined as the sum of Aitken and accumulation modes, while PM_{10} is given by the sum of the three modes. Chemical speciation is performed in the pre-processing phase by the emission manager (EMMA) based on the profiles from the US EPA model SPECIATE (v3.2, 2002; cf. https://www.epa.gov/air-emissions-modeling/speciate-version-45-through-40 for more recent versions). To simulate hygroscopic growth by aerosols in high relative humidity conditions, water uptake by aerosol particles is taken into account based on the ISORROPIA model (Nenes et al., 1998) and added to the PM_{10} dry mass concentration from FARM. The resulting output species is called PM_{10w} in FARM version 4.7.

The FARM output concentrations are 4-D fields at 1 km spatial resolution along the horizontal dimensions, 16 different vertical levels (from the surface to 9290 m, corresponding to equispaced pressure levels) and 1-hour temporal resolution. The PM_{10w} concentration profiles from FARM are extracted at the grid cell corresponding to Aosta–Saint Christophe for comparison with the profiles measured by the ALC. Indeed, since FARM is not able to calculate the aerosol optical properties needed to simulate the backscatter coefficient measured by the ALC, the comparison between the profiles measured by the ALC and estimated by the CTM is here performed in terms of mass concentration (by converting the ALC data into PM_{10}, see Sect. 3.1.1).

Supplying a detailed and precise emission inventory to the CTM is crucial to accurately assess the magnitude of the pollutants loads and their variability in both time and space. Additional information regarding the regional emission inventory and the boundary conditions is provided in the Supplement (~~Sect. S2 and S3~~Sects. S2–S3). The geographic coverage of the regional and the national emission inventories is shown in Fig. 2. Local sources and boundary conditions can be switched on/off for sensitivity analyses.

3.2.3 Back-trajectories

The publicly-available LAGRANTO Lagrangian analysis tool, version 2.0 (Sprenger and Wernli, 2015), is used to numerically integrate the high-resolution 3-D wind fields from COSMO and to determine the origin of the air masses sampled by the ALC over Aosta–Saint Christophe. The software also enables to trace 3-D and 2-D meteorological fields along each trajectory. In particular, the algorithm was set up to start 8 trajectories in a circle of 1 km around the observing site and at 7 different altitudes from the ground to 4000 m a.s.l., for a total of 56 trajectories for every run. From a one-year (2016) analysis of the trajectories arriving to the Aosta Valley, it is found that a backward run time of 48 hours is sufficient, on average, to cover most of the domain of the meteorological model. Therefore, ~~to reduce errors in trajectories with increasing running time,~~ we limit the computation to this duration.

4 Results

The observed ~~phenomena are~~ phenomenon is presented through three case studies (~~26–31 August ,~~ August 2015~~; 26–29 January,~~ , January 2017~~;~~ , 25–30 May ~~,~~ 2017), chosen for their relevance and clarity. The episodes are also representative of three different atmospheric conditions (seasons) and were observed with slightly different sets of operating instruments (Table 1). The case studies were also selected among those showing long sequences of days characterised by the recurrent appearance of a thick aerosol layer from the ALC, to emphasise the periodicity of the phenomenon. Indeed, as explained in more detail by Diémoz et al. (2019), the elevated aerosol layer can be observed very frequently, i.e. ~~at least 40–50~~ about 50% of the days, depending on the season.

4.1 Case study 1: Summer (~~26–31~~ August 2015)

One of the longest and most notable episodes of unexpected high aerosol loads in the northwestern Alps was registered from 26 August to 3 September 2015~~(here we present the period 26–31 August)~~, few months after the ALC installation in Aosta–Saint Christophe (here we focus on the period 25–31 August, this allowing to show the typical clear conditions before the arrival of the polluted air mass). In those days, a wide anticyclonic area extended from northern Africa to central and eastern Europe. The period is thus representative of fair weather conditions, with only few cirrus clouds on days 27 and 28, and absence of strong synoptic flows at ground, which favoured the regular development of thermally-driven winds from the plain to the mountains triggered by temperature and pressure gradients between the valley and the foreground.

4.1.1 ALC observations

A thick aerosol layer is detected by the ALC over the Aosta–Saint Christophe observatory from the afternoon of 26 August (Fig. 3a). Very clear conditions are visible in the low troposhere on 25 August, while the high-altitude layer in the morning of the same day, which is not considered here, is due to smoke transport from North America). The appearance of the PBL layer is clearly noticeable on ~~this day~~ 26 August as an increase in the backscatter coefficient up to an altitude of 3 km a.s.l., with scattering ratios ~~,~~ $\mathrm{SR} \simeq 4$ at midday (light-blue area in the figure) almost doubling ($\mathrm{SR} > 8$, ~~red) in~~ orange-yellow) in a few hours. This layer persists during the night, when SR reaches values above 30. ~~The day after, when convection starts in the valley after sunrise, the aerosol-rich layer is observed to entrain into the developing mixing layer, thus impacting the lower levels, with potential consequences on the surface air quality, as previously observed in other areas (e.g., Bader and Whiteman, 1989; Curci et al., 2015).~~ On 27 August, the ALC backscatter is then observed to decrease in the central part of the day and to increase again in the afternoon. This behaviour keeps very regular for almost a week, with the ~~afternoon~~ aerosol-rich layer extending from ground up to 3–3.5 km. ~~At night-time, some low clouds form~~ As further discussed in the next paragraphs, we anticipate here that the main factor driving this cycle is likely an enhanced hygroscopic growth of aerosol advected from the Po Valley from the afternoon to the early morning, this effect also leading to formation of low clouds within the aerosol layer ~~and are screened out~~ at night (screened out as white areas in the figure~~(white areas). The~~). In fact, the

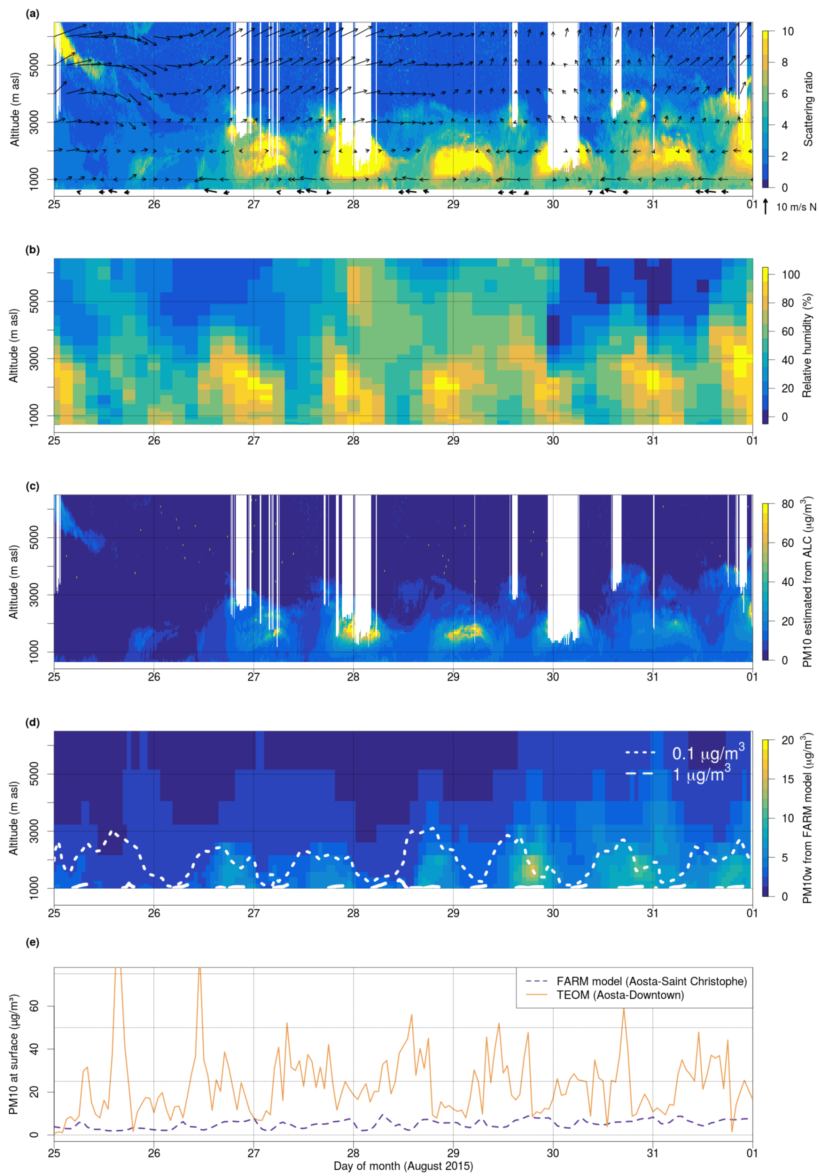

Figure 3. Case study of ~~26–31~~ 25–31 August 2015. (a) Coloured background: vertical profile of scattering ratio from ALC in Aosta–Saint Christophe. The signal above the clouds is plotted as white areas. Arrows: horizontal velocity of the wind measured at the surface (bold, lower arrows) and simulated by COSMO at several elevations (thin arrows). Calm wind (speed $< 1\ \mathrm{m\,s^{-1}}$) is not plotted. A reference arrow for a $10\ \mathrm{m\,s^{-1}}$ wind blowing from the south to the north is drawn at the bottom right corner; (b) Vertical profile of relative humidity forecasted by COSMO; (c) Vertical profile of PM_{10} mass concentration derived from ALC; (d) Mass concentration (PM_{10w}) from FARM. PM concentration from non-local sources is represented by the coloured background (the colour scale is chosen to better show the daily pattern simulated by the model) and the effect of local sources by the contour line, at logarithmic steps (dotted: 0.1 $\mathrm{\mu g\,m^{-3}}$; dashed, near the surface: 1 $\mathrm{\mu g\,m^{-3}}$); (e) Hourly PM_{10} (dry) surface concentration from FARM simulations in Aosta–Saint Christophe and observations in Aosta–Downtown, for the purpose of checking if any sudden variation in surface air quality data is noticeable.

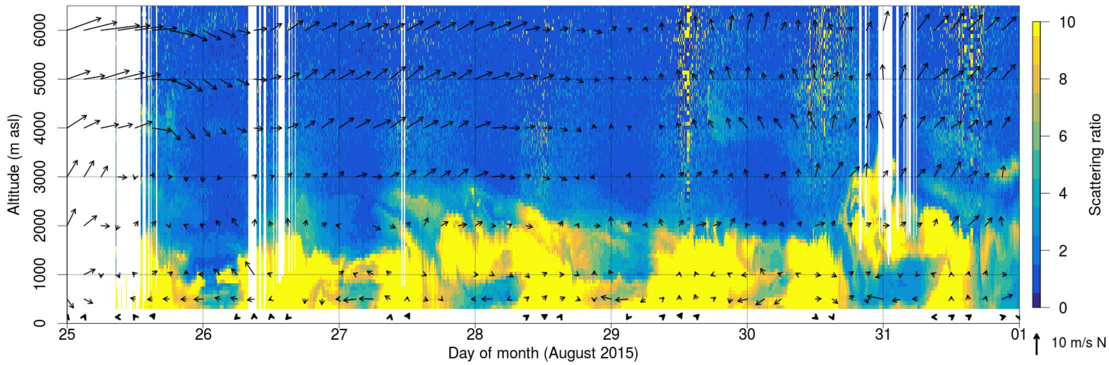

Figure 4. Vertical profile of scattering ratio from the ALC in Milan. Arrows: horizontal velocity of the wind measured at the surface (bold, lower arrows) and simulated by COSMO at several elevations (thin arrows).

transition from aerosol to the cloud phase is very sharp, as also noticeable from the sudden increase of more than 40 $\mathrm{W\,m^{-2}}$ of the downward infrared irradiance monitored at the same site (Fig. S2c).

Simultaneous ALC measurements in the city of Milan (see relative position in Fig. 2), which can be considered representative of the overall dynamics occurring ~~in~~ within the Po basin, are shown in Fig. 4. Interesting feature here is that the modulation of the scattering ratio looks almost reversed compared to the Aosta–Saint Christophe site, with maximum SR at the surface at midday and minimum values during the night and the morning. While in the uppermost levels (>3000 m a.s.l.) the synoptic circulation is blowing undisturbed from the west, the wind velocity at 500 m a.s.l. keeps alternating, likely driven by the breeze regime (the surface wind is affected by urban effects and does not show appreciable variations).

4.1.2 Meteorological variables and back-trajectories

The observed reversal behaviour in Milan and Aosta already suggests that air masses movements are driving the clean-up of the lowermost levels in the Po plain and ~~transporting~~ the transport of the aerosol plumes elsewhere. To substantiate this hypothesis, a careful analysis of the meteorological fields (observed and modelled) was performed. In particular, we verified that this selected sequence of days presents a typical pattern of plain-to-mountain wind systems during the afternoon of each day in Aosta–Saint Christophe. Surface-level eastern winds speed as high as 8 $\mathrm{m\,s^{-1}}$ is measured daily in the afternoon till sunset and is shown as bold arrows in the lowermost levels of Fig. 3a. Conversely, calm wind is detected during the night, i.e. when the aerosol layer thickens. Since no instrument is available at the measuring site to determine the vertical profile of the wind velocity, the simulations from the COSMO model are used to assess the wind field at several altitudes (thin arrows in Fig. 3a). It reproduces well the thermal wind circulation in the lowest atmospheric layers during the afternoon and slightly overestimates the mountain-to-plain drainage winds at night and early morning (this issue is discussed in Sect. 4.4). The thermally-driven wind pattern forecasted by COSMO extends up to an altitude of 3000 m, i.e. approximately the maximum height of the aerosol layer observed by the ALC (reasons for possible discrepancies of this simulated and measured altitude

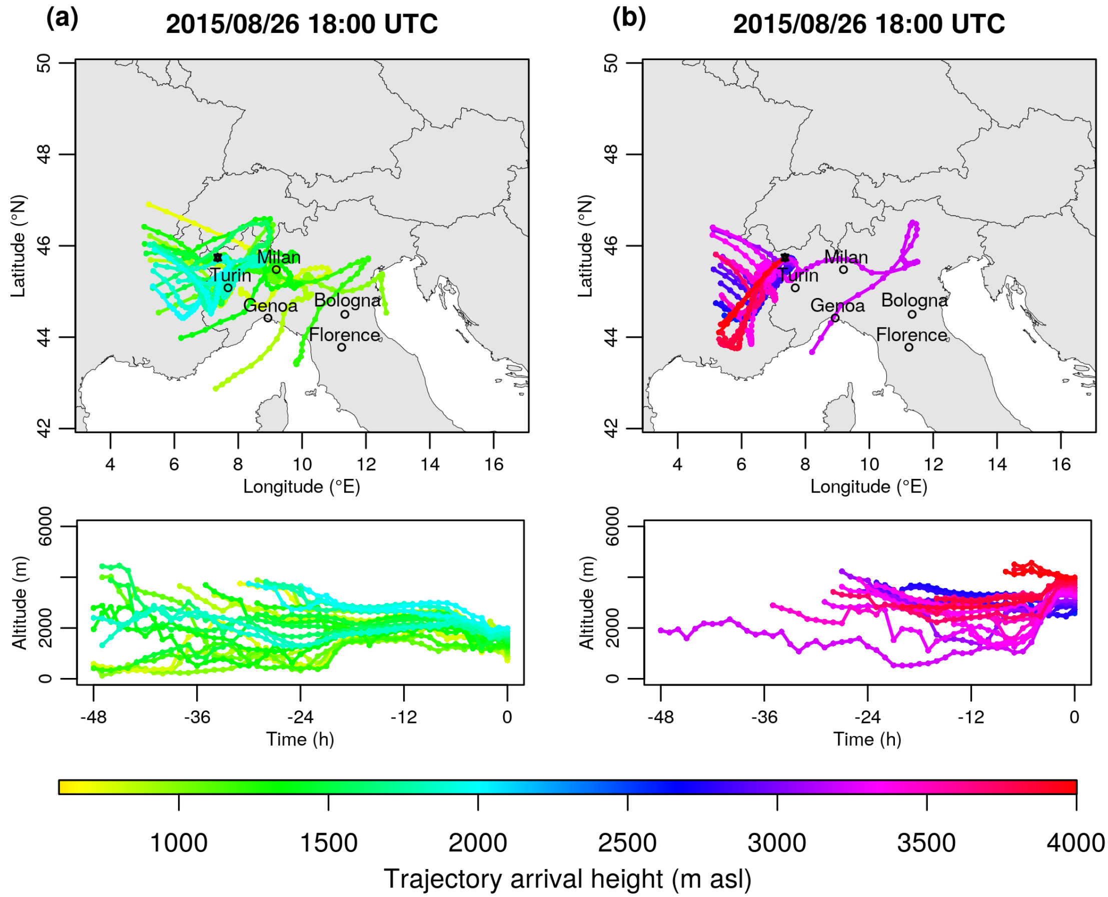

Figure 5. 48-hours back-trajectories ending at Aosta–Saint Christophe on 26 August 2015 at ~~12~~ 18 UTC at altitudes lower than 2000 m a.s.l. (a) and higher than 2500 m a.s.l. (b). The trajectories are cut at the border of the COSMO model. The colour scale represents the back-trajectory arrival height. Corresponding altitudes of the backtrajectories vs time are reported in the bottom panels. The dots along each trajectory mark a 1-hour step and the black star indicates the trajectory arrival point (Aosta–Saint Christophe). ~~The whole~~ A more complete sequence for the ~~day 26 August~~ episode is shown in Fig. S3~~, Sect. S4~~.

are discussed in Sect. 4.4). Note that wind direction is incompatible with ~~the Aosta city~~ Aosta being the potential source of the observed aerosol layer, as ~~it~~ the city is located west of the observatory. At higher elevations, the wind field is clearly decoupled from that in the PBL and follows the large-scale circulation.

Complementary information is provided by the analysis of the 48-hours back-trajectories calculated by LAGRANTO using COSMO fields (Sect. 3.2.3) ending over the Aosta Valley in the period addressed (Fig. 5 and S3). For ease of clarity, the LAGRANTO output is shown in separate panels depending on the arrival altitude of each trajectory (< 2000 and and > 2500 m a.s.l.). These results show that ~~during the night between~~ before the episode (25 ~~and~~ August and morning of 26 August, Fig. S3a and d) trajectories are driven by large-scale flows from the ~~northwest direction~~ west and are thus parallel at all altitudes. ~~This indicates air masses reaching Aosta to have crossed~~ Therefore, air masses reached Aosta after crossing the Alps, notably the Mt Blanc chain, ~~before arriving over the observatory,~~ hence transporting clear and unpolluted air from the free troposphere to the PBL. Then, in the ~~morning~~ afternoon of 26 August~~from 9 to 12 UTC~~, back-trajectories in the PBL ~~suddenly~~ change their provenance owing to the development of the thermal circulation tapping into air masses of very different origin (Fig. 5a), while higher-altitude trajectories mostly continue to follow the synoptic circulation (Fig. 5b). The lowermost trajectories cover a notable distance and cross some major conurbations of the Po basin, i.e. Milan and Turin, at altitudes lower than few hundreds meters a.s.l., and thus well within the polluted PBL. ~~The~~ This sudden reversal of the trajectories occurs simultaneously with the appearance of the elevated aerosol layers in the Aosta ALC image (Fig. 3a). These meteorological conditions persist for the rest of the day and in the following days. The analysis of the corresponding back-trajectories confirms that ~~the air masses sampled by the ALC in Aosta–Saint Christophe keep originating~~ transport of polluted air masses from the Po basin ~~for the whole episode~~also occurs in the afternoons of the other days of this episode, until the flux changes again to a north-western configuration (Fig. S3c and f).

To complete the picture, it is worth mentioning that the COSMO model also predicts an increase of the relative humidity (Fig. 3b) from evening to early morning, almost simultaneous with the SR enhancement observed by the ALC. In this time frame, RH exceeds typical summertime deliquescence values reported for the Po basin in previous studies (e.g., DRH=67%, D'Angelo et al., 2016), and reaches up to 98% at the ground (Fig. S2b). This suggests hygroscopic growth on aerosols and consequent increase in the ALC β_p~~(e.g.~~. For example, in a measurement site representative of Po Valley conditions ~~,~~Adam et al. (2012) found a median increase of the aerosol backscatter coefficient of 70% for RH=90% compared to the dry case~~)~~. During the day, RH decreases below typical crystallisation values in summer (e.g., CRH=62%, D'Angelo et al., 2016). As RH is clearly modulated by the temperature daily cycle, the measured specific humidity (SH) is also plotted on the same figure (S2b) as an additional variable ~~,~~independent of temperature, to identify potential advections of different air masses to the observation site. Indeed, an SH increase occurs on ~~the first day of the sequence~~ 26 August (starting from minimum values of $\sim$8 $\mathrm{g\,kg^{-1}}$ in the morning to about 11 $\mathrm{g\,kg^{-1}}$ in the evening) as soon as the wind starts blowing and high values ($> 13\ \mathrm{g\,kg^{-1}}$) endure for the rest of the week~~, likely indicating~~. This likely indicates that the dry air, typical of the more mixed mountain PBL (Henne et al., 2005; Mélin and Zibordi, 2005), is replaced by more stagnating, and humidified, air masses characteristic of hot summer days in the Po Valley (Bucci et al., 2018). This scenario is compatible with recent findings by Campanelli et al. (2018), who performed water vapour measurements with the POM-02 at Aosta–Saint Christophe and found that moist air masses are mainly coming from the east. A discussion about the constancy of the measured SH during each day compared to the more variable values forecasted by COSMO is provided in Sect. 4.4. We anticipate here that this behaviour confirms that COSMO overestimates the nighttime drainage winds (characterised by lower SH) and contributes to the observed discrepancies between the PM concentrations from FARM and the ALC.

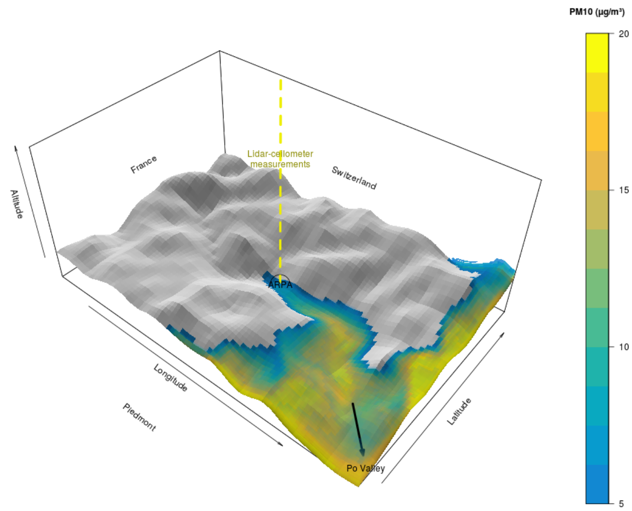

Figure 6. Still-frame of the three-dimensional simulation of $\mathrm{PM_{10}}$ concentration by FARM (image from 28 August 2015 at 15 UTC). The image clearly shows the entrance of the aerosol-rich air mass from the Po basin into the Aosta Valley (~~red and blue~~ yellow-blue area). The same colour scale as in Figs. 3d, 9d and 12d is used (the lowest concentrations are removed for ease of representation). The sequence 26–31 August 2015 is available as a video file in the Supplementary material (https://doi.org/10.5446/38391).

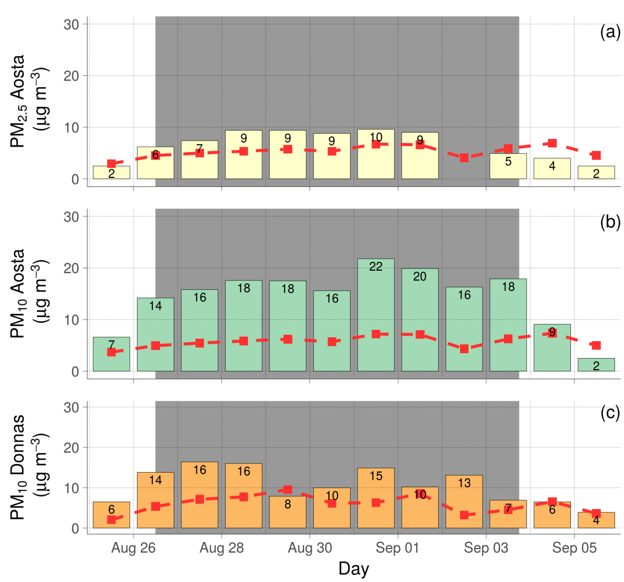

Figure 7. Measured (coloured bars) and simulated (dotted line) daily averages of $\mathrm{PM_{2.5}}$ and $\mathrm{PM_{10}}$ concentrations at Aosta–Downtown and Donnas during case study 1 (August 2015). The period when the ALC detects a thick layer above Aosta–Saint Christophe is highlighted with a grey background. $\mathrm{PM_{2.5}}$ measurements in Aosta are missing for 2 September 2015.

4.1.3 Mass concentrations

We also show in Fig. 3c the altitude-resolved aerosol mass derived from the ALC backscatter coefficient (as described in Sect. 3.1.1). The maximum concentration within the aerosol layer is $> 80\ \mu g\,m^{-3}$. The corresponding PM_{10w} profile from FARM, partitioned between the non-local (coloured background) and local (contour line) pollution, is shown in Fig. 3d. FARM qualitatively reproduces the recurrent increase of the aerosol concentration at the end of each day and mainly ascribes it to particles transported by the thermal winds from the model-box boundaries. As an example, Fig. 6 provides a 3-D snapshot of the model simulation results, clearly showing the entrance of the aerosol-rich air mass from the Po basin to the Aosta Valley. The picture refers to 28 August 2015 at 15 UTC – the whole sequence 26–31 August 2015 being available as a video file in the Supplementary material (https://doi.org/10.5446/38391). Still, there are two important differences between the FARM model simulations and the ALC observations in terms of 1) absolute PM_{10w} concentrations and 2) timing of the phenomenon. In fact:

1. PM_{10w} values from FARM are much lower than the ones retrieved from the ALC (about -40% outside the thick aerosol layer identified by the ALC at night and even -80% inside the layer);

2. the maximum PM_{10w} simulated concentration during the advections is anticipated by several hours (up to 6–7 hours, in the worst cases) compared to the ALC measurements, which, in contrast, show a better correlation with the relative humidity profile by COSMO.

Possible reasons, such as hygroscopicity effects and modelling deficiencies, explaining the above-mentioned issues are further discussed in Sect. 4.4.

To evaluate the impacts on surface air quality parameters during the episode, hourly PM_{10} concentrations at the surface as measured in Aosta–Downtown and simulated by FARM in Aosta–Saint Christophe are presented in Fig. 3e (PM_{10} monitoring at La Thuile was not yet operational, at that time). Apart ~~from one spike~~ two spikes ($80\ \mu g\,m^{-3}$) on 25 and 26 August (presumably of local origin), the concentrations measured in Aosta–Downtown by the TEOM show a slight increase after the arrival of the layer, but without sudden jumps. Also, PM concentrations are generally higher during daytime compared to the night~~and do not show any noticeable increase corresponding to the arrival of the layer. This feature~~, according to the expected cycle of the summertime local sources (e.g., traffic, resuspension, etc.). This features, however, can be connected to the fact that mass loss occurs in TEOM due to secondary aerosol volatility, as ~~also found by Diémoz et al. (2019)~~ better discussed in the companion paper by comparing the daily PM_{10} cycle from this instrument and the Fidas OPC in Aosta–Saint Christophe. Moreover, this volatility could be different between nighttime and daytime, which would also contribute to the observed daily behaviour. Besides, FARM estimates at the surface are again lower than measurements (-60%, on average). Daily PM_{10} concentrations observed by Opsis SM200 instruments during the case study in Aosta–Downtown and Donnas are shown in Fig. 7, ~~the shaded area corresponding~~ which includes the whole episode (correlation index with TEOM measurements $\rho = 0.84$). The shaded area corresponds to those dates affected by the thick layers as revealed by the ALC. ~~Unlike hourly measurements by TEOM, an~~ An increase in daily concentrations (up to ~~7~~ maximum values of 10 $\mu g\,m^{-3}$ for $PM_{2.5}$ and ~~11–15~~ 16–22 $\mu g\,m^{-3}$ for PM_{10}) can be clearly noticed at both sites, leading to concentrations slightly higher than average for the same period (7 $\mu g\,m^{-3}$ for $PM_{2.5}$ in Aosta–Downtown and 12 $\mu g\,m^{-3}$ for PM_{10} at both sites, considering the 2015–2017 series). The statistical significance of such PM increases during these transport episodes, compared to the natural variability of the aerosol load in non-advection conditions, is assessed in the companion paper using the full dataset. The daily averages of the simulated aerosol concentrations at the surface are superimposed on the same figure (dashed lines). While the model qualitatively reproduces the average load of $PM_{2.5}$ and its variations in Aosta–Downtown, it underestimates PM_{10} at both stations as already noticed.

4.1.4 Sun photometer measurements

Since sun photometric measurements can be only performed in daylight, results are often unavailable at those times when the ALC shows the greatest backscatter signal, i.e. in the evening and at night. However, data collected by the POM-02 radiometer can still be effective to monitor the first (late afternoon) and last (early morning) dynamics of the aerosol layer as seen by the ALC (Fig. 3a), and particularly tell us if this signal is detectable in the sun photometer-derived, column-integrated aerosol load. AOD obtained from the sun photometer (Fig. S2d) varies from 0.02 (25 and 26 August ~~,~~ before appearance of the layer) to 0.07 (29 August, morning) at 1064 nm (approximately 0.05 to 0.2 at 500 nm) and closely follows the AOD obtained by vertically integrating the extinction coefficient from the ALC over the atmospheric column. The two independent AOD retrievals present a mean bias of -0.007 and standard deviation of the differences of 0.006, both lower than the declared uncertainty of the POM sun photometer itself (about 0.01) (Campanelli et al., 2007). The good closure with the AOD from the photometer demonstrates the reliability of the functional relationships derived by Dionisi et al. (2018) and employed in our ALC inversion algorithm, at least during the daytime.

Further retrieval products from SUNRAD.pack and SKYRAD.pack (displayed in Fig. S2e) show the Ångström exponent to increase from 1.2 to 1.7 on ~~the first day~~ 26 August from 8 to 17 UTC, suggesting the advection of smaller particles in the atmosphere, and to remain almost constant (about 1.6, a typical value for the Po Valley, as already described by Mélin and Zibordi (2005), and Kambezidis and Kaskaoutis (2008)) in the following days. These values should be compared to the lower Ångström exponents typically measured in the Aosta Valley, i.e. $\sim$1.1 on average (Diémoz et al., 2014a, 2019). Likewise, the single scattering albedo (SSA) at 500 nm increases (from 0.7 to 0.95) on 26 August, which is compatible with the arrival of more scattering (likely secondary aerosol, as described in Sects. 4.2.4 and 4.3.4) and/or more aged aerosol, such as that from the Po Valley (Barnaba et al., 2007; Gilardoni et al., 2014). The sun photometer-derived, total-column, aerosol volume distribution (Fig. S2f) peaks in the accumulation mode (about 0.3 μm). A slight decrease of the peak diameter in the morning (from about 0.4 μm to 0.2 μm) can be noticed on some days (e.g., 27–30 August) and might be ascribed to the dehydration of the particles as temperature increases and RH decreases. The same behaviour can be observed better in the third case study (Sect. 4.3.5 and Fig. S9g).

4.1.5 Spatial extent of the observed phenomenon

In order to provide a first evaluation of whether the phenomenon observed and described in detail for the Aosta area could have a more general validity in the Alpine region, we used AOD data retrieved from space over Northern Italy. In particular,

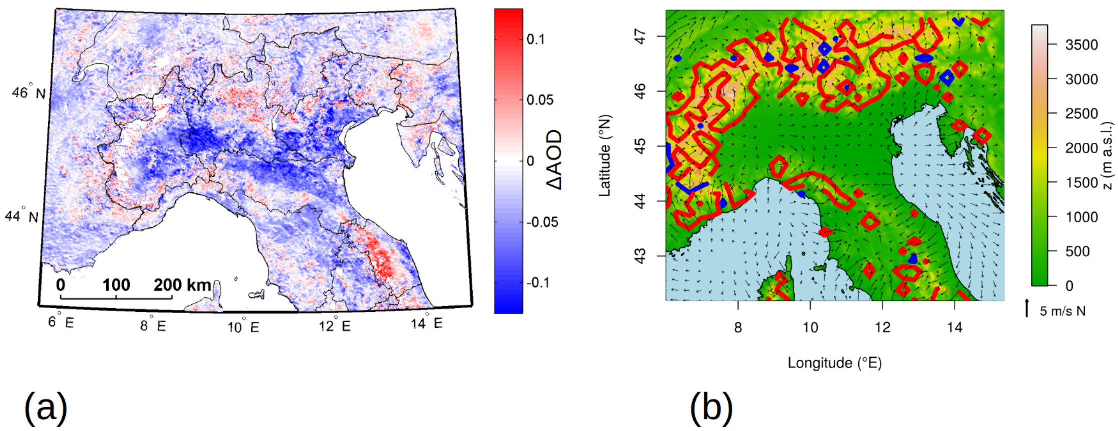

Figure 8. (a) Average difference between AOD estimated from Aqua and Terra satellites during days 27–31 August 2015 using the MAIAC algorithm. (b) Horizontal wind velocity from COSMO (arrows), vertical velocity (red/blue contours, $\pm 0.1\ \mathrm{ms}^{-1}$) over the same domain and the same hours as in Fig. (a).

we exploited the high resolution capabilities of the MODIS-MAIAC AOD product (Sect. 3.1.3) and the availability of two MODIS overpasses during the day (Terra and Aqua platforms), to detect signs of the described effects at the regional scale. Figure 8a shows the average difference between the AOD retrieved each day from MODIS-Aqua (overpass time between 12–13 UTC) and that from MODIS-Terra (10-11 UTC). Despite the short time lag between the Terra (AM) and Aqua (PM) satellite overpasses, this figure shows that the data are sufficient to start detecting an overall reduction of the AOD in the Po basin (blue area) and a reverse increase in the mountain areas (Alps and Apennines) surrounding it. The general picture suggests a sort of aerosol drainage from the Po Valley (negative AOD difference, blue) to the Alps (positive AOD difference, red), although some aerosol dehydration from the morning to the afternoon could also partially contribute to the observed PM–AM differences. ~~The~~ This provides an observation-based confirmation to the hypothesis of aerosol transport, in agreement with our previous results from FARM (e.g., Fig. 6 and the relative video file), ~~is strengthened by the~~ and with wind simulations from COSMO over the same area ~~and~~ (averaged over the same hours between Terra and Aqua overpasses~~(~~, Fig 8b). Valley-mountain (and sea-land~~breezes)~~) breezes are clearly reproduced, as expected in days with weak synoptic flows and strong heating by the sun.

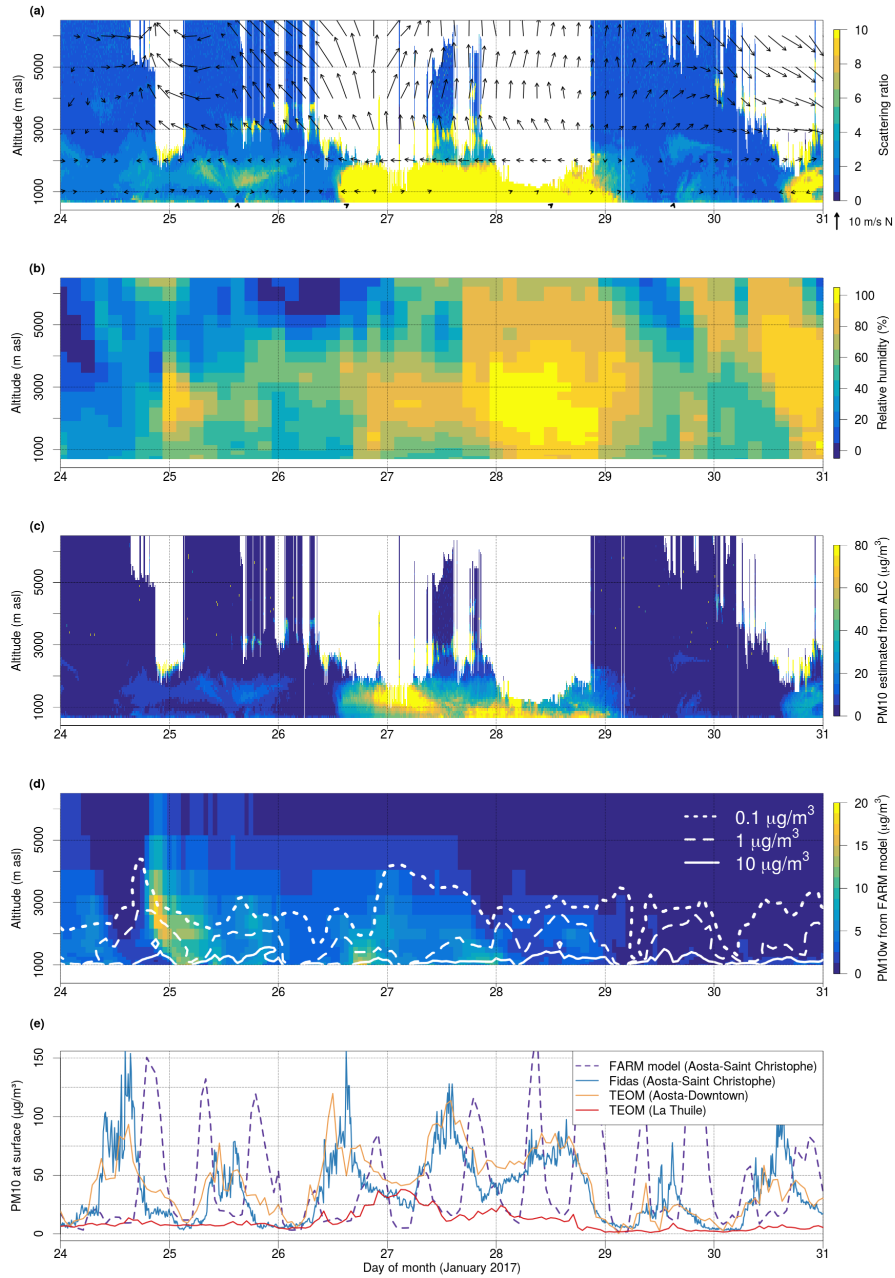

Figure 9. Case study of ~~26–29~~ 24–30 January 2017. (a) Coloured background: vertical profile of scattering ratio from ALC in Aosta–Saint Christophe. Arrows: horizontal velocity of the wind measured at the surface and simulated by COSMO at several elevations; (b) Vertical profile of relative humidity forecasted by COSMO; (c) Vertical profile of PM_{10} mass concentration derived from the ALC using the functional relationships; (d) Mass concentration (PM_{10w}) from FARM; (e) Hourly and sub-hourly PM_{10} (dry) surface concentration from FARM simulations and observations in Aosta–Saint Christophe, Aosta–Downtown and La Thuile (the y-scale of this panel is extended compared to Fig. 3 and 12).

4.2 Case study 2: Winter (~~26–29~~ January 2017)

A second pollution transport episode was chosen for its significance and its consequences on air quality. Indeed, the last days of January 2017 and the first ones of February 2017 were characterised by heavy exceedances of $\mathrm{PM_{10}}$ in the whole Po basin with concentrations of nearly 300 $\mu\mathrm{g\,m^{-3}}$ in some stations of northern Italy (Bacco et al., 2017). This situation was driven by conditions of strong atmospheric stability, weak winds, low mixing height and presence of clouds, and additionally worsened by the transit of a warmer air mass aloft, i.e. the typical circumstances causing the most severe air pollution episodes in the Po basin in winter (Finardi and Pellegrini, 2004). Chemical analyses accomplished in the framework of the air quality monitoring network in northern Italy identified considerable formation of secondary particulate (e.g., ammonium nitrate), also confirmed by very large $\mathrm{PM_{2.5}}$/$\mathrm{PM_{10}}$ ratios (almost 90%).

In the Aosta Valley, this pollution episode lasted only from 26 to 29 January. At that time, the Alps were contended by a pressure trough at the north and a ridge at the south. At the beginning of the period, the influence of the low-pressure system prevailed and brought cloudy skies over the valley~~, thus enforcing the atmospheric stability in the PBL. The~~. Although local emissions (e.g., residential heating and traffic, additionally worsened by the temperature inversion), might have also increased in this period, the influence of pollution transport from the Po basin is unambiguous. As a result of the advection, the PM concentrations measured in the Aosta Valley ~~, although lower than the ones detected in the Po basin,~~ were found to be significant in the whole region (e.g., $\mathrm{PM_{10}}$>100 $\mu\mathrm{g\,m^{-3}}$ in Aosta–Downtown and Donnas), even at some remote measuring sites (e.g., ~~$\mathrm{PM_{10}}$ ∼~~$\mathrm{PM_{10}}$∼70 $\mu\mathrm{g\,m^{-3}}$ in Antey, Sect. 4.2.3)~~. Another peculiarity of this case study is the fact that, owing to a temperature inversion close to the ground, the phenomenon could be mainly identified and fully understood by using profiling instruments, such as the ALC, rather than the data from the air quality and weather surface networks~~, and remarkably higher than the average concentrations in the same period (e.g., 33 $\mu\mathrm{g\,m^{-3}}$ for $\mathrm{PM_{10}}$ and 23 $\mu\mathrm{g\,m^{-3}}$ for $\mathrm{PM_{2.5}}$ in Aosta–Downtown in 2015–2017). No sun photometric measurements were available for this period due to clouds and major maintenance to the POM-02 instrument.

4.2.1 ALC observations

The ~~SR~~ profiles from the ALC in Aosta–Saint Christophe for this winter case are depicted in Fig. 9a and show the sudden appearance of a thick aerosol layer in the afternoon of 26 January. Unlike the previous case, the ALC measurements do not reveal distinct features for each day of the sequence, but rather a continuous and persisting layer during the whole episode. The SR reaches values above 30 in the night between 26 and 27 at altitude, and, more close to the surface, between the evening of 27 and the morning of 29 January. The layer extends up to 2000 m a.s.l., a clear signature of the non-local origin of the air mass~~in view of the presence of a temperature inversion close to the ground~~. Some clouds are visible above and within the aerosol layer~~, thus further inhibiting the mixing in the PBL~~. The episode ends on 29 January as quickly as it began, with clearer air taking the place of the polluted air mass starting from above and subsequently eroding the ~~temperature inversion at~~ layer down to the surface.

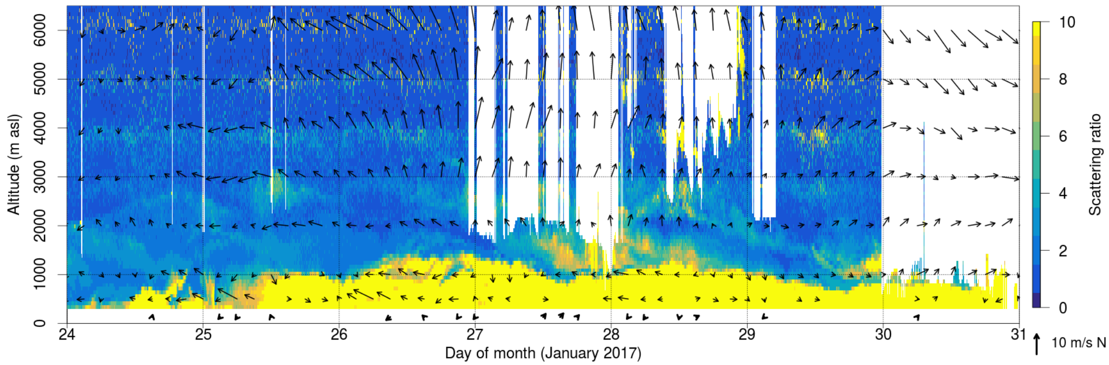

Figure 10. Vertical profile of scattering ratio from the ALC in Milan (~~26–29~~ 24–30 January 2017). Arrows: horizontal velocity of the wind measured at the surface (bold, lower arrows) and simulated by COSMO at several elevations (thin arrows).

Simultaneous ALC profiles over Milan are depicted in Fig. 10. As opposed to the Aosta Valley, the aerosol layer does not vanish on 29 January, but remains for some days more, although the winds at altitude change their provenance from the west on that day. Clouds only form from 27 January, presumably allowing solar radiation to trigger a weak breeze tide in the lowest 2000 m on that day, whilst strong stability favours calm wind in the following days.

4.2.2 Meteorological variables and back-trajectories

The wind field over Aosta–Saint Christophe, depicted in Fig. 9a, presents a very different pattern compared to the first case addressed (Fig. 3a). Firstly, calm wind is measured for the whole period at the ~~surface~~bottom of the valley. This is due to a shallow temperature inversion in the lower atmospheric layers in the main valley~~, as revealed by the thermometers along the mountain slope (Fig. S5, Sect. S5). Indeed~~. Conversely, at the Saint-Denis station, located above the inversion layer, and at the Donnas station, where the temperature inversion is weaker, the wind pattern is more representative of the wider circulation: for example, the average wind speed in Saint-Denis is about 4 $\mathrm{m\,s^{-1}}$ on 26 January afternoon (Fig. S4e~~, Sect. S5~~) and the wind clearly turns from west (morning) to east (afternoon), simultaneously with the appearance of the layer. The same wind change is detected in Donnas on the same day (Fig. S4f), with easterly wind speeds > 1 $\mathrm{m\,s^{-1}}$ for several hours in the afternoon. As a further difference with the first case, the forecasted wind at 1000–2000 m a.s.l. does not show any change in direction typical of the thermal winds. For example, at 2000 m a.s.l. the circulation is continuous, and vigorous (up to 6 $\mathrm{m\,s^{-1}}$), from the afternoon of 26 to the beginning of 29 January. Indeed, this winter case study interestingly shows that thermally-driven winds are not the only mechanism, especially in winter, driving the advection of air masses from the Po Valley to the Alps. Rather, the synoptical circulation can push the air masses towards the Alpine valleys, as in this case. In fact, the flow clearly reveals its southern origin at elevations above the mountain crest (e.g., 3000 m a.s.l.), where the wind is not channelled within the main valley. At that altitude, the wind speed is even greater than 20 $\mathrm{m\,s^{-1}}$. Finally, on 29 January, the measurements in Saint-Denis (gradual increase of the speed of westerly wind) and in Donnas (even stronger wind, again from the west), and COSMO simulations (wind reversal at 1000–2000 m a.s.l) correlate with the disappearance of the layer better than observations performed at the bottom of the valley (calm wind).

Back-trajectories for 26 January are plotted in Fig. S6 ~~(Sect. S5)~~ and indicate transit over the Po basin starting from the morning (panels a, d), which seems to contradict the fact that the layer arrival over the Aosta Valley is detected by the ALC only since the afternoon. This can be explained by noting that the mean altitude of the trajectories crossing the Po basin during the morning exceeds 1500 m a.s.l. ~~(not shown),~~ and is thus higher than the Po Valley aerosol layer observed by the ALC in Milan (Fig. 10). The trajectory altitude tends to decrease in the afternoon ~~to~~ reaching the elevations of the polluted boundary layer ~~,~~ (Fig. S6b), thus leading to effective aerosol transport to the Aosta Valley~~(the trajectory~~. In fact, considering that each dot in Fig. S6b represents a 1-hour step, we estimate a mean air masses residence time in the Po Valley PBL ~~being~~ of 30–35 hours before arriving over the observing site. Finally, trajectories turn westerly on 29 January, in agreement with the removal of the layer over Aosta (Fig. S6c and f).

Together with the appearance of the aerosol layer, an increase in the COSMO RH can be noticed (Fig. 9b). The latter remains higher, above typical wintertime deliquescence values (e.g., DRH=54%, D'Angelo et al., 2016), for the whole duration of the episode and never drops below the crystallisation point (e.g., CRH=47%), which can be partly attributed also to the presence of low clouds forecasted by the NWP model, as actually occurred. The advection is detected more clearly by the increase in specific humidity measured at ground (from less than $2\,\mathrm{g\,km^{-1}}$ to a maximum of $4\,\mathrm{g\,kg^{-1}}$ on 28 January, Fig. S4b). For this episode, the arrival of a different air mass is additionally revealed by the temperature/humidity sensors along the mountain slope. Pseudo-equivalent potential temperatures at different altitudes are shown in Fig. S5. As clearly noticeable, the spread among the series recorded at 550 m a.s.l. and the ones at higher altitudes remarkably, and quickly, decreases on 26 January, especially during the night, suggesting that the strong (and very shallow) temperature inversion weakens and mixing of the upper aerosol layers down to the surface is favoured.

4.2.3 Mass concentrations and particle measurements at the surface

The mass concentration retrieved within the layer by the ALC (Fig. 9c) is quite variable (from $30\,\mathrm{\mu g\,m^{-3}}$ at the edge of the layer to more than $100\,\mathrm{\mu g\,m^{-3}}$ at the core) and reveals the heterogeneous distribution of the particulate inside the layer. FARM predicts a very different scenario, with three separate increases at the end of 26, 27 and 28 January of non-local origin (coloured background in Fig. 9d, much lower than the concentration retrieved by the ALC) and a clear diurnal cycle close to the surface of local origin (Fig. 9e). The diurnal cycle in the simulations is characterised by two peaks corresponding to the combined effect of traffic rush hours, residential heating and variation of the mixing layer height. Hourly and sub-hourly $\mathrm{PM_{10}}$ surface concentration measurements at both Aosta–Downtown and Aosta–Saint Christophe, however, only exhibit one peak at midday. ~~The~~ Taking into consideration these different daily evolution patterns and the sources included in the emission inventory, the most likely reasons for the differences between the model and the measurements at the surface ~~are due to~~ appear to be an underestimation of the residential heating (actually switched on all day during these very cold days) and an overestimation of the traffic road contribution, together with an overestimation of the mixing layer height growth at midday by the NWP model. Anyway, Fig. 11 shows that the daily averages of PM concentrations measured at several sites of the region are higher on 27–28

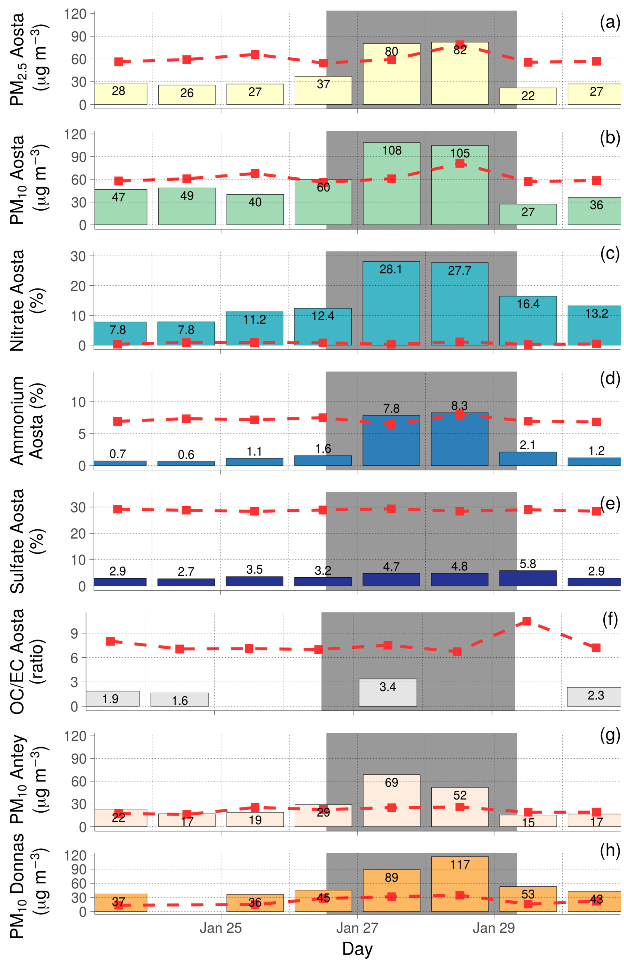

Figure 11. Measured (coloured bars) and simulated (dotted line) $\mathrm{PM}_{2.5}$ and PM_{10} daily concentrations at several sites of the Aosta Valley (a,b,g,h); percentage concentrations of nitrate (c), ammonium (d) and sulfate (e), and OC/EC ratio (f) at Aosta–Downtown during case study 2 (January 2017). The period when the ALC detects a thick layer above Aosta–Saint Christophe is highlighted with a grey background.

January than on the neighbouring days. Specifically, the increase is similar (more than 40 $\mu g\,m^{-3}$) for both $PM_{2.5}$ and PM_{10} in Aosta–Downtown, which results from the fact that the increment is mainly driven by particles with diameter less than 2.5 μm. The maximum PM_{10} concentration (117 $\mu g\,m^{-3}$) was measured on 28 January in Donnas (Fig. 11h), which is the closest station to the Po basin. The spatial pattern of the observed increase, not fully captured by the model, is evident in Fig. S7 ~~, Sect. S5~~ and represents a further indication of the Po Valley being the source of the polluted air masses. Moreover, Fig. 11(c,d) shows this increase to be associated to enhancement in Aosta–Downtown of the nitrate and ammonium components (see next paragraph), two key species of the Po Valley secondary aerosol, but minor contributors to PM_{10} in the Aosta Valley. Finally, while the daily PM concentrations from FARM are comparable, on average, to the measurements, the modulation of the PM concentration by the advection (peaks) is not captured by the model, whose output is rather constant. Most interestingly, data collected at remote and usually pristine sites also show a remarkable increase: at La Thuile (PM_{10} winter average 7 $\mu g\,m^{-3}$), the hourly PM_{10} concentration (Fig. 9e) reaches nearly 40 $\mu g\,m^{-3}$ (some hours later than the appearance of the aerosol layer in Aosta–Saint Christophe) and correlates well with the increasing NO_2 concentration (from about 2 $\mu g\,m^{-3}$ before and after the event to 44 $\mu g\,m^{-3}$ during the event on a hourly basis) measured by a co-located detector. Additionally, the mobile laboratory in Antey (winter average 20 $\mu g\,m^{-3}$) measures increasing daily PM_{10} concentrations with a maximum of 69 $\mu g\,m^{-3}$ on 27 January (Fig. 11g) and increasing NO_2 concentrations from about 30 $\mu g\,m^{-3}$ to 56 $\mu g\,m^{-3}$.

For this selected sequence of days, the data collected by the OPC in Aosta–Saint Christophe are additionally available. The instrument reveals a notable increase in the number concentration for particles smaller than 0.5 µm (Fig. S4c) in coincidence to the arrival of the aerosol layer. The total number concentration (Fig. S4d) gradually increases from few ~~hundres~~ hundreds particles cm^{-3} up to 3000 particles cm^{-3} and decreases again on 29 January (the average value in winter 2016–2017 in conditions of local pollution being 650 particles cm^{-3}).

4.2.4 Chemical analyses

Some results of anion/cation analyses performed on daily samples collected at Aosta–Downtown are also reported in Fig. 11 and presented in terms of relative concentrations (ratio between ions mass and PM_{10}). As anticipated, the fractions of nitrate and ammonium drastically increase during the event, reaching values more than double (nitrate) or even eight to ten times as much (ammonium) compared to the concentrations in the days adjacent to the case study. Indeed, wintertime low temperature and high humidity in the Po Valley represent the best conditions leading to the formation of ammonium nitrate (Schaap et al., 2004). Besides, this nitrate increase enhances the observation of a lowering of DRH (D'Angelo et al., 2016) that may influence the ALC backscatter. Sulfate also increases, but not as much as nitrate and ammonium, since unfavourable conditions are met during winter (Carbone et al., 2010). Only one sample was analysed for EC and OC during the event, and the OC/EC ratio increases only marginally, likely due to sample overloading. In general, variations of the aerosol composition are noticeable on 27–28 January and in line with transport from the Po basin (as more rigorously demonstrated using the Positive Matrix Factorisation method in the companion paper). Indeed, high presence of secondary aerosol in the Po Valley has been documented since a long time, most notably nitrate compounds (Schaap et al., 2004; Putaud et al., 2010; Saarikoski et al., 2012; Aksoyoglu et al., 2017). The latter are probably enhanced by the particular atmospheric conditions during the examined period

(Bacco et al., 2017). All together, nitrate, ammonium and sulfate can explain about 40% of the PM_{10} mass during the episode (as a reference, this fraction represents 15% of the PM_{10} mass for non-advection days of January–February 2017, on average, owing to missing sources of precursors in the Aosta Valley), while organic matter (OM, assuming a typical conversion factor of 1.6 between the measured concentration of OC and the unknown concentration of OM, as in Turpin and Lim (2001) and Curci et al. (2015) for urban sites) and elemental carbon account for a remaining 30% and 5% fraction, respectively (similar percentages are obtained for non-advection days in January–February 2017). Finally, the relative concentration of the other measured ions, allegedly of local origin (e.g., Na^+ and Cl^- from road salting, not shown), does not follow the same pattern as observed in Fig. 11. Figures 11c–e also reveal that FARM is not able to reproduce the experimental chemical speciation: nitrate is strongly underestimated, while ammonium and sulfate are strongly overestimated, and the simulations of the OC/EC ratio do not follow the experimental data. This behaviour is probably to be ascribed to the fact that the SPECIATE v3.2 chemical characterisation implemented in the emission manager is not suitable for the considered sources and/or that the sources, and therefore their chemical profiles, are not accurately identified.

4.3 Case study 3: Spring (~~25–30~~ May 2017)

This third case, occurring in Spring, is similar to the first one (Sect. 4.1), but is included to represent a third season and because a more extended observational dataset was available. From a meteorological point of view, a wide high-pressure ridge extended from the Mediterranean Sea to western and central Europe, thus favouring sunny days with afternoon instabilities and thermally-driven winds from the Po basin to the Aosta Valley. At the end of the period, a weakening of the high-pressure area led to increased instability. The ~~overall sequence~~ whole advection episode (25 May – 3 June 2017) ~~, only partially described in the following paragraphs (25–30 May),~~ lasted for 10 consecutive days. In the next paragraphs, we will mainly focus on the interval 24–30 May.

4.3.1 ALC observations

Since the establishment of the thermally-driven wind regime, starting from 25 May, a thick aerosol layer is regularly detected by the ALC in the afternoon (Fig. 12a). The layer persists during each night, when the scattering ratio increases up to a value of 20 and clouds systematically form within the layer. This aerosol layer extends from the ground to an altitude increasing from 2.5 km at the beginning of the case study to more than 3 km at the end of the episode. ~~Entrainment of the elevated layer to the surface in the middle of the day is repeatedly observed by the ALC.~~

4.3.2 Meteorological variables and back-trajectories

The plain-to-mountain circulation, driving the phenomenon under investigation, is well captured by both measurements at the surface (Fig. 12a, bold arrows) and COSMO forecasts (thin arrows). Eastern winds with speeds $> 10\ \mathrm{m\,s^{-1}}$ are measured in the afternoon till sunset at the surface, while nights are characterised by calm wind. At higher elevations, the wind provenance turns from the north, at the start of the depicted sequence, to the south.

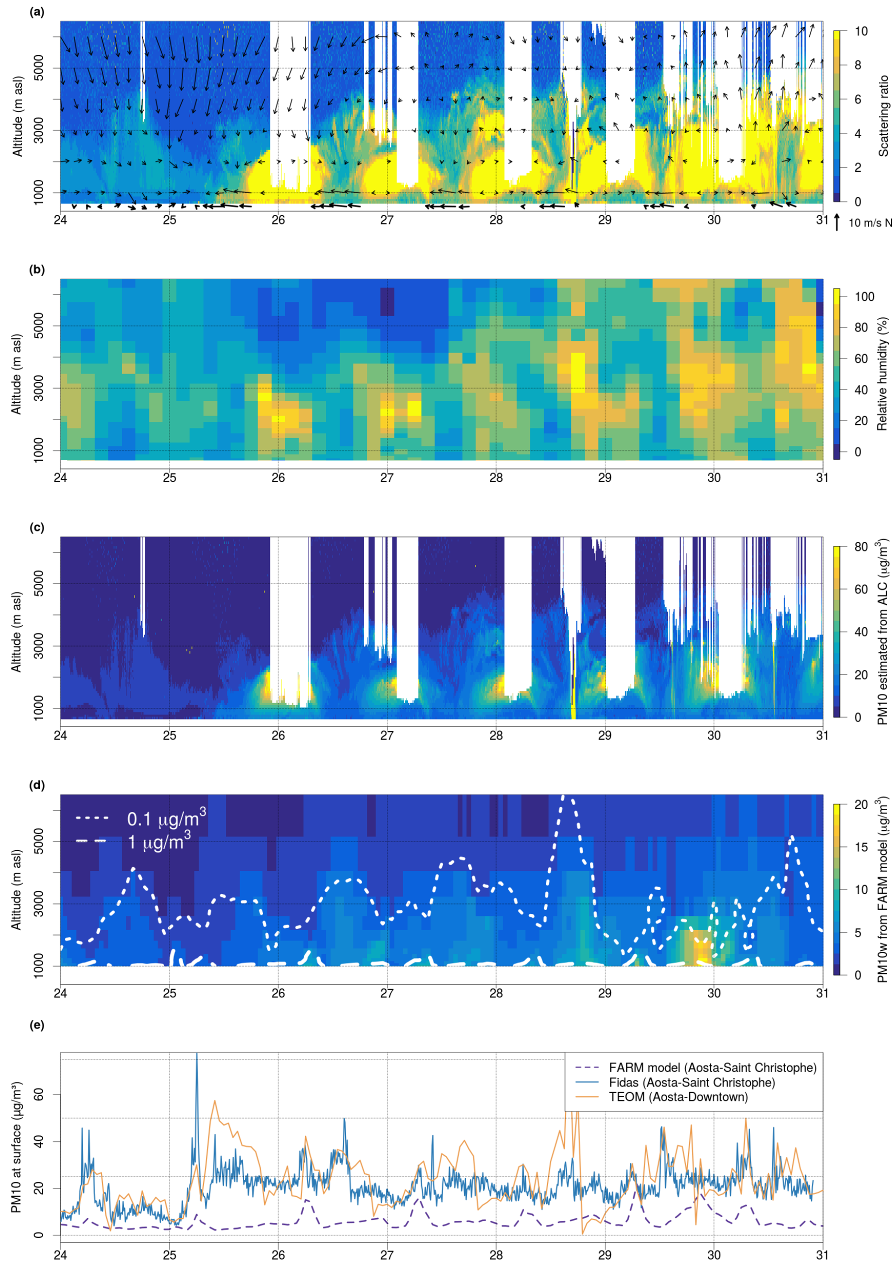

Figure 12. Case study of ~~25–30~~ 24–30 May 2017. (a) Coloured background: vertical profile of scattering ratio from ALC in Aosta–Saint Christophe. Arrows: horizontal velocity of the wind measured at the surface and simulated by COSMO at several elevations; (b) Vertical profile of relative humidity forecasted by COSMO; (c) Vertical profile of PM_{10} mass concentration derived from the ALC using the functional relationships; (d) Mass concentration (PM_{10w}) from FARM; (e) Hourly and sub-hourly PM_{10} (dry) surface concentration from FARM simulations and observations in Aosta–Saint Christophe and Aosta–Downtown.

The back-trajectories ending over the Aosta Valley ~~on 25 May~~ during the third episode are plotted in Fig. ~~S9, Sect. S6. The~~ S8. On 25 May, the large-scale circulation from the north generally dominates the air mass origin (Fig. S8a and d). However, during the day, the low-level thermal circulation becomes strong enough to influence the lowest trajectories, which start to cross the Po Valley in the second part of the day (Fig. S8b), in line with the simultaneous appearance of an aerosol layer in the ALC measurements. Together with their rotation during this day, the trajectories also decrease their altitude. At the end of the day, the air masses reaching the station have slithered for more than 20 hours on the surface of the Po basin. The ~~analysis of the trajectories for the following days indicates that the air masses keep crossing the Po basin~~end of the episode is marked again by north-western provenance (Fig. S8c and f).

As in the first case, COSMO accurately predicts the advection of humid air at the same times as the ALC detects a thickening of the layer (Fig. 12b). At night, the simulated and measured RH exceed 90% at altitude and 80% at ground, respectively (Figs. 12 and ~~S8b~~S9b). Contrary to RH, specific humidity does not show any daily cycle (Fig. ~~S8b~~S9b). A sudden SH increase (5 to 10 $\mathrm{g\,kg^{-1}}$) is clearly visible on ~~the first day (~~25 May ~~)~~ at the time of the advection, while the values for the following days are almost constant except on the occasion of short showers (e.g., evening of 28 May).

4.3.3 Mass concentrations and particle measurements at the surface

The aerosol mass derived from the ALC is presented in Fig. 12c. The maximum concentration retrieved by this method within the aerosol layer is higher than 60 $\mathrm{\mu g\,m^{-3}}$ just before the formation of clouds at night. Again, FARM (Fig. 12d) qualitatively reproduces the afternoon increase of aerosol concentrations owing to transport from the boundaries, however the simulated concentrations are much lower (about 4–5 times) than the retrievals from the ALC and the advection arrival times are anticipated compared to the appearance of the thick layer from the ceilometer.

Hourly and sub-hourly $\mathrm{PM_{10}}$ surface concentrations (measured in Aosta–Downtown and Aosta–Saint Christophe and simulated by FARM) are presented in Fig. 12e. FARM correctly reproduces the morning rush-hours peak, but the concentrations are about half those from the PM samplers. The series in Fig. 12e shows an increase of $\mathrm{PM_{10}}$ surface concentration during ~~the first day~~25 May, with persisting high values for the rest of the week, most noticeably during the night. Accordingly, PM daily means in Fig. 13(a,b,g,h) show a distinct increase in the whole region (the concentrations doubles) during the case study compared to the preceding and following days (and also compared to the 2015–2017 average concentrations for the same period, i.e. 12 $\mathrm{\mu g\,m^{-3}}$ for $\mathrm{PM_{10}}$ in Aosta–Downtown and Donnas, and 6 $\mathrm{\mu g\,m^{-3}}$ for $\mathrm{PM_{2.5}}$ in Aosta–Downtown).

The number distribution and total particle number measured by the OPC in Aosta–Saint Christophe are plotted in Fig. ~~S8c~~ S9c and d, respectively. ~~A~~ It shows a notable increase in the number concentration during ~~the first day~~ 25 May (from less than 200 to more than 800 particles $\mathrm{cm^{-3}}$) and in the afternoon of each day, and a decrease in the central part of each day as soon as the valley convection starts and the mixing layer height increases~~is clearly visible~~.

4.3.4 Chemical analyses

Percentage concentrations of nitrate, ammonium and sulfate are represented in Fig. 13(c–e) and account for about 20–25% of the total $\mathrm{PM_{10}}$ mass (as a reference, this fraction represents less than 15% for non-advection days in May–June 2017). Inter-

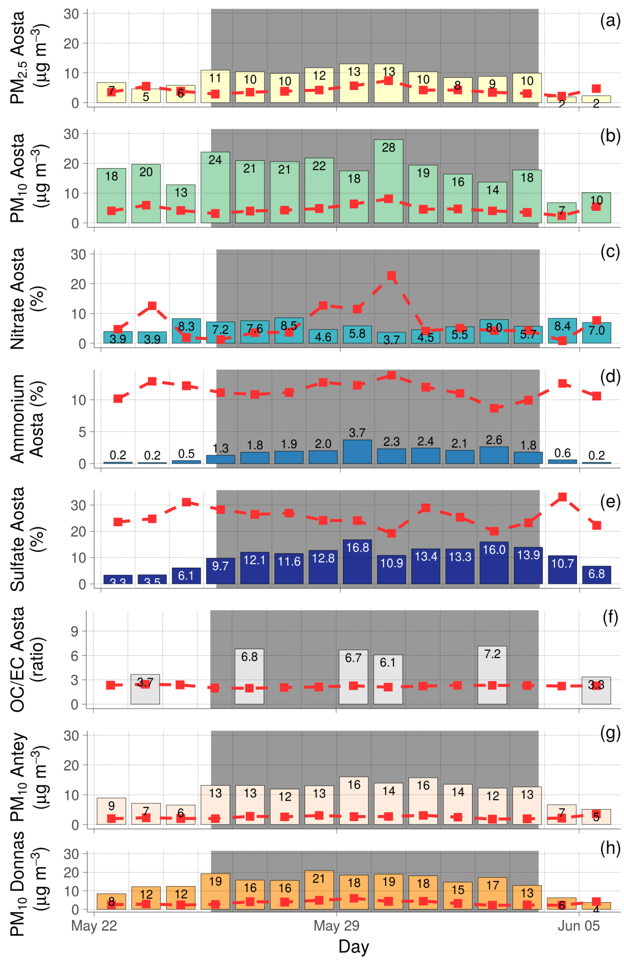

Figure 13. Measured (coloured bars) and simulated (dotted line) $PM_{2.5}$ and PM_{10} concentrations at several sites of the Aosta Valley (a,b,g,h); percentage concentrations of nitrate (c), ammonium (d) and sulfate (e), and OC/EC ratio (f) at Aosta–Downtown during case study 3 (May–June 2017). The period when the ALC detects a thick layer above Aosta–Saint Christophe is highlighted with a grey background.

estingly, relative nitrate concentration does not change much and does not reach the extreme values of the winter case study. Indeed, transfer of ammonium nitrate from particles to gas-phase, which is not measured, is favoured by higher temperatures (Saarikoski et al., 2012). Conversely, ammonium and sulfate increase remarkably during the advection, reaching typical concentrations of the Po Valley in that period (Putaud et al., 2010). In particular, the sulfate concentration is much higher and more affected by the advection in May than during the winter case. The role reversal between nitrate and sulfate in case studies 2 and 3 results from the different sensitivity of those compounds to temperature and atmospheric conditions (Carbone et al., 2014). Again, the contribution of inorganic species from the model does not agree with the analyses: the contribution by ammonium and sulfate is strongly underestimated, while the peaks in the simulated nitrate concentration are not reflected in the analyses.

As for the organic part, OM and EC are the main constituents of the remaining fraction, with about 60% and 6%, respectively. Although the available dataset is rather short, the OC/EC ratio during the event almost doubles (values of 6.1–7.2) compared to the value before (3.7) and after (3.3) the event. This increase of the OC fraction during transport episodes is confirmed by the long-term analysis (Diémoz et al., 2019).

4.3.5 Sun photometer measurements

The same morning-midday-afternoon modulation can be observed in the AOD from both the ALC and the sun photometer (Fig. ~~S8e~~S9e). The high AOD values in the first and last part of the day (up to 0.30–0.40 at 500 nm) and the decrease in the middle of the day (down to 0.12 at 500 nm) match the appearance of the layer seen by the ALC and its enhancement due to hygroscopic effects, in accordance with the results of Adam et al. (2012) for a typical site in the Po basin (in that case, for RH=90%, the extinction coefficient increased on average to 180% of the value measured for RH=0%). The steep rise (from 0.8 to 1.7) in the Ångström exponent on ~~the first day~~ 25 May (Fig. ~~S8f~~S9f) and its continuous increase in the following days (up to nearly 2.0) may be attributed to the advection of small particles to the measuring site. The SSA fluctuates around large values (generally between 0.9 and 1.0), typical of weakly light-absorbing or aged aerosol. Most interestingly, the volume distribution (Fig. ~~S8g~~S9g) exhibits an abrupt decrease of the peak diameter during the morning hours (e.g., from 0.5 at 6.40 UTC to 0.2 $\mu\mathrm{m}$ at midday on 27 May), strengthening the hypothesis of aerosol hydration at night and dehydration during the day as temperature increases and RH decreases.

4.4 Model–measurement discrepancies

Our CTM qualitatively reproduces the aerosol advections in all three case studies. It helps to understand the phenomenon by allowing switching on/off the non-local sources (boundary conditions), but fails to quantitatively explain the concentrations retrieved by the ALC (PM_{10w}) and measured by the air quality network (PM_{10}). ~~Notably~~As already mentioned in the description of the three cases, the model: a) underestimates the PM mass both in the layer aloft and at the surface, and ~~anticipates (by some hours)~~ b) anticipates the peak concentrations compared to the profiles from the ALC. ~~In particular, the anticipation cannot be due to inaccuracies in modelling the wind speed, since the discrepancies between forecasts and observations are $< 10\%$ during the episodes.~~ A variety of (possibly concurrent) reasons can explain ~~this behaviour~~the observed underestimation, mainly related to:

1. inaccuracies in retrieving the PM concentration from the ALC backscatter. As mentioned, ALC measures aerosol backscatter, ~~and~~ so that specific tools were developed (Dionisi et al., 2018) and are used here to associate a PM value to it~~(Dionisi et al., 2018), but expected error on these estimates are~~ . Still, the expected error associated to these estimates is of the order of 30–40%. In addition~~to the uncertainty related to this ALC-based PM retrieval, other factors also play a role. First~~, the ALC ~~is sensitive to the total suspended particulate (TSP) of any dimension, whereas FARM simulates the PM concentration for particles with diameter smaller than 10 . Secondly, and most importantly, water uptake by aerosol can be prominent, especially when RH>DRHand exceeds the conditions assumed for calculating the functional relationships (RH≤~~retrieval is based on functional relationships derived assuming maximum RH of 95%. Higher FARM-ALC discrepancies can be expected when RH>DRH, and particularly at RH>95%~~). These issues can worsen the comparison between the model (PM_{10w}) and the ALC profiles~~;

2. inaccuracies in the CTM simulations. The emission inventory used within FARM likely underestimates the real emissions, as also reported in other cases, and for different models, in the scientific literature (e.g., EMEP, 2016; Uchino et al., 2017). In particular, the boundary conditions could not be accurate enough for our aims owing to the abrupt change of the national emission inventory grid resolution (12 km) to the local scale (1 km). This issue can affect the comparison between the model (dry PM_{10}) and surface measurements, especially in winter, as discussed more extensively in the companion paper (Diémoz et al., 2019). Additionally, the aerosol hygroscopicity may be not optimally simulated by FARM, e.g. due to a wrong characterisation of the chemical properties of the modelled aerosol, which again impacts on the comparison between the vertical profiles from the model and the ALC. Finally, some underestimation of PM values could also be due to overestimation of the FARM simulated PBL height. An evaluation of this kind of effect is in principle possible by comparing the simulations with the ALC-derived PBL height (e.g., Angelini et al., 2009; Haeffelin et al., 2012) . However, this should be performed only selecting non-advection conditions, i.e., those in which the ceilometer signal is only affected by local aerosols and is thus able to follow the daily evolution of the local PBL using local particles as tracers. This kind of investigation was, however, beyond the scope of the present work. Challenges and recent efforts to define a PBL in mountainous areas (“Mountain Boundary Layer”, MBL) and discrepancies between the MBL and the aerosol layer are more extensively described by Lehner and Rotach (2018).

The case studies described here show that several of the previous points most likely play a significant role. Some sensitivity tests were performed addressing point 2. In particular, for the first case study (August 2015, Sect. 4.1) we performed two additional tests. 1) We doubled the PM concentrations from the boundary conditions to assess the sensitivity of the simulated vertical profiles to the accuracy of the national emission inventory and to the transport from outside the administrative boundaries of the Aosta Valley, while leaving the regional emission inventory unchanged. The perturbation of the boundary conditions used for the test may appear excessively large, however this choice could be supported by the fact that the resolution of the national inventory grid is much coarser than the local one, which may be a source of inaccuracies. 2) We employed two different, more empirical, parametrisations of the aerosol hygroscopicity to recalculate water uptake by aerosol. As shown in the Supplementary material (Sect. S7), the results of the two tests support the hypothesis that both the national inventory and the parametrisation of the hygroscopic effects in the model are responsible for the discrepancies between simulations and measurements in the first case study. Doubling the boundary conditions also slightly improves the comparison between simulations and measurements at the surface for the winter case study (first introduced in Sect. 4.2), although some discrepancies in the geographic distribution of the concentrations persist (~~Sect. S7,~~ Fig. S12~~), probably due to inaccurate NWP input data (~~, e.g., overestimation on 25 January 2017 and underestimation on the following days)~~.~~, probably due to inaccurate NWP input data. Finally, it is worth to mention that, during the winter episode, a small fraction of the detected secondary particulate might form locally due to heterogeneous chemical reactions taking place on the advected particles themselves (e.g., Gilardoni et al., 2016; Kim et al., 2018; Lim et al., 2018). These dynamics could contribute to the observed underestimation, however they are too complex to be simulated by present CTMs. Further efforts on this topic are scheduled for the future.

The previous considerations, however, fail at comprehensively explaining the time shifts sometimes noticeable between the model and the measurements, i.e. anticipation of the advection arrival time (even in "dry" conditions in the afternoon on the first day of each sequence) and of the layer disappearance in the morning (where hygroscopicity may have an important role). Although an accurate assessment would require a more sophisticated set of instruments to characterise the vertical profile of the wind velocity, here we formulate some hypotheses:

1. the NWP model likely anticipates and overestimates the easterly thermally-driven winds in the first hours of the afternoon. This is noticeable, for example, in Fig. S13, where the zonal component of the wind from both COSMO and the surface measurements for case study 1 (August 2015) is plotted, and, on a longer statistical basis, in Fig. S1(b,c), showing that the model has the tendency to see easterly winds more often and with higher intensity compared to the observations. A possible reason for that is the smoothed valley orography used in the NWP model compared to the real one. This is displayed in Fig. S14, showing the difference of the Digital Elevation Model (DEM) used within COSMO and a more realistic DEM (10 m resolution): both valleys and mountain crests are clearly smoothed out by COSMO, with absolute differences well > 500 m (and up to 1000 m). This difference could additionally explain why the altitude of the entrainment zone (i.e., the boundary between the free atmosphere and the boundary layer where the thermally-driven circulation develops) is underestimated by COSMO compared to the height of the aerosol layer detected by the ALC (e.g., Figs. 3 and 12);

2. COSMO overestimates the nighttime drainage winds (katabatic winds), as noticeable, again, from Fig. S13 for case study 1. This might trigger enhanced cleansing of the lower atmospheric layers during the night as simulated by FARM (see, e.g., the supplementary video file relative to Fig. 6, https://doi.org/10.5446/38391), but undetected by the ALC. An overestimation of the drainage winds would also explain the differences between the simulated and measured daily cycle of specific humidity, represented in Fig. S15 for case study 1 as an example. In fact, the measured SH usually increases during the first advection day as a result of the transport from source areas with more stagnating conditions (cf. Figs. 3, 9 and 12), but stays rather constant for the rest of the episode. Conversely, COSMO yields larger dynamics, with SH maxima in the late afternoon and subsequent decrease, likely owing to overestimated drainage winds developing after sunset (this results in SH minimum in the late morning).

As a final remark, we also mention that the 2.8 km grid resolution of the COSMO-I2 model might still be insufficient for resolving the complex 3-D flow field of an Alpine valley and is too coarse to reproduce the mountain atmosphere with its various mixing processes. Follow-up studies using next generation NWP models with increased resolution (1 km or lower) would be of great interest. On the other hand it should also be noticed that decreasing the grid spacing below the scale for which turbulence parametrisations have been developed, i.e. modelling the “grey zone” (or “terra incognita”, e.g., Wyngaard, 2004), does not necessary lead to better performances. In this context, comparison of high-resolution simulations with our vertically-resolved dataset could represent a challenging future benchmark for this relevant topic of ongoing research.

5 Conclusions

We investigated the phenomenology of recurrent episodes of wind-driven arrival of aerosol layers in the northwestern Italian Alps, and specifically in the Aosta Valley. The analysis was performed by combining a multiple-site, multiple-sensor measurement dataset with modelling tools. Through a deep examination of three case studies, specifically-selected within a 3-year dataset as clear examples of the phenomenon under investigation, we can provide the following answers to the scientific questions driving the study (see Introduction)~~.~~:

1. What is the origin of the aerosol layers detected in the northwestern Alps?

   All results agreed in showing these episodes to be associated to the arrival of polluted air masses originating from the Po basin, one of the EU pollution hotspots. To reach this conclusion, we examined wind flows from both the experimental (surface observations of the wind velocity from the meteorological network at multiple elevations) and modelling (high-resolution NWP models, back-trajectories and CTM simulations) perspective. Interestingly, in one case (Sect. 4.2.2), calm wind measurements at the bottom of the valley ~~during a~~ in cold-pool conditions at the beginning of the advection episode could give the mistaken impression that the aerosol originated from local sources, since the circulation in the lowermost levels was inactive, while the wind was blowing undisturbed above the temperature inversion. However, the ALC capacities of sounding the vertical profile of the atmosphere, together with the experimental/modelling data at different elevations, turned out to be a substantial benefit for the clear understanding of the phenomenon;

2. What conditions are favourable to the aerosol flow into the valley?

   We show that these advections are due to thermally-driven winds (especially in the warm period of the year, e.g. case studies 1 and 3) or synoptic flows (mainly in the cold season, e.g. case 2) from the east (Po basin) to the west. ~~These meteorological conditions are frequently met, especially during fair weather days in the warm period of the year. Comprehensive statistics of the cases~~ A more systematic analysis of the flow regimes and their impacts on transport based on comprehensive statistics are provided in the companion paper (Diémoz et al., 2019) exploiting the full 3-year record of ALC measurements~~, show these conditions to occur at least 50~~. These show that conditions favourable for the development of the advections occur >50% of the days ~~in summer and spring. We~~ on average. Also, we expect the frequency of the advections to increase with increasing proximity to the source (Po basin);

3. How do the advected aerosol layers evolve in both altitude and time?

   Thanks to the monitoring capacity (24/7) of the ALCs, we could follow the evolution of the aerosol layer in both altitude and time. We show that the advected aerosol layers can extend up to 4000 m a.s.l. in the warm season, which incidentally points out the potential impacts of aerosol dry and wet depositions on the remote, high-altitude ecosystems. On the other side, the altitude of the layer sounded by the ALC is a clear indication that the emissions are not local. As for the evolution in time, the layers were usually detected to arrive over Aosta in the afternoon, when the plain-mountain thermal regime is established. However, the backscatter from the ALC was found to reach its maximum during the night, when water uptake on aerosol took place and clouds could frequently form within the aerosol layer~~. In the days following the advection episodes, a residual layer was seen to sink towards the surface, with possible, further impacts on the air quality~~;

4. What is the impact of the transported aerosol on PM surface concentrations and chemical composition?

   An important increase in $\mathrm{PM_{10}}$ and $\mathrm{PM_{2.5}}$ was detectable during the investigated advections, with up to 80 $\mu\mathrm{g\,m^{-3}}$ of $\mathrm{PM_{10}}$ likely transported in Donnas (Fig. 11). The size distribution of the advected particles generally peaks in the accumulation mode, with a diameter of few tenths of $\mu\mathrm{m}$ (as observed by both the OPC, at the surface, and the sun photometer, in the uppermost layers). Moreover, this kind of particulate is weakly light-absorbing (sun photometer). Chemical analyses reveal these layers to produce an increase of the secondary inorganic fraction, composed by nitrate, sulphate and ammonium, i.e. three typical compounds found in the Po Valley atmosphere, and with low deliquescence RH. Weak local formation of secondary particulate could not be excluded during episodes of severe advection (e.g., case study 2), probably also due to aqueous phase chemistry. However, including these latter processes in current CTMs is still challenging. In one of the case studies, the OC/EC ratio was also observed to increase, a possible sign of the transport of organic compounds from the Po basin;

5. Are the presently used chemical transport models able to reproduce and explain the observations along the vertical profile?

   ~~In this investigation ,~~ Our investigation allowed an evaluation of the FARM model~~was very useful to interpret and complement the observations, and particularly to evaluate the relative weight of local and non-local contributions~~. Notably, FARM could reproduce the observed arrival ~~and persistence~~ of elevated aerosol layers and it correctly attributed them to sources external to the Aosta Valley. However, ~~the timing and~~ absolute values of PM concentrations and the timing of the advections were poorly reproduced, with ~~anticipations (in time) and underestimations (~~underestimations of aerosol concentrations ~~)~~ and time anticipations compared to the measurements. On the basis of a sensitivity study, ~~these issues were~~ the former issue may be partly attributed to both water uptake ~~on those~~ by highly-hygroscopic particles, not fully taken into account in the model, and deficiencies in the emission inventories, especially owing to the coarse resolution of the national one (12 km). ~~From a modelling perspective~~As for the timing discrepancies, suboptimal performances of the NWP model to simulate daytime (thermally-driven) and nighttime (katabatic) winds are the most likely sources of error. Despite these limitations, FARM brought insights on the phenomenology addressed, supporting the observations and helping to interpret them. On the other hand, the observation-based results of this work ~~represent a motivation to improve~~ could drive the improvement of the emission inventories, thus enhancing the reliability of the CTM ~~simulation~~(e.g., Diémoz et al., 2019). In turn, this ~~would~~ could allow extending the findings of this work to a wider domain, not covered (or not fully covered) by observations.

The phenomenology described in detail in the current study through the selected ~~case studies~~ cases has been further investigated in ~~a companion paper(Diémoz et al., 2019)~~the companion paper, exploiting the complete observational dataset over the period 2015–2017, complemented by a long-term simulation by the FARM model. This wider dataset, inspected by statistical techniques and classification schemes, allowed a quantitative evaluation of the long-term impact of the aerosol transported from the Po basin to the air quality in the northwestern Alps. Still, future work is needed to investigate possible local and basin-wide strategies to effectively mitigate this impact.

Data availability. The ALC data are available upon request from the Alice-net (alicenet@isac.cnr.it) and E-PROFILE (http://data.ceda.ac.uk/badc/eprofile/data/) networks. The sun photometer data can be downloaded from the EuroSkyRad network web site (http://www.euroskyrad.net/index.html) after authentication (credentials may be requested to M. Campanelli, m.campanelli@isac.cnr.it). The measurements from ARPA air quality surface network are available at the web page http://www.arpa.vda.it/it/aria/la-qualit%C3%A0-dell-aria/stazioni-di-monitoraggio/inquinanti-export-dati. The wind data in Milan refer to the ClimateNetwork®weather station Milan Bicocca and were kindly provided by Fondazione OMD. The weather data from the Aosta–Saint Christophe and Saint-Denis stations can be retrieved from http://cf.regione.vda.it/richiesta_dati.php upon request to Centro Funzionale della Valle d'Aosta. The MAIAC data were made available by Alexei Lyapustin (NASA). The rest of the data can be asked to the corresponding author (h.diemoz@arpa.vda.it).

Author contributions. HD, FB and GPG conceived and designed the study and contributed to the interpretation of the results. TM supplied the meteorological observations and numerical weather predictions. GP performed the chemical transport simulations. DD provided the ALC functional relationships and assistance on the Rayleigh ALC calibration with inputs from MH. SP carried out the EC/OC analyses and IKFT helped with the interpretation of the chemical speciation. MC supplied the POM calibration factors. FB and LDC prepared the satellite radiometer data. LDL and LF provided the ALC data from Milan. HD analysed the data and wrote the manuscript with contribution from FB, GPG, and all co-authors.

Competing interests. The authors declare that they have no conflict of interest.

Acknowledgements. The authors would like to thank: A. Brunier, G. Lupato, P. Proment, S. Vaccari, and M.C. Gibellino (ARPA Valle d'Aosta) for carrying out the chemical analyses; M. Pignet, C. Tarricone, and M. Zublena (ARPA Valle d'Aosta) for providing the data from the air quality surface network; Fondazione OMD and Centro Funzionale della Valle d'Aosta for the additional meteorological series; ~~Alexei~~

~~Lyapustin~~ A. Lyapustin (NASA) for the MAIAC data; S. Ferrarese (Turin University) for the exchange about high-resolution models in the "terra incognita" regime. The authors would like to acknowledge the valuable contribution of the discussions in the working group meetings organised by COST Action ES1303 (TOPROF). They also gratefully acknowledge the Institute for Atmospheric and Climate Science, ETH Zurich, Switzerland for the provision of the LAGRANTO software used in this publication. The contribution of L. Ferrero is an outcome of GEMMA Center, in the framework of Project MIUR – Dipartimenti di Eccellenza 2018–2022.

References

Adam, M., Putaud, J. P., Martins dos Santos, S., Dell'Acqua, A., and Gruening, C.: Aerosol hygroscopicity at a regional background site (Ispra) in Northern Italy, Atmos. Chem. Phys., 12, 5703–5717, https://doi.org/10.5194/acp-12-5703-2012, 2012.

Agnesod, G., Moulin, P.-A., Pession, G., Villard, H., and Zublena, M.: Étude Air Espace Mont-Blanc - Rapport Technique, Tech. rep., Espace Mont Blanc, http://www.arpa.vda.it/images/stories/ARPA/aria/progetti/progairmb_agnesod_2003.pdf, 2003.

Aksoyoglu, S., Ciarelli, G., El-Haddad, I., Baltensperger, U., and Prévôt, A. S. H.: Secondary inorganic aerosols in Europe: sources and the significant influence of biogenic VOC emissions, especially on ammonium nitrate, Atmos. Chem. Phys., 17, 7757–7773, https://doi.org/10.5194/acp-17-7757-2017, 2017.

Anfossi, D., Cassardo, C., Giraud, C., Longhetto, A., Villone, B., Bacci, P., Bonelli, P., Carboni, G., Bonafè, U., Bonasoni, P., and Giovanelli, G.: Experimental study of transalpine transport of trace effluents: a comparison with synoptic trajectories of airflow, Nuovo Ciment. C, 11, 489–526, https://doi.org/10.1007/BF02506997, 1988.

Angelini, F., Barnaba, F., Landi, T. C., Caporaso, L., and Gobbi, G. P.: Study of atmospheric aerosols and mixing layer by LIDAR, Radiat. Prot. Dosim., 137, 275–279, https://doi.org/10.1093/rpd/ncp219, 2009.

Bacco, D., Trentini, A., Minguzzi, E., Amorati, R., Zigola, C., Deserti, M., and Poluzzi, V.: Chimica del particolato e meteo, un'analisi sul campo, Ecoscienza, 1, https://www.arpae.it/cms3/documenti/_cerca_doc/ecoscienza/ecoscienza2017_1/bacco_et_al_es2017_01.pdf, 2017.

Bader, D. and Whiteman, C.: Numerical Simulation of Cross-Valley Plume Dispersion during the Morning Transition Period, J. Appl. Meteorol., 28, 652–664, https://doi.org/10.1175/1520-0450(1989)028<0652:NSOCVP>2.0.CO;2, 1989.

Baldauf, M., Seifert, A., Förstner, J., Majewski, D., Raschendorfer, M., and Reinhardt, T.: Operational Convective-Scale Numerical Weather Prediction with the COSMO Model: Description and Sensitivities, Mon. Weather Rev., 139, 3887–3905, https://doi.org/10.1175/MWR-D-10-05013.1, 2011.

Barnaba, F. and Gobbi, G. P.: Lidar estimation of tropospheric aerosol extinction, surface area and volume: Maritime and desert-dust cases, J. Geophys. Res., 106, 3005–3018, https://doi.org/10.1029/2000JD900492, 2001.

Barnaba, F. and Gobbi, G. P.: Modeling the Aerosol Extinction versus Backscatter Relationship for Lidar Applications: Maritime and Continental Conditions, J. Atmos. Ocean. Tech., 21, 428–442, https://doi.org/10.1175/1520-0426(2004)021<0428:MTAEVB>2.0.CO;2, 2004.

Barnaba, F., Gobbi, G. P., and de Leeuw, G.: Aerosol stratification, optical properties and radiative forcing in Venice (Italy) during ADRIEX, Q. J. Roy. Meteor. Soc., 133, 47–60, https://doi.org/10.1002/qj.91, 2007.

Barnaba, F., Putaud, J. P., Gruening, C., dell'Acqua, A., and Dos Santos, S.: Annual cycle in co-located in situ, total-column, and height-resolved aerosol observations in the Po Valley (Italy): Implications for ground-level particulate matter mass concentration estimation from remote sensing, J. Geophys. Res., 115, https://doi.org/10.1029/2009JD013002, 2010.

Belis, C., Blond, N., Bouland, C., Carnevale, C., Clappier, A., Douros, J., Fragkou, E., Guariso, G., Miranda, A. I., Nahorski, Z., Pisoni, E., Ponche, J.-L., Thunis, P., Viaene, P., and Volta, M.: Strengths and Weaknesses of the Current EU Situation, pp. 69–83, Springer International Publishing, https://doi.org/10.1007/978-3-319-33349-6_4, 2017.

Bigi, A. and Ghermandi, G.: Trends and variability of atmospheric $PM_{2.5}$ and $PM_{10-2.5}$ concentration in the Po Valley, Italy, Atmos. Chem. Phys., 16, 15 777–15 788, https://doi.org/10.5194/acp-16-15777-2016, 2016.

Binkowski, F.: Science Algorithms of the EPA Models-3 Community Multiscale Air Quality (CMAQ) Modeling System, vol. EPA/600/R-99/030, chap. The aerosol portion of Models-3 CMAQ,, DW Byun, and JKS Ching (Eds), 1999.

Birch, M. E. and Cary, R. A.: Elemental Carbon-Based Method for Monitoring Occupational Exposures to Particulate Diesel Exhaust, Aerosol Sci. Tech., 25, 221–241, https://doi.org/10.1080/02786829608965393, 1996.

Borghi, S. and Giuliacci, M.: Circulation features driven by diurnal heating in the lower atmospheric layers of the Po Valley, Nuovo Cimento C, 3, 1–16, https://doi.org/10.1007/BF02509187, 1980.

Bourgeois, I., Savarino, J., Caillon, N., Angot, H., Barbero, A., Delbart, F., Voisin, D., and Clément, J.-C.: Tracing the Fate of Atmospheric Nitrate in a Subalpine Watershed Using Δ17O, Environ. Sci. Tech., 52, 5561–5570, https://doi.org/10.1021/acs.est.7b02395, 2018.

Bucci, S., Cristofanelli, P., Decesari, S., Marinoni, A., Sandrini, S., Größ, J., Wiedensohler, A., Di Marco, C. F., Nemitz, E., Cairo, F., Di Liberto, L., and Fierli, F.: Vertical distribution of aerosol optical properties in the Po Valley during the 2012 summer campaigns, Atmos. Chem. Phys., 18, 5371–5389, https://doi.org/10.5194/acp-18-5371-2018, 2018.

Burkhardt, J., Zinsmeister, D., Grantz, D. A., Vidic, S., Sutton, M. A., Hunsche, M., and Pariyar, S.: Camouflaged as degraded wax: hygroscopic aerosols contribute to leaf desiccation, tree mortality, and forest decline, Environ. Res. Lett., 13, 085 001, https://doi.org/10.1088/1748-9326/aad346, 2018.

Calori, G., Silibello, C., and Marras, G.: FARM (Flexible Air quality Regional Model) Model formulation and user's Manual, Arianet, 4.7 edn., 2014.

Campanelli, M., Estellés, V., Tomasi, C., Nakajima, T., Malvestuto, V., and Martínez-Lozano, J. A.: Application of the SKYRAD Improved Langley plot method for the in situ calibration of CIMEL Sun-sky photometers, Appl. Opt., 46, 2688–2702, https://doi.org/10.1364/AO.46.002688, 2007.

Campanelli, M., Mascitelli, A., Sanò, P., Diémoz, H., Estellés, V., Federico, S., Iannarelli, A. M., Fratarcangeli, F., Mazzoni, A., Realini, E., Crespi, M., Bock, O., Martínez-Lozano, J. A., and Dietrich, S.: Precipitable water vapour content from ESR/SKYNET sun–sky radiometers: validation against GNSS/GPS and AERONET over three different sites in Europe, Atmos. Meas. Tech., 11, 81–94, https://doi.org/10.5194/amt-11-81-2018, 2018.

Carbone, C., Decesari, S., Mircea, M., Giulianelli, L., Finessi, E., Rinaldi, M., Fuzzi, S., Marinoni, A., Duchi, R., Perrino, C., Sargolini, T., Vardè, M., Sprovieri, F., Gobbi, G., Angelini, F., and Facchini, M.: Size-resolved aerosol chemical composition over the Italian Peninsula during typical summer and winter conditions, Atmos. Environ., 44, 5269 – 5278, https://doi.org/10.1016/j.atmosenv.2010.08.008, 2010.

Carbone, C., Decesari, S., Paglione, M., Giulianelli, L., Rinaldi, M., Marinoni, A., Cristofanelli, P., Didiodato, A., Bonasoni, P., Fuzzi, S., and Facchini, M. C.: 3-year chemical composition of free tropospheric PM1 at the Mt. Cimone GAW global station – South Europe – 2165 m a.s.l., Atmos. Environ., 87, 218 – 227, https://doi.org/10.1016/j.atmosenv.2014.01.048, 2014.

Carslaw, K. S., Boucher, O., Spracklen, D. V., Mann, G. W., Rae, J. G. L., Woodward, S., and Kulmala, M.: A review of natural aerosol interactions and feedbacks within the Earth system, Atmos. Chem. Phys., 10, 1701–1737, https://doi.org/10.5194/acp-10-1701-2010, 2010.

Carter, W.: Documentation of the SAPRC-99 Chemical Mechanism for VOC Reactivity Assessment. Final Report to California Air Resources Board, Contract 92-329 and 95-308, SAPRC, Tech. rep., University of California, Riverside,CA, http://www.engr.ucr.edu/~carter/pubs/s99doc.pdf, 2000.

Caserini, S., Giani, P., Cacciamani, C., Ozgen, S., and Lonati, G.: Influence of climate change on the frequency of daytime temperature inversions and stagnation events in the Po Valley: historical trend and future projections, Atmos. Res., 184, 15 – 23, https://doi.org/https://doi.org/10.1016/j.atmosres.2016.09.018, 2017.

Cavalli, F., Viana, M., Yttri, K. E., Genberg, J., and Putaud, J.-P.: Toward a standardised thermal-optical protocol for measuring atmospheric organic and elemental carbon: the EUSAAR protocol, Atmos. Meas. Tech., 3, 79–89, https://doi.org/10.5194/amt-3-79-2010, 2010.

Cesaroni, G., Badaloni, C., Gariazzo, C., Stafoggia, M., Sozzi, R., Davoli, M., and Forastiere, F.: Long-term exposure to urban air pollution and mortality in a cohort of more than a million adults in Rome, Environ. Health Persp., 121, 324, https://doi.org/10.1289/ehp.1205862, 2013.

Charron, A., Harrison, R. M., Moorcroft, S., and Booker, J.: Quantitative interpretation of divergence between PM10 and PM2.5 mass measurement by TEOM and gravimetric (Partisol) instruments, Atmos. Environ., 38, 415 – 423, https://doi.org/10.1016/j.atmosenv.2003.09.072, 2004.

Chu, D. A., Kaufman, Y. J., Zibordi, G., Chern, J. D., Mao, J., Li, C., and Holben, B. N.: Global monitoring of air pollution over land from the Earth Observing System-Terra Moderate Resolution Imaging Spectroradiometer (MODIS), J. Geophys. Res., 108, https://doi.org/10.1029/2002JD003179, 2003.

Chudnovsky, A. A., Koutrakis, P., Kloog, I., Melly, S., Nordio, F., Lyapustin, A., Wang, Y., and Schwartz, J.: Fine particulate matter predictions using high resolution Aerosol Optical Depth (AOD) retrievals, Atmos. Environ., 89, 189–198, https://doi.org/10.1016/j.atmosenv.2014.02.019, 2014.

Clerici, M. and Mélin, F.: Aerosol direct radiative effect in the Po Valley region derived from AERONET measurements, Atmos. Chem. Phys., 8, 4925–4946, https://doi.org/10.5194/acp-8-4925-2008, 2008.

Collaud Coen, M., Andrews, E., Aliaga, D., Andrade, M., Angelov, H., Bukowiecki, N., Ealo, M., Fialho, P., Flentje, H., Hallar, A. G., Hooda, R., Kalapov, I., Krejci, R., Lin, N.-H., Marinoni, A., Ming, J., Nguyen, N. A., Pandolfi, M., Pont, V., Ries, L., Rodríguez, S., Schauer, G., Sellegri, K., Sharma, S., Sun, J., Tunved, P., Velasquez, P., and Ruffieux, D.: Identification of topographic features influencing aerosol observations at high altitude stations, Atmos. Chem. Phys., 18, 12 289–12 313, https://doi.org/10.5194/acp-18-12289-2018, 2018.

Cong, Z., Kawamura, K., Kang, S., and Fu, P.: Penetration of biomass-burning emissions from South Asia through the Himalayas: new insights from atmospheric organic acids, Scientific reports, 5, https://doi.org/10.1038/srep09580, 2015.

Cristofanelli, P., Marinoni, A., Arduini, J., Bonafè, U., Calzolari, F., Colombo, T., Decesari, S., Duchi, R., Facchini, M. C., Fierli, F., Finessi, E., Maione, M., Chiari, M., Calzolai, G., Messina, P., Orlandi, E., Roccato, F., and Bonasoni, P.: Significant variations of trace gas composition and aerosol properties at Mt. Cimone during air mass transport from North Africa – contributions from wildfire emissions and mineral dust, Atmos. Chem. Phys., 9, 4603–4619, https://doi.org/10.5194/acp-9-4603-2009, 2009.

Cugerone, K., De Michele, C., Ghezzi, A., Gianelle, V., and Gilardoni, S.: On the functional form of particle number size distributions: influence of particle source and meteorological variables, Atmos. Chem. Phys., 18, 4831–4842, https://doi.org/10.5194/acp-18-4831-2018, 2018.

Curci, G., Ferrero, L., Tuccella, P., Barnaba, F., Angelini, F., Bolzacchini, E., Carbone, C., Denier van der Gon, H. A. C., Facchini, M. C., Gobbi, G. P., Kuenen, J. P. P., Landi, T. C., Perrino, C., Perrone, M. G., Sangiorgi, G., and Stocchi, P.: How much is particulate matter near the ground influenced by upper-level processes within and above the PBL? A summertime case study in Milan (Italy) evidences the distinctive role of nitrate, Atmos. Chem. Phys., 15, 2629–2649, https://doi.org/10.5194/acp-15-2629-2015, 2015.

D'Angelo, L., Rovelli, G., Casati, M., Sangiorgi, G., Perrone, M. G., Bolzacchini, E., and Ferrero, L.: Seasonal behavior of PM2.5 deliquescence, crystallization, and hygroscopic growth in the Po Valley (Milan): Implications for remote sensing applications, Atmos. Res., 176-177, 87 – 95, https://doi.org/10.1016/j.atmosres.2016.02.011, http://www.sciencedirect.com/science/article/pii/S016980951630028X, 2016.

de Freitas, C. R.: Tourism climatology: evaluating environmental information for decision making and business planning in the recreation and tourism sector, Int. J. Biometeorol., 48, 45–54, https://doi.org/10.1007/s00484-003-0177-z, 2003.

De Wekker, S. F. J., Kossmann, M., Knievel, J. C., Giovannini, L., Gutmann, E. D., and Zardi, D.: Meteorological Applications Benefiting from an Improved Understanding of Atmospheric Exchange Processes over Mountains, Atmosphere, 9, https://doi.org/10.3390/atmos9100371, 2018.

Decesari, S., Allan, J., Plass-Duelmer, C., Williams, B. J., Paglione, M., Facchini, M. C., O'Dowd, C., Harrison, R. M., Gietl, J. K., Coe, H., Giulianelli, L., Gobbi, G. P., Lanconelli, C., Carbone, C., Worsnop, D., Lambe, A. T., Ahern, A. T., Moretti, F., Tagliavini, E., Elste, T., Gilge, S., Zhang, Y., and Dall'Osto, M.: Measurements of the aerosol chemical composition and mixing state in the Po Valley using multiple spectroscopic techniques, Atmos. Chem. Phys., 14, 12 109–12 132, https://doi.org/10.5194/acp-14-12109-2014, 2014.

Della Ceca, L., García Ferreyra, M. F., Lyapustin, A., Chudnovsky, A., Otero, L., Carreras, H., and Barnaba, F.: Satellite-based view of the aerosol spatial and temporal variability in the Córdoba region (Argentina) using over ten years of high-resolution data, ISPRS J. Photogramm., https://doi.org/https://doi.org/10.1016/j.isprsjprs.2018.08.016, 2018.

Dhungel, S., Kathayat, B., Mahata, K., and Panday, A.: Transport of regional pollutants through a remote trans-Himalayan valley in Nepal, Atmos. Chem. Phys., 18, 1203–1216, https://doi.org/10.5194/acp-18-1203-2018, 2018.

Diémoz, H., Siani, A. M., Casale, G. R., di Sarra, A., Serpillo, B., Petkov, B., Scaglione, S., Bonino, A., Facta, S., Fedele, F., Grifoni, D., Verdi, L., and Zipoli, G.: First national intercomparison of solar ultraviolet radiometers in Italy, Atmos. Meas. Tech., 4, 1689–1703, https://doi.org/10.5194/amt-4-1689-2011, 2011.

Diémoz, H., Campanelli, M., and Estellés, V.: One Year of Measurements with a POM-02 Sky Radiometer at an Alpine EuroSkyRad Station, J. Meteorol. Soc. Jpn., 92A, 1–16, https://doi.org/10.2151/jmsj.2014-A01, 2014a.

Diémoz, H., Siani, A. M., Redondas, A., Savastiouk, V., McElroy, C. T., Navarro-Comas, M., and Hase, F.: Improved retrieval of nitrogen dioxide (NO_2) column densities by means of MKIV Brewer spectrophotometers, Atmos. Meas. Tech., 7, 4009–4022, https://doi.org/10.5194/amt-7-4009-2014, 2014b.

Diémoz, H., Gobbi, G. P., Magri, T., Pession, G., Pittavino, S., Tombolato, I. K. F., Campanelli, M., and Barnaba, F.: Transport of Po Valley aerosol pollution to the northwestern Alps. Part 2: long-term impact on air quality, submitted to Atmos. Chem. Phys., 2019.

Dionisi, D., Barnaba, F., Diémoz, H., Di Liberto, L., and Gobbi, G. P.: A multiwavelength numerical model in support of quantitative retrievals of aerosol properties from automated lidar ceilometers and test applications for AOT and PM_{10} estimation, Atmos. Meas. Tech., 11, 6013–6042, https://doi.org/10.5194/amt-11-6013-2018, 2018.

Dosio, A., Galmarini, S., and Graziani, G.: Simulation of the circulation and related photochemical ozone dispersion in the Po plains (northern Italy): Comparison with the observations of a measuring campaign, J. Geophys. Res., 107, LOP 2–1–LOP 2–24, https://doi.org/10.1029/2000JD000046, 2002.

EEA: Air Quality in Europe - 2015 Report, Tech. rep., https://doi.org/10.2800/62459, 2015.

EEA: Air Quality in Europe - 2017 Report, Tech. rep., https://doi.org/10.2800/850018, 2017.

EMEP: Transboundary particulate matter, photo-oxidants, acidifying and eutrophying components, Tech. rep., MSC-W, CCC and CEIP, 2016.

Emili, E., Lyapustin, A., Wang, Y., Popp, C., Korkin, S., Zebisch, M., Wunderle, S., and Petitta, M.: High spatial resolution aerosol retrieval with MAIAC: Application to mountain regions, J. Geophys. Res., 116, https://doi.org/10.1029/2011JD016297, 2011.

Estellés, V., Campanelli, M., Smyth, T. J., Utrillas, M. P., and Martínez-Lozano, J. A.: Evaluation of the new ESR network software for the retrieval of direct sun products from CIMEL CE318 and PREDE POM01 sun-sky radiometers, Atmos. Chem. Phys., 12, 11 619–11 630, https://doi.org/10.5194/acp-12-11619-2012, 2012.

EU Commission: Directive 2008/50/EC of the European Parliament and of the Council of 21 May 2008 on ambient air quality and cleaner air for Europe, Official Journal of the European Union, pp. L152/1–44, 2008.

Federico, S., Torcasio, R. C., Sanò, P., Casella, D., Campanelli, M., Meirink, J. F., Wang, P., Vergari, S., Diémoz, H., and Dietrich, S.: Comparison of hourly surface downwelling solar radiation estimated from MSG–SEVIRI and forecast by the RAMS model with pyranometers over Italy, Atmos. Meas. Tech., 10, 2337–2352, https://doi.org/10.5194/amt-10-2337-2017, 2017.

Fernald, F. G.: Analysis of atmospheric lidar observations: some comments, Appl. Opt., 23, 652–653, https://doi.org/10.1364/AO.23.000652, 1984.

Ferrero, L., Perrone, M. G., Petraccone, S., Sangiorgi, G., Ferrini, B. S., Lo Porto, C., Lazzati, Z., Cocchi, D., Bruno, F., Greco, F., Riccio, A., and Bolzacchini, E.: Vertically-resolved particle size distribution within and above the mixing layer over the Milan metropolitan area, Atmos. Chem. Phys., 10, 3915–3932, https://doi.org/10.5194/acp-10-3915-2010, 2010.

Ferrero, L., Castelli, M., Ferrini, B. S., Moscatelli, M., Perrone, M. G., Sangiorgi, G., D'Angelo, L., Rovelli, G., Moroni, B., Scardazza, F., Močnik, G., Bolzacchini, E., Petitta, M., and Cappelletti, D.: Impact of black carbon aerosol over Italian basin valleys: high-resolution measurements along vertical profiles, radiative forcing and heating rate, Atmos. Chem. Phys., 14, 9641–9664, https://doi.org/10.5194/acp-14-9641-2014, 2014.

Ferrero, L., Močnik, G., Cogliati, S., Gregorič, A., Colombo, R., and Bolzacchini, E.: Heating Rate of Light Absorbing Aerosols: Time-Resolved Measurements, the Role of Clouds, and Source Identification, Environ. Sci. Tech., 52, 3546–3555, https://doi.org/10.1021/acs.est.7b04320, 2018.

Finardi, S. and Pellegrini, U.: Systematic analysis of meteorological conditions causing severe urban air pollution episodes in the central Po Valley, in: 9th Int. Conf. on Harmonisation within Atmospheric Dispersion Modelling for Regulatory Purposes, http://www.harmo.org/Conferences/proceedings/_Garmisch/publishedSections/6.13.pdf, 2004.

Finardi, S., Silibello, C., D'Allura, A., and Radice, P.: Analysis of pollutants exchange between the Po Valley and the surrounding European region, Urban Clim., 10, 682 – 702, https://doi.org/https://doi.org/10.1016/j.uclim.2014.02.002, source apportionment and modelling of urban air pollution, 2014.

Freney, E. J., Sellegri, K., Canonaco, F., Boulon, J., Hervo, M., Weigel, R., Pichon, J. M., Colomb, A., Prévôt, A. S. H., and Laj, P.: Seasonal variations in aerosol particle composition at the puy-de-Dôme research station in France, Atmos. Chem. Phys., 11, 13 047–13 059, https://doi.org/10.5194/acp-11-13047-2011, 2011.

Fuzzi, S., Baltensperger, U., Carslaw, K., Decesari, S., Denier van der Gon, H., Facchini, M. C., Fowler, D., Koren, I., Langford, B., Lohmann, U., Nemitz, E., Pandis, S., Riipinen, I., Rudich, Y., Schaap, M., Slowik, J. G., Spracklen, D. V., Vignati, E., Wild, M., Williams, M., and Gilardoni, S.: Particulate matter, air quality and climate: lessons learned and future needs, Atmos. Chem. Phys., 15, 8217–8299, https://doi.org/10.5194/acp-15-8217-2015, 2015.

Gariazzo, C., Silibello, C., Finardi, S., Radice, P., Piersanti, A., Calori, G., Cecinato, A., Perrino, C., Nussio, F., Cagnoli, M., et al.: A gas/aerosol air pollutants study over the urban area of Rome using a comprehensive chemical transport model, Atmos. Environ., 41, 7286–7303, https://doi.org/10.1016/j.atmosenv.2007.05.018, 2007.

Gilardoni, S., Massoli, P., Giulianelli, L., Rinaldi, M., Paglione, M., Pollini, F., Lanconelli, C., Poluzzi, V., Carbone, S., Hillamo, R., Russell, L. M., Facchini, M. C., and Fuzzi, S.: Fog scavenging of organic and inorganic aerosol in the Po Valley, Atmos. Chem. Phys., 14, 6967–6981, https://doi.org/10.5194/acp-14-6967-2014, 2014.

Gilardoni, S., Massoli, P., Paglione, M., Giulianelli, L., Carbone, C., Rinaldi, M., Decesari, S., Sandrini, S., Costabile, F., Gobbi, G. P., Pietrogrande, M. C., Visentin, M., Scotto, F., Fuzzi, S., and Facchini, M. C.: Direct observation of aqueous secondary organic aerosol from biomass-burning emissions, P. Natl. A. Sci., 113, 10 013–10 018, https://doi.org/10.1073/pnas.1602212113, 2016.

Gohm, A., Harnisch, F., Vergeiner, J., Obleitner, F., Schnitzhofer, R., Hansel, A., Fix, A., Neininger, B., Emeis, S., and Schäfer, K.: Air Pollution Transport in an Alpine Valley: Results From Airborne and Ground-Based Observations, Bound.-Lay. Meteorol., 131, 441–463, https://doi.org/10.1007/s10546-009-9371-9, 2009.

Green, D. C., Fuller, G. W., and Baker, T.: Development and validation of the volatile correction model for PM10 – An empirical method for adjusting TEOM measurements for their loss of volatile particulate matter, Atmos. Environ., 43, 2132 – 2141, https://doi.org/10.1016/j.atmosenv.2009.01.024, 2009.

Guariso, G. and Volta, M.: Air Quality Integrated Assessment: A European Perspective, Springer, https://doi.org/10.1007/978-3-319-33349-6, 2017.

Haeffelin, M., Angelini, F., Morille, Y., Martucci, G., Frey, S., Gobbi, G. P., Lolli, S., O'Dowd, C. D., Sauvage, L., Xueref-Rémy, I., Wastine, B., and Feist, D. G.: Evaluation of Mixing-Height Retrievals from Automatic Profiling Lidars and Ceilometers in View of Future Integrated Networks in Europe, Bound.-Lay. Meteorol., 143, 49–75, https://doi.org/10.1007/s10546-011-9643-z, 2012.

Henne, S., Furger, M., Nyeki, S., Steinbacher, M., Neininger, B., de Wekker, S. F. J., Dommen, J., Spichtinger, N., Stohl, A., and Prévôt, A. S. H.: Quantification of topographic venting of boundary layer air to the free troposphere, Atmos. Chem. Phys., 4, 497–509, https://doi.org/10.5194/acp-4-497-2004, 2004.

Henne, S., Furger, M., and Prévôt, A. S. H.: Climatology of Mountain Venting–Induced Elevated Moisture Layers in the Lee of the Alps, J. Appl. Meteorol., 44, 620–633, https://doi.org/10.1175/JAM2217.1, 2005.

Italian Ministry of the Environment: Nuovo accordo di programma per l'adozione coordinata e congiunta di misure per il miglioramento della qualità dell'aria nel bacino padano, Legislative acts of the Lombardy region, http://www.regione.lombardia.it/wps/wcm/connect/5f880847-0a8c-4f20-b220-0685af81d03c/allegato+dgr+6675.pdf?MOD=AJPERES&CACHEID=5f880847-0a8c-4f20-b220-0685af81d03c, 2018.

Kambezidis, H. and Kaskaoutis, D.: Aerosol climatology over four AERONET sites: An overview, Atmos. Environ., 42, 1892 – 1906, https://doi.org/10.1016/j.atmosenv.2007.11.013, 2008.

Kaufman, Y. and Tanré, D.: Algorithm for remote sensing of tropospheric aerosol form MODIS, MODIS ATBD MOD02, 9, 1–85, Tech. rep., 1998.

Kazadzis, S., Kouremeti, N., Diémoz, H., Gröbner, J., Forgan, B. W., Campanelli, M., Estellés, V., Lantz, K., Michalsky, J., Carlund, T., Cuevas, E., Toledano, C., Becker, R., Nyeki, S., Kosmopoulos, P. G., Tatsiankou, V., Vuilleumier, L., Denn, F. M., Ohkawara, N., Ijima, O., Goloub, P., Raptis, P. I., Milner, M., Behrens, K., Barreto, A., Martucci, G., Hall, E., Wendell, J., Fabbri, B. E., and Wehrli, C.: Results from the Fourth WMO Filter Radiometer Comparison for aerosol optical depth measurements, Atmos. Chem. Phys., 18, 3185–3201, https://doi.org/10.5194/acp-18-3185-2018, 2018.

Khan, M., Masiol, M., Formenton, G., Di Gilio, A., de Gennaro, G., Agostinelli, C., and Pavoni, B.: Carbonaceous PM2.5 and secondary organic aerosol across the Veneto region (NE Italy), Sci. Total Environ., 542, 172 – 181, https://doi.org/https://doi.org/10.1016/j.scitotenv.2015.10.103, 2016.

Khatri, P. and Takamura, T.: An Algorithm to Screen Cloud-Affected Data for Sky Radiometer Data Analysis, J. Meteorol. Soc. Jpn., 87, 189–204, https://doi.org/10.2151/jmsj.87.189, 2009.

Kim, H., Zhang, Q., and Heo, J.: Influence of intense secondary aerosol formation and long-range transport on aerosol chemistry and properties in the Seoul Metropolitan Area during spring time: results from KORUS-AQ, Atmos. Chem. Phys., 18, 7149–7168, https://doi.org/10.5194/acp-18-7149-2018, 2018.

Klett, J. D.: Lidar inversion with variable backscatter/extinction ratios, Appl. Opt., 24, 1638–1643, https://doi.org/10.1364/AO.24.001638, 1985.

Lang, M. N., Gohm, A., and Wagner, J. S.: The impact of embedded valleys on daytime pollution transport over a mountain range, Atmos. Chem. Phys., 15, 11 981–11 998, https://doi.org/10.5194/acp-15-11981-2015, 2015.

Larsen, B., Gilardoni, S., Stenström, K., Niedzialek, J., Jimenez, J., and Belis, C.: Sources for PM air pollution in the Po Plain, Italy: II. Probabilistic uncertainty characterization and sensitivity analysis of secondary and primary sources, Atmos. Environ., 50, 203 – 213, https://doi.org/https://doi.org/10.1016/j.atmosenv.2011.12.038, 2012.

Lau, W. K., Kim, M.-K., Kim, K.-M., and Lee, W.-S.: Enhanced surface warming and accelerated snow melt in the Himalayas and Tibetan Plateau induced by absorbing aerosols, Environ. Res. Lett., 5, 025 204, https://doi.org/10.1088/1748-9326/5/2/025204, 2010.

Lehner, M. and Rotach, M. W.: Current Challenges in Understanding and Predicting Transport and Exchange in the Atmosphere over Mountainous Terrain, Atmosphere, 9, https://doi.org/10.3390/atmos9070276, 2018.

Lim, Y. B., Seo, J., Kim, J. Y., and Turpin, B. J.: Multiday haze in the East Asia: Transport and chemical aging of hygroscopic particles, Atmos. Chem. Phys. Discuss., 2018, 1–28, https://doi.org/10.5194/acp-2018-364, 2018.

Lyapustin, A., Wang, Y., Laszlo, I., Kahn, R., Korkin, S., Remer, L., Levy, R., and Reid, J. S.: Multiangle implementation of atmospheric correction (MAIAC): 2. Aerosol algorithm, J. Geophys. Res., 116, https://doi.org/10.1029/2010JD014986, 2011.

Lyapustin, A., Wang, Y., Laszlo, I., and Korkin, S.: Improved cloud and snow screening in MAIAC aerosol retrievals using spectral and spatial analysis, Atmos. Meas. Tech., 5, 843–850, https://doi.org/10.5194/amt-5-843-2012, 2012.

Manara, V., Bassi, M., Brunetti, M., Cagnazzi, B., and Maugeri, M.: 1990–2016 surface solar radiation variability and trend over the Piedmont region (northwest Italy), Theor. Appl. Climatol., https://doi.org/10.1007/s00704-018-2521-6, 2018.

Mélin, F. and Zibordi, G.: Aerosol variability in the Po Valley analyzed from automated optical measurements, Geophy. Res. Lett., 32, https://doi.org/10.1029/2004GL021787, 2005.

Mercalli, L., Castellano, C., Cat Berro, D., and Di Napoli, G.: Atlante climatico della Valle d'Aosta, vol. 2, Società Meteorologica Subalpina, 2003.

Moroni, B., Castellini, S., Crocchianti, S., Piazzalunga, A., Fermo, P., Scardazza, F., and Cappelletti, D.: Ground-based measurements of long-range transported aerosol at the rural regional background site of Monte Martano (Central Italy), Atmos. Res., 155, 26 – 36, https://doi.org/10.1016/j.atmosres.2014.11.021, 2015.

Nakajima, T., Tonna, G., Rao, R., Boi, P., Kaufman, Y., and Holben, B.: Use of sky brightness measurements from ground for remote sensing of particulate polydispersions, Appl. Opt., 35, 2672–2686, https://doi.org/10.1364/AO.35.002672, 1996.

Neftel, A., Spirig, C., Prévôt, A. S. H., Furger, M., Stutz, J., Vogel, B., and Hjorth, J.: Sensitivity of photooxidant production in the Milan Basin: An overview of results from a EUROTRAC-2 Limitation of Oxidant Production field experiment, J. Geophys. Res., 107, LOP 1–1–LOP 1–10, https://doi.org/10.1029/2001JD001263, 2002.

Nenes, A., Pandis, S. N., and Pilinis, C.: ISORROPIA: A new thermodynamic equilibrium model for multiphase multicomponent inorganic aerosols, Aquat. Geochem., 4, 123–152, https://doi.org/10.1023/A:1009604003981, 1998.

Nyeki, S., Eleftheriadis, K., Baltensperger, U., Colbeck, I., Fiebig, M., Fix, A., Kiemle, C., Lazaridis, M., and Petzold, A.: Airborne Lidar and in-situ Aerosol Observations of an Elevated Layer, Leeward of the European Alps and Apennines, Geophys. Res. Lett., 29, 33–1–33–4, https://doi.org/10.1029/2002GL014897, 2002.

Osborne, S. R., Haywood, J. M., and Bellouin, N.: In situ and remote-sensing measurements of the mean microphysical and optical properties of industrial pollution aerosol during ADRIEX, Q. J. Roy. Meteor. Soc., 133, 17–32, https://doi.org/10.1002/qj.92, 2007.

Patashnick, H. and Rupprecht, E. G.: Continuous PM-10 Measurements Using the Tapered Element Oscillating Microbalance, J. Air Waste Manage., 41, 1079–1083, https://doi.org/10.1080/10473289.1991.10466903, 1991.

Pletscher, K., Weiss, M., and Moelter, L.: Simultaneous determination of PM fractions, particle number and particle size distribution in high time resolution applying one and the same optical measurement technique, Gefahrst. Reinhalt. L., 76, 425–436, http://www.gefahrstoffe.de/gest/article.php?data[article_id]=86622, 2016.

Putaud, J.-P., Dingenen, R. V., Alastuey, A., Bauer, H., Birmili, W., Cyrys, J., Flentje, H., Fuzzi, S., Gehrig, R., Hansson, H., Harrison, R., Herrmann, H., Hitzenberger, R., Hüglin, C., Jones, A., Kasper-Giebl, A., Kiss, G., Kousa, A., Kuhlbusch, T., Löschau, G., Maenhaut, W., Molnar, A., Moreno, T., Pekkanen, J., Perrino, C., Pitz, M., Puxbaum, H., Querol, X., Rodriguez, S., Salma, I., Schwarz, J., Smolik, J., Schneider, J., Spindler, G., ten Brink, H., Tursic, J., Viana, M., Wiedensohler, A., and Raes, F.: A European aerosol phenomenology – 3: Physical and chemical characteristics of particulate matter from 60 rural, urban, and kerbside sites across Europe, Atmos. Environ., 44, 1308 – 1320, https://doi.org/10.1016/j.atmosenv.2009.12.011, 2010.

Rampanelli, G., Zardi, D., and Rotunno, R.: Mechanisms of Up-Valley Winds, J. Atmos. Sci., 61, 3097–3111, https://doi.org/10.1175/JAS-3354.1, 2004.

Raut, J.-C. and Chazette, P.: Assessment of vertically-resolved PM_{10} from mobile lidar observations, Atmos. Chem. Phys., 9, 8617–8638, https://doi.org/10.5194/acp-9-8617-2009, 2009.

Remer, L. A., Mattoo, S., Levy, R. C., and Munchak, L. A.: MODIS 3 km aerosol product: algorithm and global perspective, Atmos. Meas. Tech., 6, 1829–1844, https://doi.org/10.5194/amt-6-1829-2013, 2013.

Rosati, B., Gysel, M., Rubach, F., Mentel, T. F., Goger, B., Poulain, L., Schlag, P., Miettinen, P., Pajunoja, A., Virtanen, A., Klein Baltink, H., Henzing, J. S. B., Größ, J., Gobbi, G. P., Wiedensohler, A., Kiendler-Scharr, A., Decesari, S., Facchini, M. C., Weingartner, E., and Baltensperger, U.: Vertical profiling of aerosol hygroscopic properties in the planetary boundary layer during the PEGASOS campaigns, Atmos. Chem. Phys., 16, 7295–7315, https://doi.org/10.5194/acp-16-7295-2016, 2016.

Saarikoski, S., Carbone, S., Decesari, S., Giulianelli, L., Angelini, F., Canagaratna, M., Ng, N. L., Trimborn, A., Facchini, M. C., Fuzzi, S., Hillamo, R., and Worsnop, D.: Chemical characterization of springtime submicrometer aerosol in Po Valley, Italy, Atmos. Chem. Phys., 12, 8401–8421, https://doi.org/10.5194/acp-12-8401-2012, 2012.

Schaap, M., van Loon, M., ten Brink, H. M., Dentener, F. J., and Builtjes, P. J. H.: Secondary inorganic aerosol simulations for Europe with special attention to nitrate, Atmos. Chem. Phys., 4, 857–874, https://doi.org/10.5194/acp-4-857-2004, 2004.

Schmidli, J.: Daytime Heat Transfer Processes over Mountainous Terrain, J. Atmos. Sci., 70, 4041–4066, https://doi.org/10.1175/JAS-D-13-083.1, 2013.

Schnitzhofer, R., Norman, M., Wisthaler, A., Vergeiner, J., Harnisch, F., Gohm, A., Obleitner, F., Fix, A., Neininger, B., and Hansel, A.: A multimethodological approach to study the spatial distribution of air pollution in an Alpine valley during wintertime, Atmos. Chem. Phys., 9, 3385–3396, https://doi.org/10.5194/acp-9-3385-2009, 2009.

Serafin, S. and Zardi, D.: Daytime Heat Transfer Processes Related to Slope Flows and Turbulent Convection in an Idealized Mountain Valley, J. Atmos. Sci., 67, 3739–3756, https://doi.org/10.1175/2010JAS3428.1, 2010.

Serafin, S., Adler, B., Cuxart, J., De Wekker, S. F. J., Gohm, A., Grisogono, B., Kalthoff, N., Kirshbaum, D. J., Rotach, M. W., Schmidli, J., Stiperski, I., Večenaj, Ž., and Zardi, D.: Exchange Processes in the Atmospheric Boundary Layer Over Mountainous Terrain, Atmosphere, 9, https://doi.org/10.3390/atmos9030102, 2018.

Siani, A. M., Modesti, S., Casale, G. R., Diémoz, H., and Colosimo, A.: Biologically effective surface UV climatology at Rome and Aosta, Italy, AIP Conf. Proc., 1531, 903–906, https://doi.org/10.1063/1.4804917, 2013.

Siani, A. M., Scarlatti, F., Religi, A., Diémoz, H., Casale, G. R., Pedone, M., and Savastiouk, V.: Examination on total ozone column retrievals by Brewer spectrophotometry using different processing software, Atmos. Meas. Tech. Discuss., 2018, 1–28, https://doi.org/10.5194/amt-2017-441, 2018.

Silibello, C., Calori, G., Brusasca, G., Giudici, A., Angelino, E., Fossati, G., Peroni, E., and Buganza, E.: Modelling of PM 10 concentrations over Milano urban area using two aerosol modules, Environ. Modell. Softw., 23, 333–343, https://doi.org/10.1016/j.envsoft.2007.04.002, 2008.

Sokhi, R., Kitwiroon, N., and Luhana, L.: FUMAPEX Datasets of Urban Air Pollution Models and Meteorological Preprocessors, in: Fumapex Report D, vol. 2, pp. 1–D2, 2003.

Sprenger, M. and Wernli, H.: The LAGRANTO Lagrangian analysis tool – version 2.0, Geosci. Model Dev., 8, 2569–2586, https://doi.org/10.5194/gmd-8-2569-2015, 2015.

Straif, K., Cohen, A., and Samet, J., eds.: Air pollution and cancer, WHO Press, World Health Organization, 2013.

Tampieri, F., Trombetti, F., and Scarani, C.: Summer daily circulation in the Po Valley, Italy, Geophys. Astro. Fluid, 17, 97–112, https://doi.org/10.1080/03091928108243675, 1981.

Thyer, N. H.: A theoretical explanation of mountain and valley winds by a numerical method, Archiv für Meteorologie, Geophysik und Bioklimatologie, Serie A, 15, 318–348, https://doi.org/10.1007/BF02247220, 1966.

Turpin, B. J. and Lim, H.-J.: Species Contributions to PM2.5 Mass Concentrations: Revisiting Common Assumptions for Estimating Organic Mass, Aerosol Sci. Tech., 35, 602–610, https://doi.org/doi:10.1080/02786820152051454, 2001.

Uchino, O., Sakai, T., Izumi, T., Nagai, T., Morino, I., Yamazaki, A., Deushi, M., Yumimoto, K., Maki, T., Tanaka, T. Y., Akaho, T., Okumura, H., Arai, K., Nakatsuru, T., Matsunaga, T., and Yokota, T.: Lidar detection of high concentrations of ozone and aerosol transported from northeastern Asia over Saga, Japan, Atmos. Chem. Phys., 17, 1865–1879, https://doi.org/10.5194/acp-17-1865-2017, 2017.

Van Donkelaar, A., Martin, R. V., Brauer, M., Kahn, R., Levy, R., Verduzco, C., and Villeneuve, P. J.: Global estimates of ambient fine particulate matter concentrations from satellite-based aerosol optical depth: development and application, Environ. Health Persp., 118, 847, https://doi.org/10.1289/ehp.0901623, 2010.

Vuillermoz, M., Berlier, F., Borlino, M. C., Crea, D., Tartin, C., and Tibone, C.: Influence of vertical temperature gradients on outdoor sound propagation in a narrow valley, in: AIA-DAGA 2013 proceedings of the International Conference on Acoustics, 2013.

Wagner, J. S., Gohm, A., and Rotach, M. W.: The impact of valley geometry on daytime thermally driven flows and vertical transport processes, Q. J. Roy. Meteor. Soc., 141, 1780–1794, https://doi.org/10.1002/qj.2481, 2014.

Weissmann, M., Braun, F. J., Gantner, L., Mayr, G. J., Rahm, S., and Reitebuch, O.: The Alpine Mountain–Plain Circulation: Airborne Doppler Lidar Measurements and Numerical Simulations, Mon. Weather Rev., 133, 3095–3109, https://doi.org/10.1175/MWR3012.1, 2005.

WHO: Ambient air pollution: a global assessment of exposure and burden of disease, Tech. rep., 2016.

Wiegner, M. and Gasteiger, J.: Correction of water vapor absorption for aerosol remote sensing with ceilometers, Atmos. Meas. Tech., 8, 3971–3984, https://doi.org/10.5194/amt-8-3971-2015, 2015.

Wiegner, M. and Geiß, A.: Aerosol profiling with the Jenoptik ceilometer CHM15kx, Atmos. Meas. Tech., 5, 1953–1964, https://doi.org/10.5194/amt-5-1953-2012, 2012.

WMO: WMO/IGAC Impacts of megacities on air pollution and climate, Tech. rep., World Meteorological Organization, https://library.wmo.int/pmb_ged/gaw_205.pdf, 2012.

Wotawa, G., Kröger, H., and Stohl, A.: Transport of ozone towards the Alps – results from trajectory analyses and photochemical model studies, Atmos. Environ., 34, 1367 – 1377, https://doi.org/https://doi.org/10.1016/S1352-2310(99)00363-5, 2000.

Wyngaard, J. C.: Toward Numerical Modeling in the “Terra Incognita”, J. Atmos. Sci., 61, 1816–1826, https://doi.org/10.1175/1520-0469(2004)061<1816:TNMITT>2.0.CO;2, 2004.

Zeng, Z., Chen, A., Ciais, P., Li, Y., Li, L. Z. X., Vautard, R., Zhou, L., Yang, H., Huang, M., and Piao, S.: Regional air pollution brightening reverses the greenhouse gases induced warming-elevation relationship, Geophys. Res. Lett., 42, 4563–4572, https://doi.org/10.1002/2015GL064410, 2015.

Zhang, Q., Jiang, X., Tong, D., Davis, S. J., Zhao, H., Geng, G., Feng, T., Zheng, B., Lu, Z., Streets, D. G., Ni, R., Brauer, M., van Donkelaar, A., Martin, R. V., Huo, H., Liu, Z., Pan, D., Kan, H., Yan, Y., Lin, J., He, K., and Guan, D.: Transboundary health impacts of transported global air pollution and international trade, Nature, 543, 705–709, https://doi.org/10.1038/nature21712, 2017.

Zuev, V. V., Burlakov, V. D., Nevzorov, A. V., Pravdin, V. L., Savelieva, E. S., and Gerasimov, V. V.: 30-year lidar observations of the stratospheric aerosol layer state over Tomsk (Western Siberia, Russia), Atmos. Chem. Phys., 17, 3067–3081, https://doi.org/10.5194/acp-17-3067-2017, 2017.

Ångström, A.: On the Atmospheric Transmission of Sun Radiation and on Dust in the Air, Geografiska Annaler, 11, 156–166, 1929.

S1 Numerical weather prediction model performances

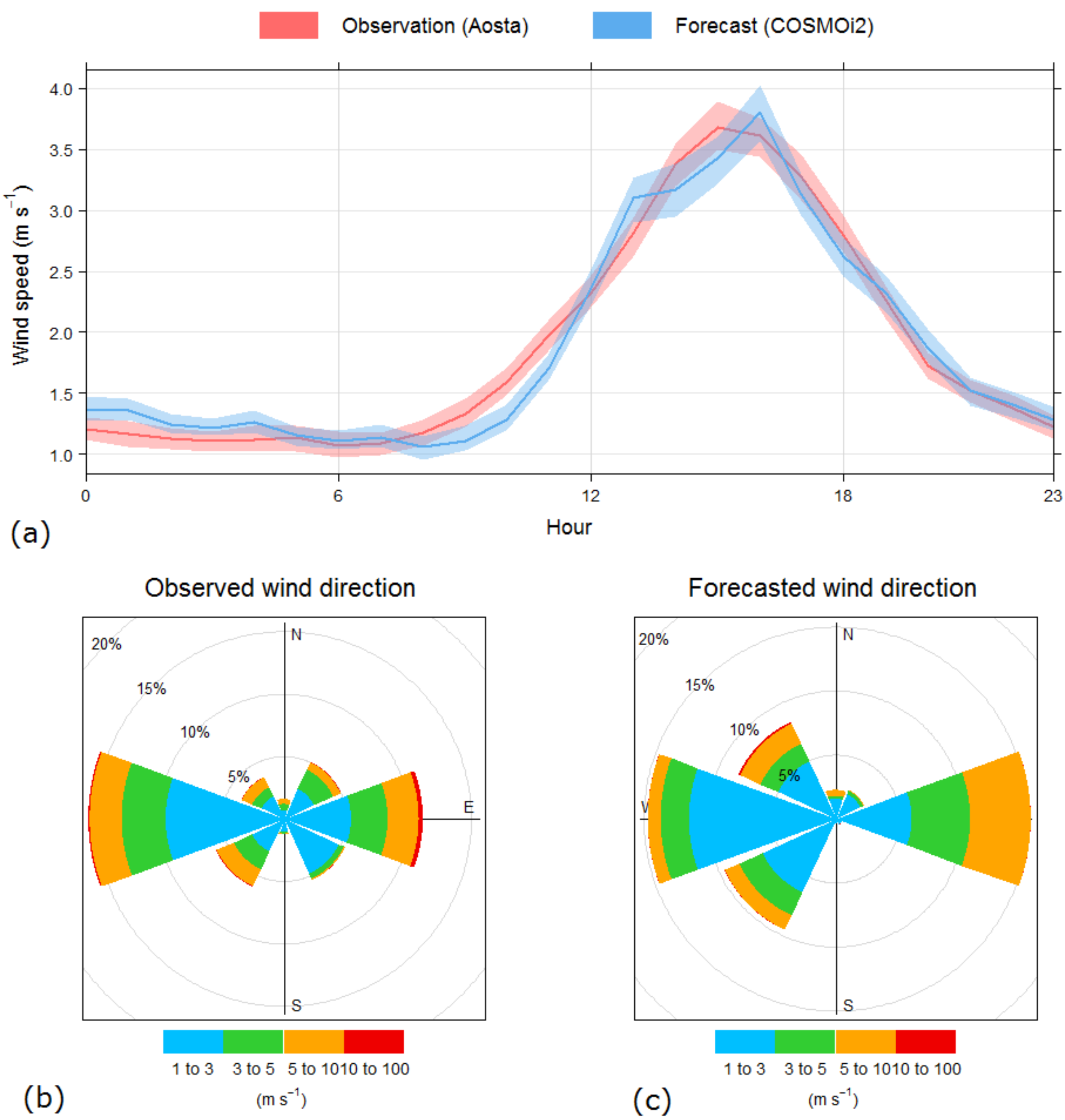

Figure S1: Comparison between average (2015–2016) wind observations at the Aosta–Downtown weather station and forecasts by COSMO-I2 for the corresponding grid cell. (a) Daily cycle of wind speed. The effect of regular winds blowing in the afternoon, especially the plain-mountain winds, is detectable as a peak between 12 and 18 LT. (b,c) Observed and forecasted wind direction. The distance from the centre of the wind rose identifies the frequency of each class of wind speed (colours) and provenance direction (polar angle).

S2 Details on the regional emission inventory

The Aosta Valley emission inventory is managed by ARPA and is currently updated to 2015. Emissions of pollutants are estimated from the best available understanding of the local sources weighted by appropriate emission factors. The latter are generally taken from the Atmospheric Emission Inventory Guidebook (EEA, 2016), unless more specific or up-to-date information is applicable based on the expertise of the operator and knowledge of the processes acting on a regional scale. The Aosta Valley inventory and the emission calculation methodologies were successfully compared to their national equivalents during an Italian comparison exercise (Pignatelli et al., 2007) in the framework of the Regional Air Pollution Information and Simulation (RAINS) European Program, aimed at harmonizing the European emissions inventories and the calculation methodologies.

In the last inventory (2015), the PM_{10} emissions in the Aosta Valley were evaluated in 690 tonnes/year, mainly attributed to domestic heating emissions (74%). Other contributors are road and off-road transports (15%) and agriculture or farming activities (11%).

S3 Details on the boundary conditions

The boundary conditions employed for this study at an intermediate (Italian and European) scale are provided by the system QualeAria (`http://www.aria-net.it/qualearia/en/`; Menut and Bessagnet (2010); Kukkonen et al. (2012)). The Global Forecast System (GFS) synoptic-scale weather forecasts from the National Center for Environmental Prediction (NCEP) are given as meteorological inputs to QualeAria. The outer air quality boundary conditions are taken from the global scale forecasts provided daily by the ECMWF MACC-C-IFS-TM5 model as part of the Copernicus Atmosphere Monitoring Service (CAMS; `http://macc.copernicus-atmosphere.eu/oper_info/nrt_info_for_users/`). The national and European emissions inventories are distributed by the Italian Institute for Environmental Protection and Research (ISPRA; Taurino et al. (2016)) for Italy and by the TNO/MEGAPOLI project for Europe (`http://megapoli.dmi.dk`, Baklanov et al. (2010)).

The described configuration was successfully tested in previous studies on air quality forecasts in the Aosta Valley (e.g., Silibello et al., 2007; Pession et al., 2008, 2016).

S4 Supporting material to case study 1

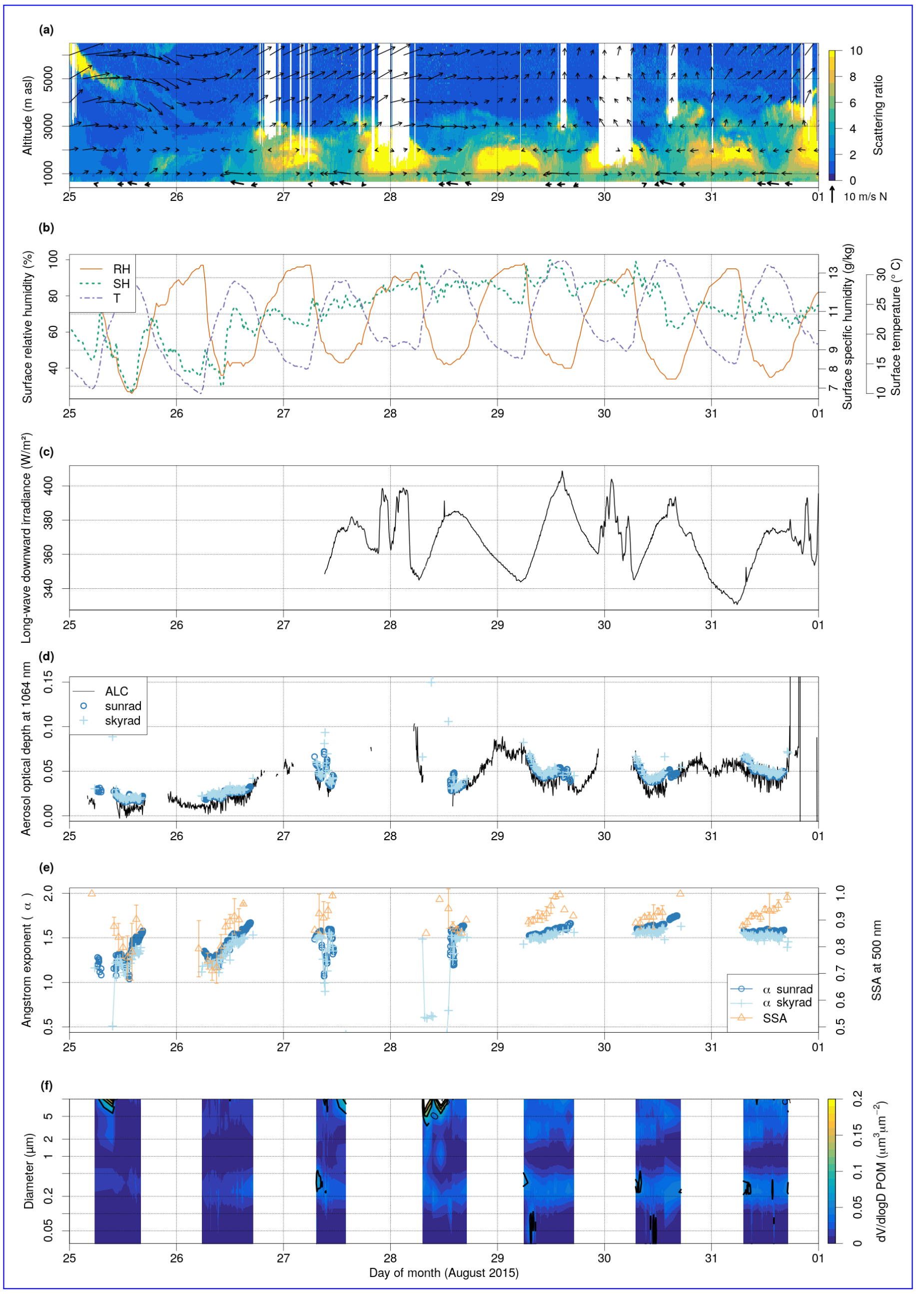

Figure S2: Case study of 26–31 August 2015. (a) Same as in Fig. ~~4~~ 3 in the main paper; (b) Surface relative humidity (RH), specific humidity (SH) and temperature (T) measured at the Aosta–Saint Christophe weather station; (c) Downward infrared irradiance measured at Aosta–Saint Christophe. Some of the infrared irradiance spikes occur at the same time as clouds in panel (a) and reveal the quick transition from the aerosol to the cloud phase. The pyrgeometer was calibrated in August 2015 and got back in the field on 27th; (d) AOD at 1064 nm from ALC (derived from the functional relationships and filtered for clouds) and photometer (both sunrad and skyrad algorithms); (e) Ångström exponent from both sunrad and skyrad algorithms (left axis), and SSA (right axis) from the photometer; (f) Volume size distribution from the photometer (cut at 10 μm diameter for ease of visualisation of the smallest sizes).

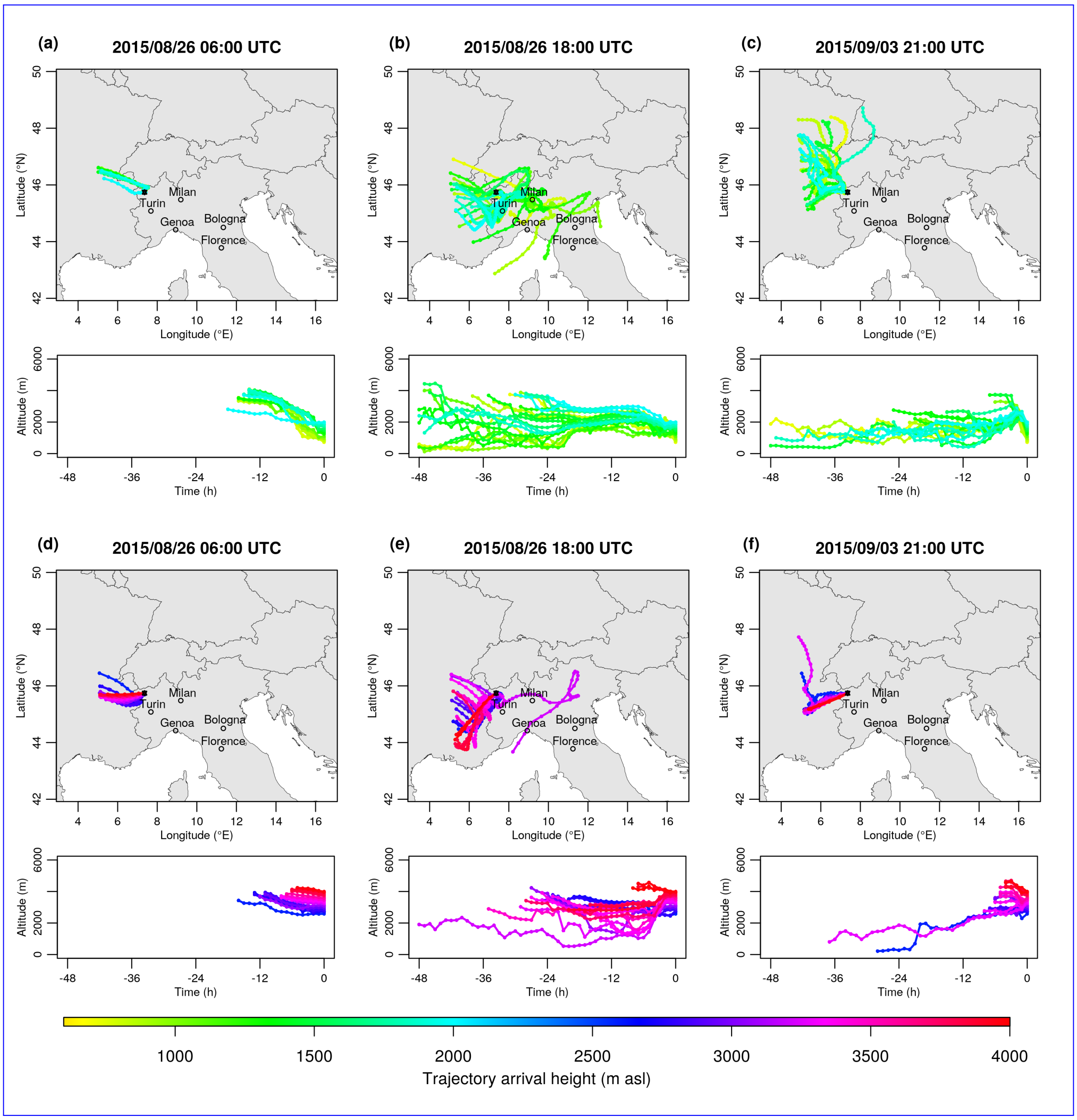

Figure S3: 48-hours back-trajectories ending at Aosta–Saint Christophe ~~on 26~~ at altitudes < 2000 m a.s.l. (a, b and c) and > 2500 m a.s.l. (d, e and f) during the summer episode (August ~~2015.~~ 2015). Before the arrival of the polluted air mass over Aosta all trajectories follow the synoptics circulation from the west (a, d). Later on the same day, the lowest trajectories turn and cross the Po basin, leading to advection of polluted air over Aosta, while the highest ones still come from the west (b, e). At the end of the episode, all trajectories turn back to the west (c, f). The trajectories are cut at the border of the COSMO model. The colour scale represents the arrival height. The dots along each trajectory mark a 1-hour step.

S5 Supporting material to case study 2

~~Case study of 26–29 January 2017. (a) Same as in Fig. 10 in the main paper; (b) Surface relative humidity, specific humidity and temperature measured at the Aosta–Saint Christophe weather station; (c) Particle number distribution from the Palas optical counter; (d) Particle number concentration (sum of all channels) from the Palas optical counter; (e) Wind speed and direction at the Saint-Denis station (800 m a.s.l). No data from the photometer are available for the selected period, since the instrument was not operating.~~

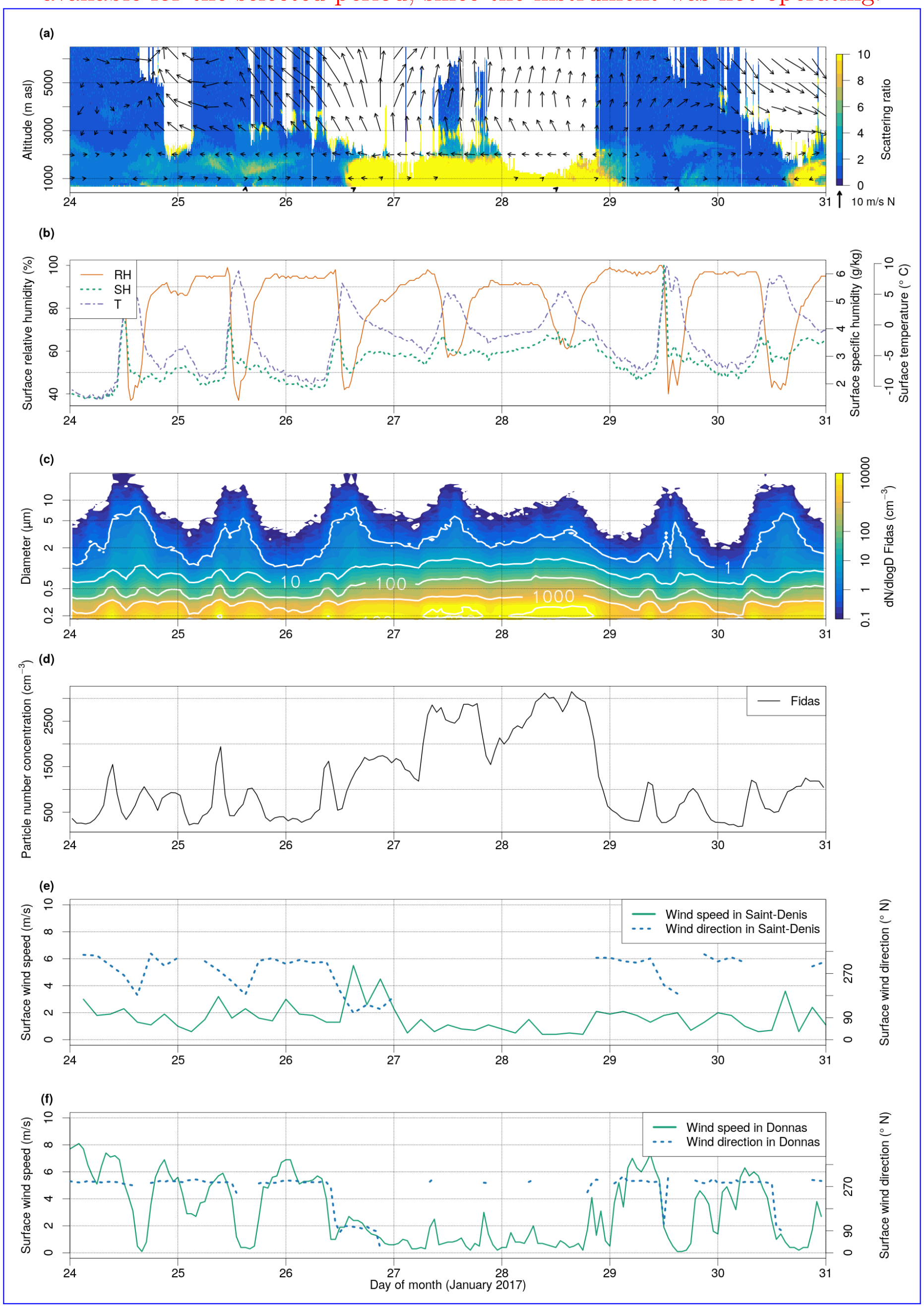

Figure S4: Case study of 26–29 January 2017. (a) Same as in Fig. 9 in the main paper; (b) Surface relative humidity, specific humidity and temperature measured at the Aosta–Saint Christophe weather station; (c) Particle number distribution from the Palas optical counter; (d) Particle number concentration (sum of all channels) from the Palas optical counter; (e) Wind speed and direction at the Saint-Denis station (800 m a.s.l); (f) Wind speed and direction at the Donnas station (316 m a.s.l). No data from the photometer are available for the selected period, since the instrument was not operating.

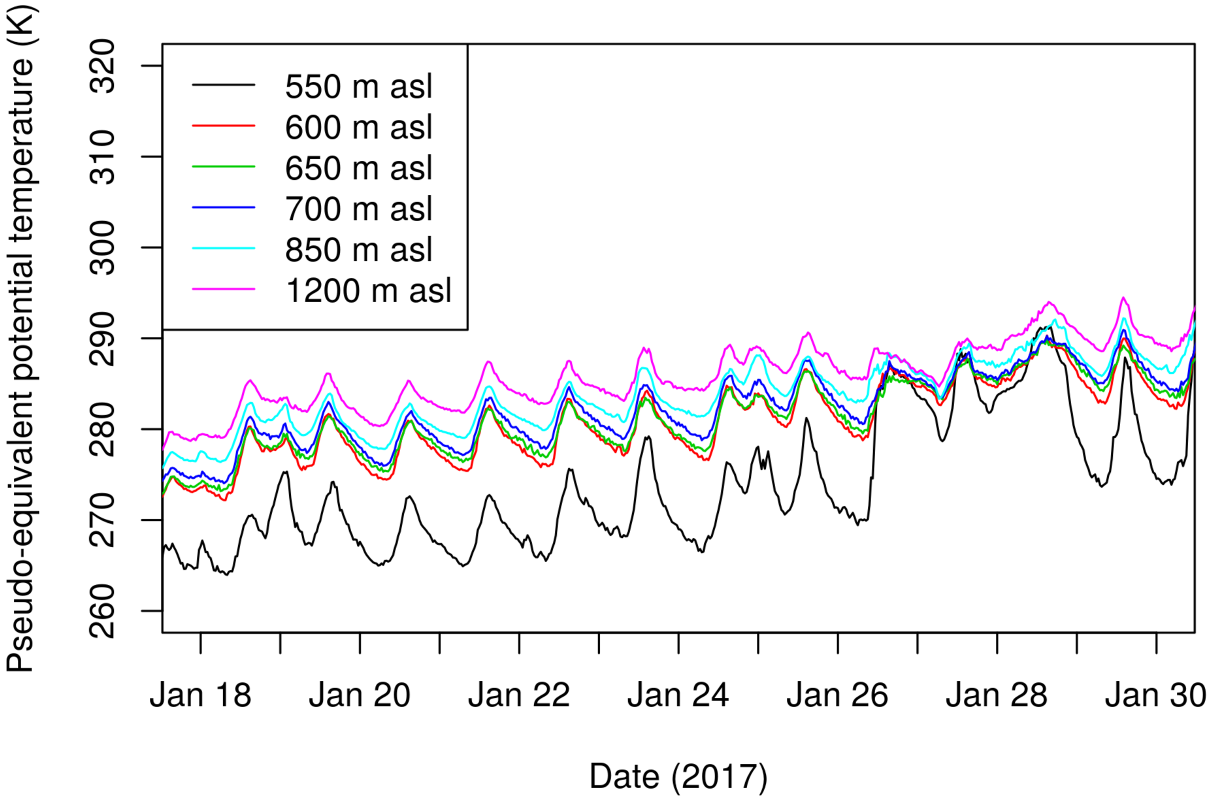

Figure S5: ~~Surface~~ Profile of pseudo-equivalent potential temperature measured along the mountain slope on January 2017. A weakening of the temperature inversion, and a more mixed boundary layer, are clearly detected from 26 to 28 January, i.e. during the advection episode.

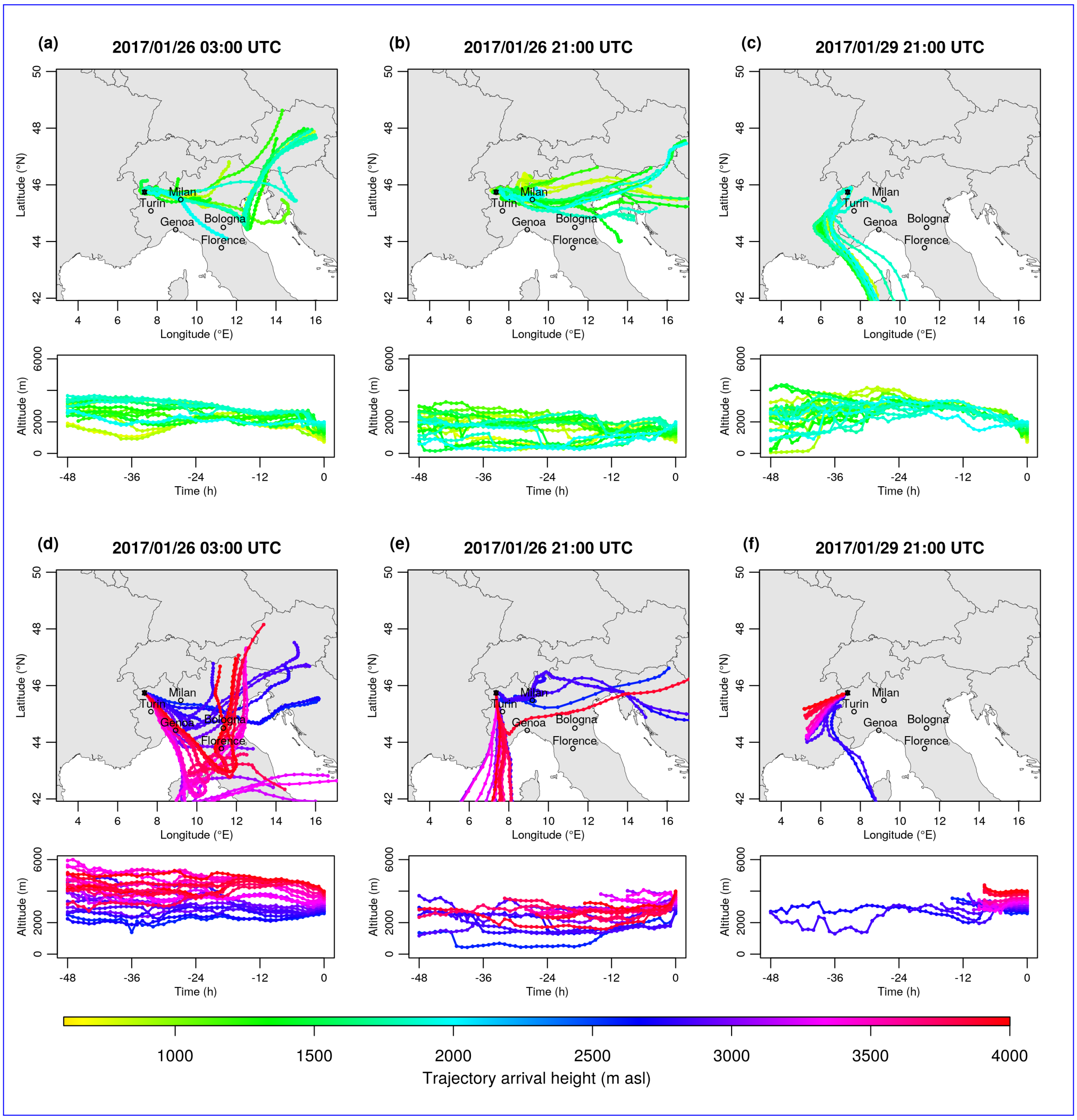

Figure S6: 48-hours back-trajectories ending at ~~Aosta Saint Christophe on 26~~ altitudes < 2000 m a.s.l. (a, b and c) and > 2500 m a.s.l. (d, e and f) during the winter episode (January ~~2017.~~2017): (a, d) morning of the advection day, (b, e) after the arrival of the layer over Aosta, and (c, f) end of the episode. Before the arrival of the layer, the trajectories are higher than the polluted mixing layer over the Po basin (a), whilst their altitude progressively decrease (b), leading to a more effective transport of pollution.

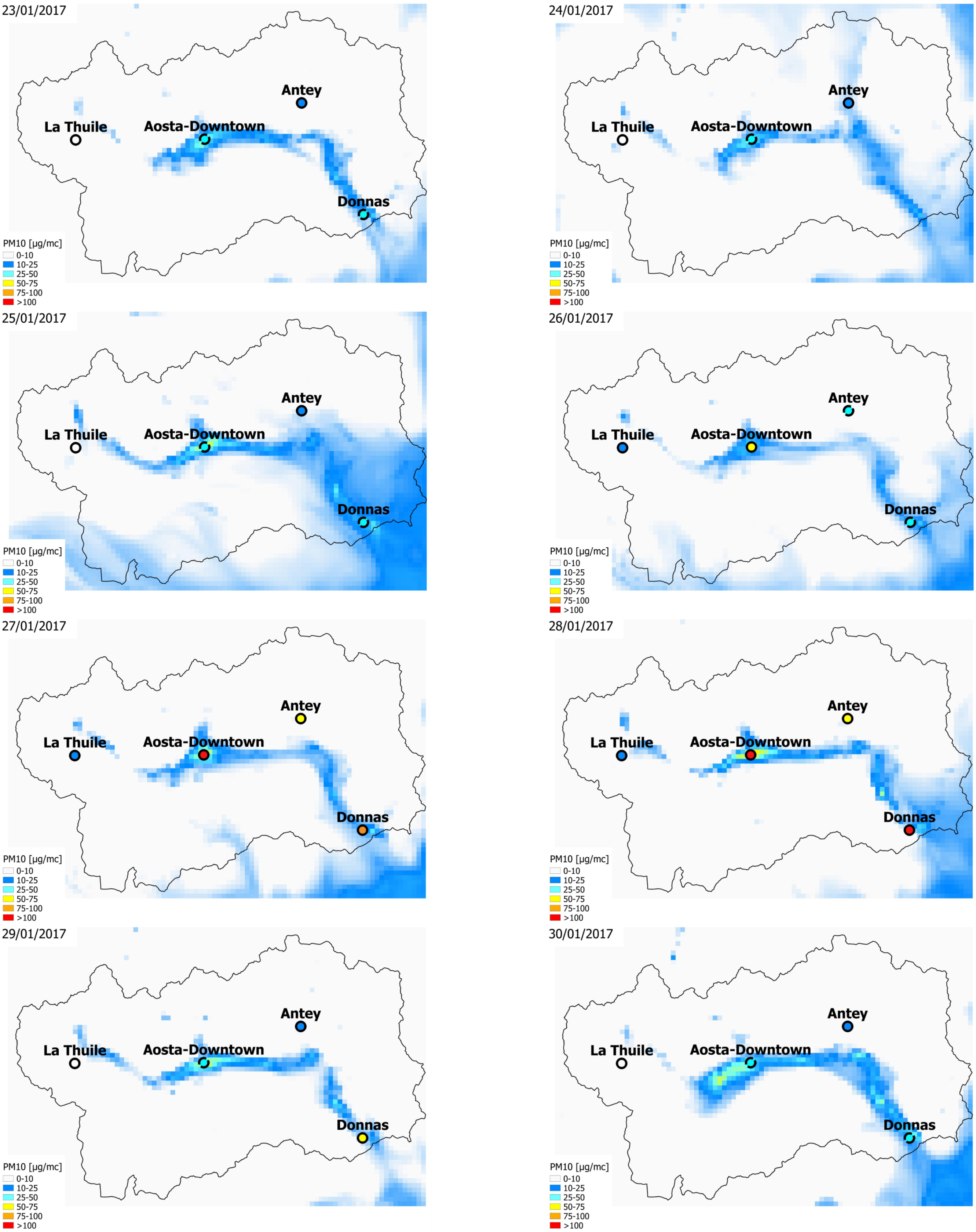

Figure S7: Daily PM_{10} surface (2D) simulations from FARM over the Aosta Valley (background colour) and in-situ measurements (circles) for case sudy 2 (January 2017).

S6 Supporting material to case study 3

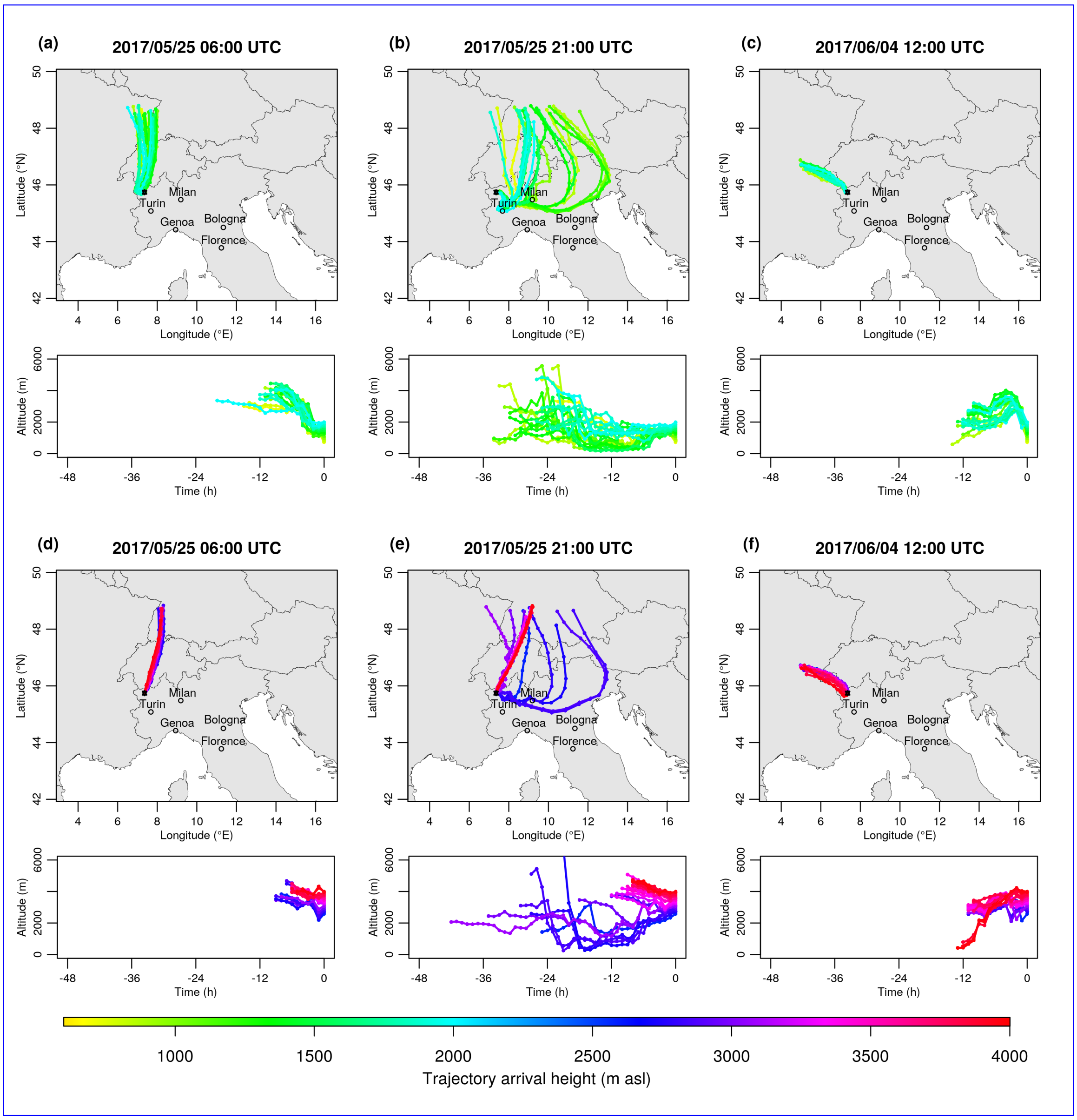

Figure S8: 48-hours back-trajectories ending at Aosta–Saint Christophe at altitudes < 2000 m a.s.l. (a, b and c) and > 2500 m a.s.l. (d, e and f) during the spring episode (May 2017): (a, d) morning of the advection day, trajectories following the synoptic circulation; (b, e) evening of the same day, lowest trajectories diverted owing to the breeze circulation and crossing the Po basin; (c, f) end of the episode, all trajectories coming from north-west.

~~48-hours back-trajectories ending at Aosta–Saint Christophe on 25 May 2017.~~

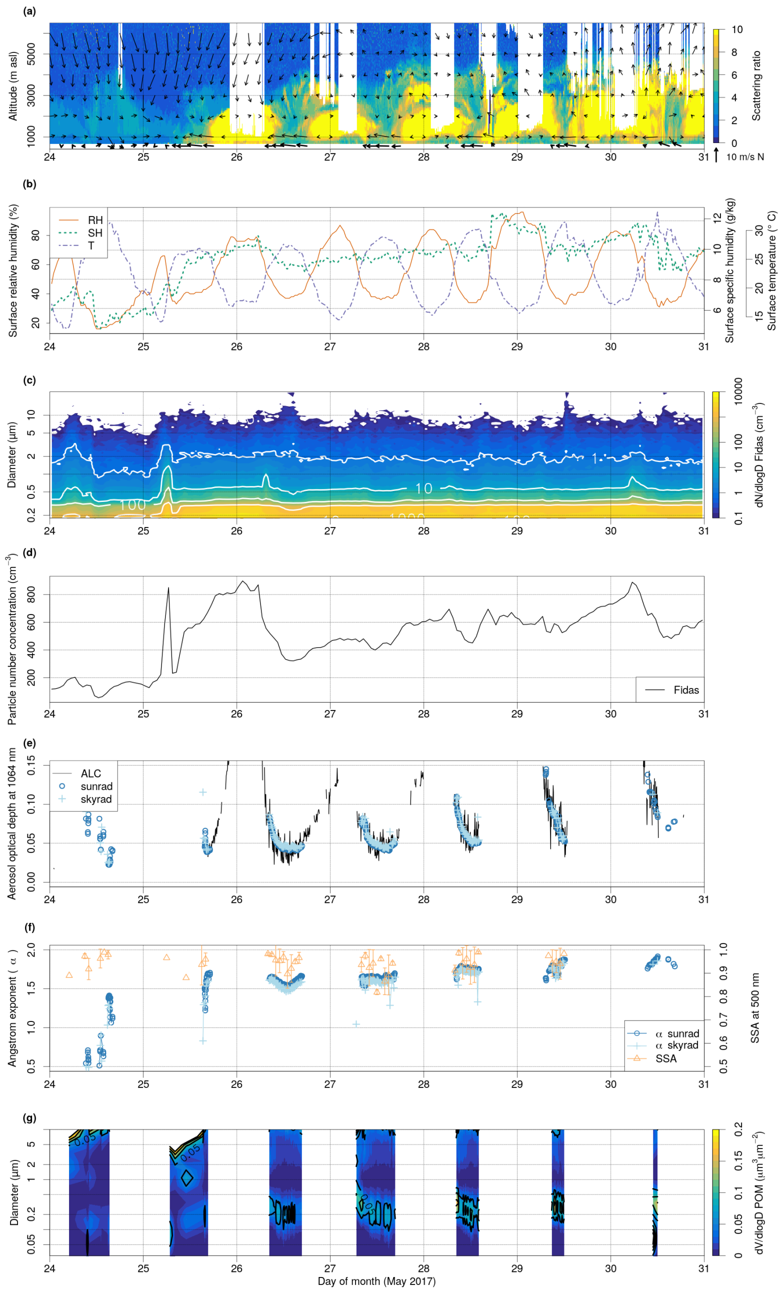

Figure S9: Case study of 25–30 May 2017. (a) Same as in Fig. ~~13~~ 12 in the main paper; (b) Surface relative humidity, specific humidity and temperature measured at the Aosta-Saint Christophe weather station; (c) Particle number distribution from the Palas optical counter; (d) Particle number concentration from the Palas optical counter; (e) AOD at 1064 nm from ALC (derived from the functional relationships and filtered for clouds) and photometer (both sunrad and skyrad algorithms); (f) Ångström exponent from both sunrad and skyrad algorithms (left axis), and SSA (right axis) from the photometer; (g) Volume size distribution from the photometer (cut at 10 μm diameter for ease of visualisation of the smallest sizes).

S7 Sensitivity studies on boundary conditions and alternative approach to estimate the hygroscopic effects

This section describes some additional tests that we performed on simulations for case study 1 (August 2015): 1) increase (doubling) of concentrations from the boundary conditions (BC). This large perturbation can be justified by the abrupt change of the national emission inventory grid resolution (12 km) to the local scale (1 km); 2) use of two different schemes, in place of the one employed by FARM, to simulate the aerosol hygroscopic effects. To this purpose, two empirical parametrisations were adopted, since the chemical composition of the elevated aerosol layer is not available experimentally, and might differ from that measured at ground (e.g., Curci et al., 2015), thus thermodynamic equilibrium models (e.g., ISORROPIA) are difficult to employ with the available data.

Figure S10 shows the discrepancy between the concentration profiles retrieved by the ALC (panel a) and the ones initially simulated by FARM (panel b; PM_{10w}, local+remote sources~~, same as Fig. 13b in the main paper~~). The results with the modified boundary conditions (test 1) are displayed in Fig. S10c and represent a clear improvement. Notably, transport events at the end of each day are better distinguishable and the concentrations approach to the ones retrieved by the ALC. However, both systematic anticipation of the maximum of each event and absence of the elevated, high-concentration "blobs" visible in the measurements are still noticeable in the panel.

We thus introduced different parametrisations for water uptake by aerosols and applied them to the dry concentrations simulated by FARM with doubled BC. In the first scheme (Fig. S10d), we assumed that the aerosol ~~grow~~ growth factor (GF), describing the increase of the particle size due to water uptake relative to the dry case, can be approximated by a γ-law function of relative humidity (e.g., Adam et al., 2012),

$$\mathrm{GF} = \left(1 - \frac{\mathrm{RH}}{100}\right)^{-\gamma} \tag{1}$$

The mass concentration of the moist aerosol (PM_w) can thus be estimated from the dry concentration (PM) as follows:

$$\mathrm{PM}_w = \mathrm{PM}\left(1 + \frac{\rho_w}{\rho_d}(\mathrm{GF}^3 - 1)\right) \tag{2}$$

where ρ_w and ρ_d are pure water and dry aerosol densities, respectively. We assumed a hygroscopic parameter $\gamma =$ 0.2, typical of the Po Valley in summer months (Adam et al., 2012), a dry aerosol density $\rho_d = 1.3\ \mathrm{g\,cm^{-3}}$ as already used in our calculations, and we employed the RH profile forecasted by the COSMO model.

In the second scheme (Fig. S10e), we used experimental mass growth obtained in Milan (summer conditions, RH range 30–90%) by D'Angelo et al. (2016). The two experimental branches of the mass growth (for increasing and decreasing RH conditions) were averaged for this test. Additionally, since the simulated RH profiles by COSMO occasionally exceeded 90%, we extrapolated the curve to higher humidities based on a γ-law, fitted to the points with RH$\geq$80% (Fig. S11).

Figures S10d and S10e show the PM_{10w} concentrations obtained with the two methods. As visible from the plots, both the new approaches provide increased PM_{10w} concentration in the elevated layers compared to the FARM output, almost reaching the high values of the measurements. Moreover, the maxima are slightly shifted towards midnight, as desired, since RH maxima are attained later at night than the aerosol advections.

Finally, the results of doubling the concentrations from the boundary conditions during case study 2 (winter case, January 2017) are displayed in Fig. S12.

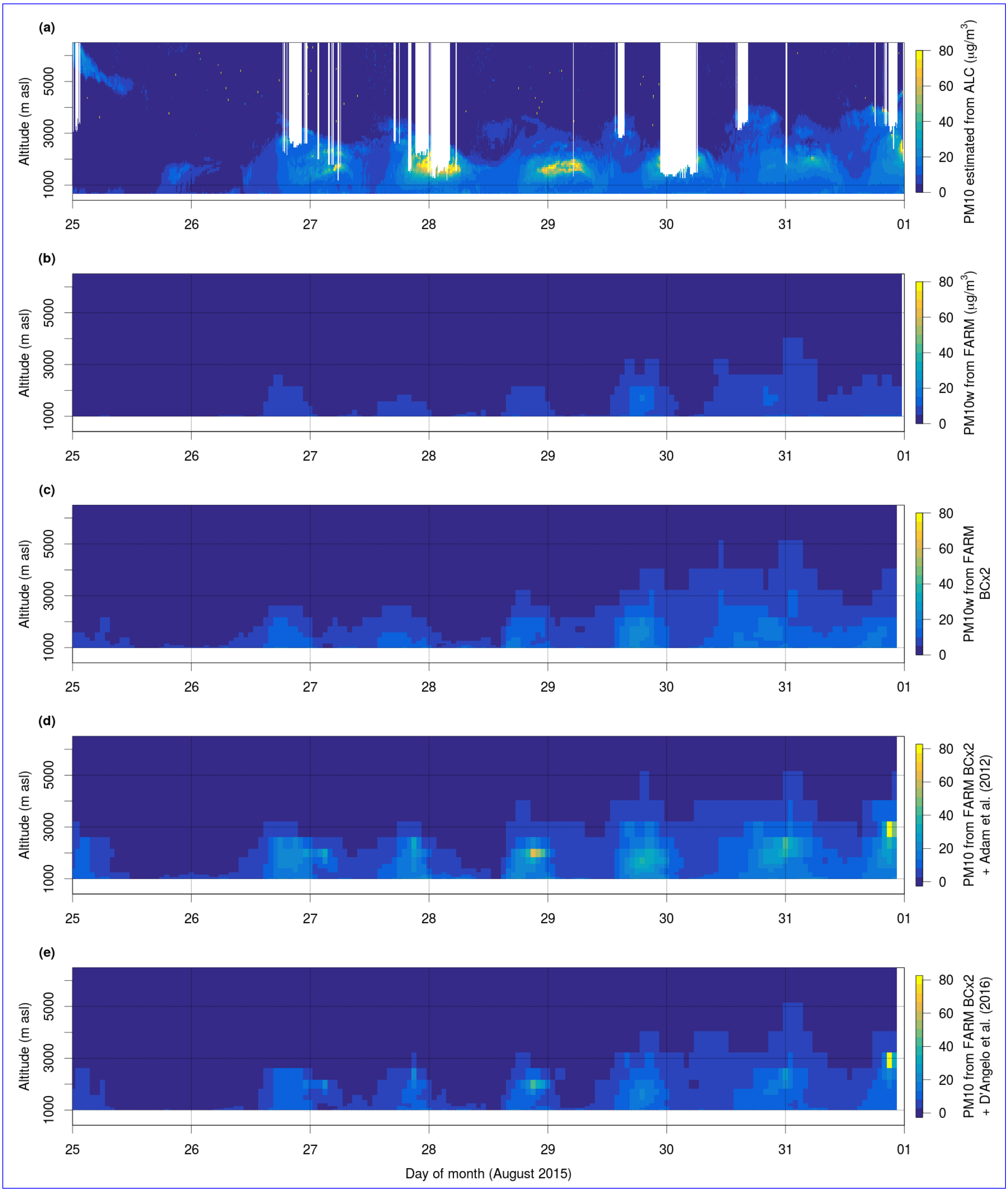

Figure S10: (a) PM_{10} concentration retrieved from ALC measurements; (b) PM_{10w} concentration initially simulated by FARM for the first case study; (c) PM_{10w} concentration simulated by FARM using doubled concentrations from the boundary conditions; (d) hydrated aerosol concentration calculated with the empirical model based on a γ-law (BC still doubled in FARM); (e) hydrated aerosol concentration calculated with the empirical model based on the function represented in Fig. S11 (BC still doubled in FARM). All units are $\mu g\ m^{-3}$.

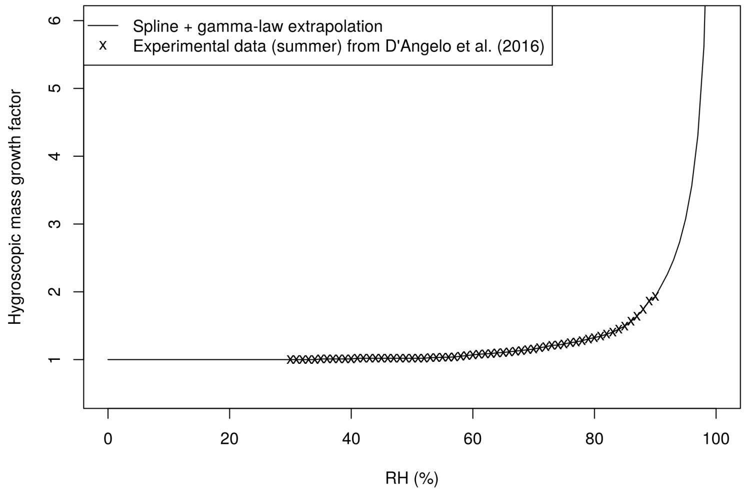

Figure S11: Hygroscopic mass growth factor (crosses) from measurements by D'Angelo et al. (2016). The continuous line represent an interpolation within the range of observations (30–90%) and an extrapolation using a γ-law to higher values of RH.

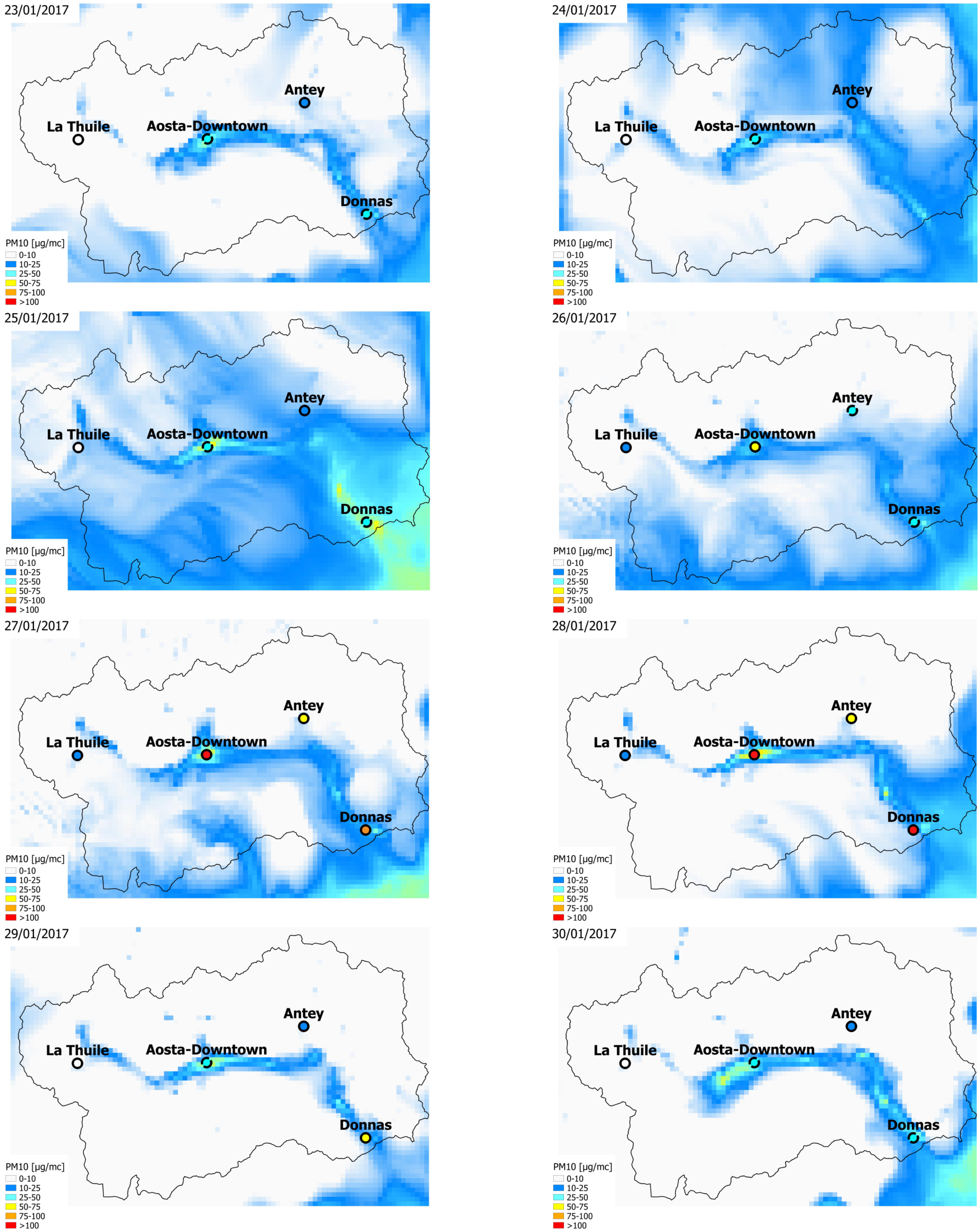

Figure S12: Same as Fig. S7, with doubled concentrations from outside the regional boundaries of the Aosta Valley.

S8 Inaccuracies of wind velocity simulations by the NWP model

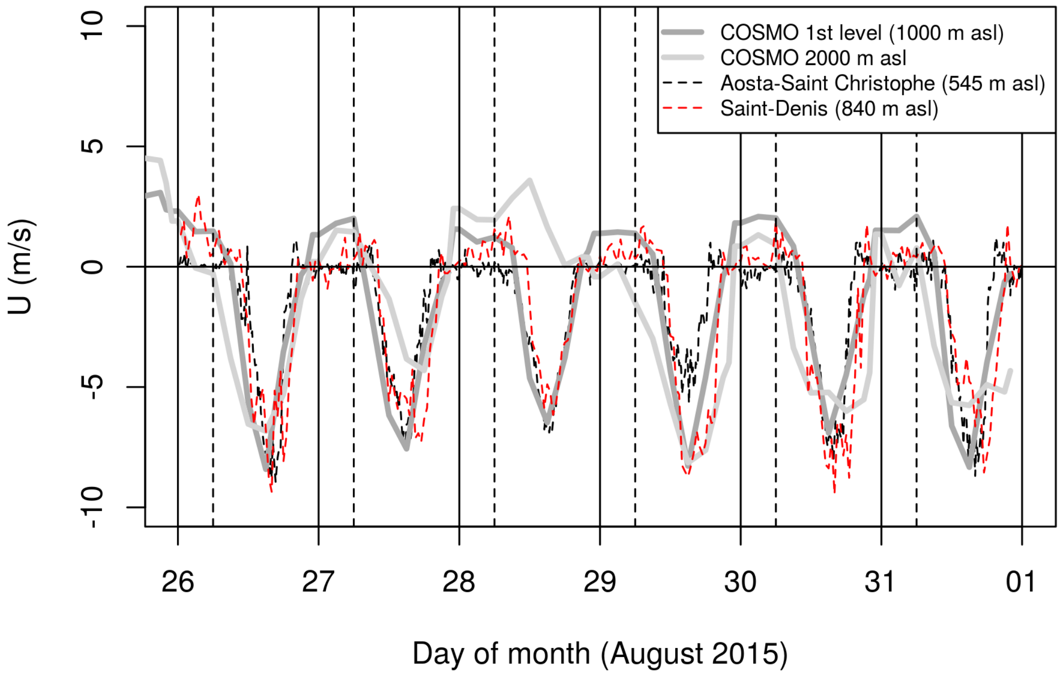

Figure S13: Zonal component of wind velocity during episode 1 (August 2015) from COSMO (1000 and 2000 m a.s.l.) and two surface stations (Aosta–Saint Christophe and Saint-Denis). Positive U represent wind from the west, negative U wind from the east.

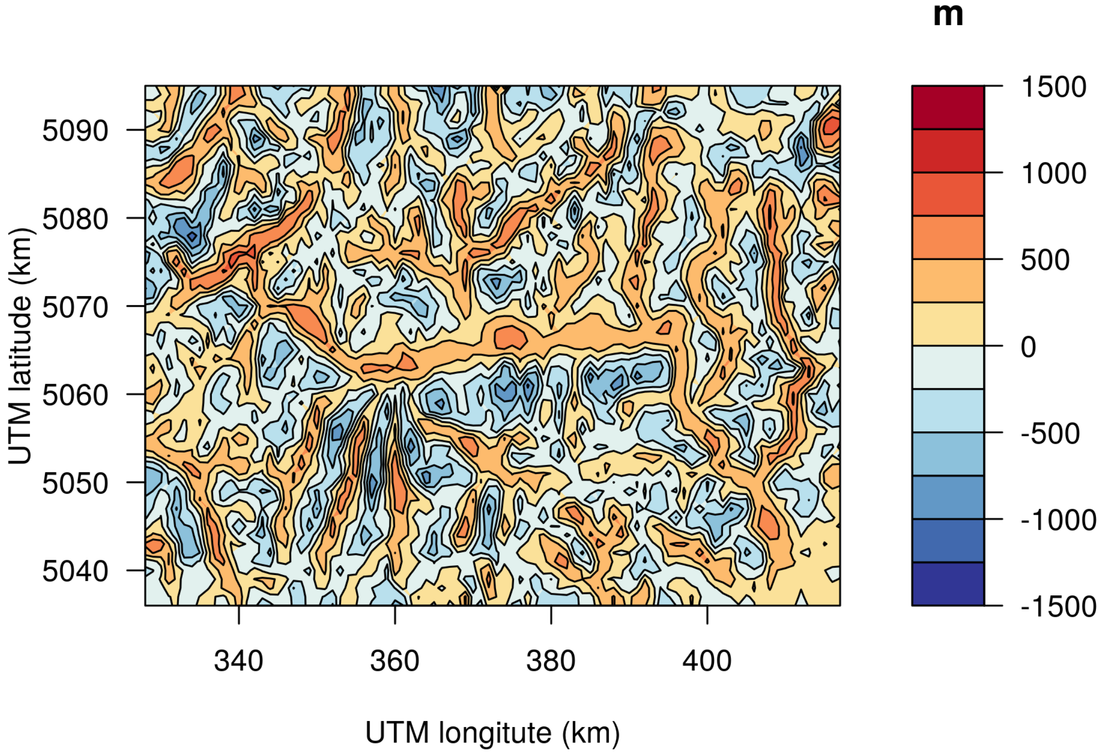

Figure S14: Difference between the (smoothed) Digital Elevation Model (DEM) used by COSMO-I2 (2.8 km resolution) and a higher-resolution DEM ("real topography", 10 m resolution).

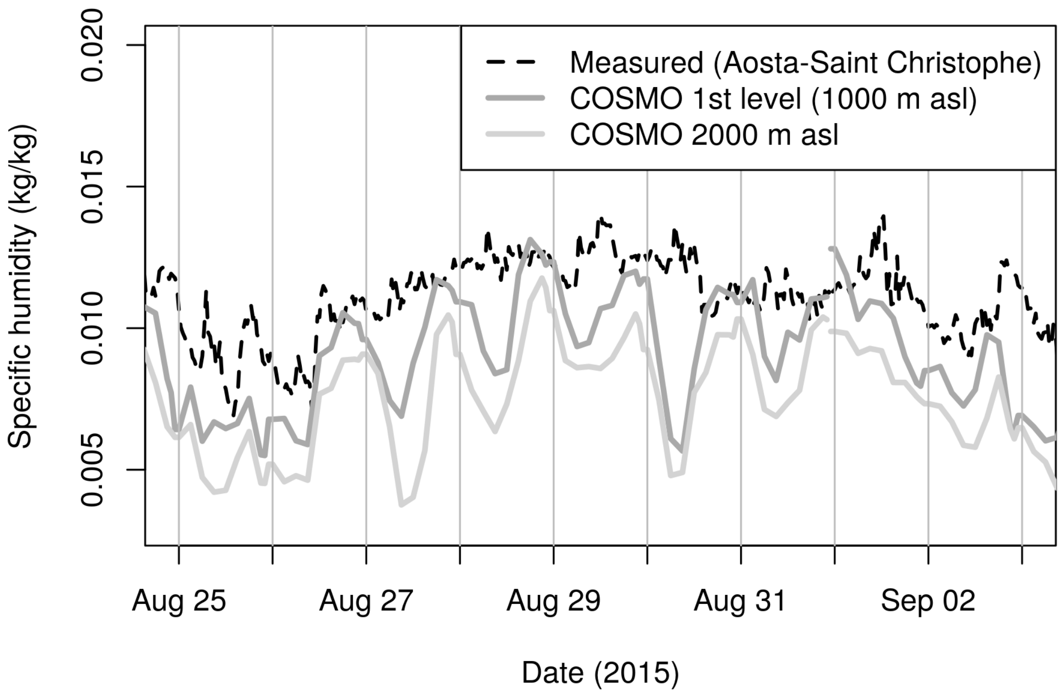

Figure S15: Comparison among specific humidity measured at Aosta–Saint Christophe and simulated by COSMO at two different altitudes (surface and 2000 m a.s.l.).

References

Adam, M., Putaud, J. P., Martins dos Santos, S., Dell'Acqua, A., and Gruening, C.: Aerosol hygroscopicity at a regional background site (Ispra) in Northern Italy, Atmos. Chem. Phys., 12, 5703–5717, doi:10.5194/acp-12-5703-2012, 2012.

Baklanov, A., Lawrence, M., Pandis, S., Mahura, A., Finardi, S., Moussiopoulos, N., Beekmann, M., Laj, P., Gomes, L., Jaffrezo, J.-L., Borbon, A., Coll, I., Gros, V., Sciare, J., Kukkonen, J., Galmarini, S., Giorgi, F., Grimmond, S., Esau, I., Stohl, A., Denby, B., Wagner, T., Butler, T., Baltensperger, U., Builtjes, P., van den Hout, D., van der Gon, H. D., Collins, B., Schluenzen, H., Kulmala, M., Zilitinkevich, S., Sokhi, R., Friedrich, R., Theloke, J., Kummer, U., Jalkinen, L., Halenka, T., Wiedensholer, A., Pyle, J., and Rossow, W. B.: MEGAPOLI: concept of multi-scale modelling of megacity impact on air quality and climate, Adv. Sci. Res., 4, 115–120, doi:10.5194/asr-4-115-2010, 2010.

Curci, G., Ferrero, L., Tuccella, P., Barnaba, F., Angelini, F., Bolzacchini, E., Carbone, C., Denier van der Gon, H. A. C., Facchini, M. C., Gobbi, G. P., Kuenen, J. P. P., Landi, T. C., Perrino, C., Perrone, M. G., Sangiorgi, G., and Stocchi, P.: How much is particulate matter near the ground influenced by upper-level processes within and above the PBL? A summertime case study in Milan (Italy) evidences the distinctive role of nitrate, Atmos. Chem. Phys., 15, 2629–2649, doi:10.5194/acp-15-2629-2015, 2015.

D'Angelo, L., Rovelli, G., Casati, M., Sangiorgi, G., Perrone, M. G., Bolzacchini, E., and Ferrero, L.: Seasonal behavior of PM2.5 deliquescence, crystallization, and hygroscopic growth in the Po Valley (Milan): Implications for remote sensing applications, Atmos. Res., 176-177, 87 – 95, doi:10.1016/j.atmosres.2016.02.011, URL `http://www.sciencedirect.com/science/article/pii/S016980951630028X`, 2016.

EEA: EMEP/EEA air pollutant emission inventory guidebook 2016 – Technical guidance to prepare national emission inventories, Tech. rep., European Environment Agency, doi:10.2800/247535, 2016.

Kukkonen, J., Olsson, T., Schultz, D. M., Baklanov, A., Klein, T., Miranda, A. I., Monteiro, A., Hirtl, M., Tarvainen, V., Boy, M., Peuch, V.-H., Poupkou, A., Kioutsioukis, I., Finardi, S., Sofiev, M., Sokhi, R., Lehtinen, K. E. J., Karatzas, K., San José, R., Astitha, M., Kallos, G., Schaap, M., Reimer, E., Jakobs, H., and Eben, K.: A review of operational, regional-scale, chemical weather forecasting models in Europe, Atmos. Chem. Phys., 12, 1–87, doi:10.5194/acp-12-1-2012, 2012.

Menut, L. and Bessagnet, B.: Atmospheric composition forecasting in Europe, Ann. Geophys., 28, 61–74, doi:10.5194/angeo-28-61-2010, 2010.

Pession, G., Magri, T., Zublena, M., Agnesod, G., Genon, G., Blanc, L., Silibello, C., Finardi, S., Calori, G., and Nanni, A.: Dust generation and dispersion (PM10 and PM2. 5) in the Aosta Valley: analysis with the FARM model, Hrvatski meteorološki časopis, 43, 603–607, URL `http://hrcak.srce.hr/file/96455`, 2008.

Pession, G., Magri, T., Calori, G., Costa, M., Bande, S., Bissardella, S., and Clemente, M.: Integrated source apportionment in support of Aosta valley and Piemonte air quality plans, in: Proceedings of Abstracts 10th International Conference on Air Quality Science and Application, Milano, University of Hertfordshire College Lane, 2016.

Pignatelli, T., De Lauretis, R., Contaldi, M., D'Elia, I., Romano, D., and Vialetto, G.: Harmonization of National inventory and projections of multi-pollutant emission scenarios. The Italian experience within the European context and the UN-ECE Convention on Long Range Transboundary Air Pollution, in: Proc. of 16th Annual Int. Emissions Inventory Conference, Raleigh (North Carolina), URL `https://www3.epa.gov/ttnchie1/conference/ei16/session8/pignatelli.pdf`, 2007.

Silibello, C., Finardi, S., Pittini, T., Pession, G., and Magri, T.: Model based yearly air quality evaluation on a very complex terrain alpine region (Valle d'Aosta), in: Proc. of the 11th Int. Conf. on Harmonization, Cambridge, UK, pp. 2–5, URL `http://www.harmo.org/conferences/proceedings/_Cambridge/publishedSections/Pp281-285.pdf`, 2007.

Taurino, E., Bernetti, A., De Lauretis, R., D'Elia, I., Di Cristofaro, E., Lena, F., Gagna, A., Gonella, B., Pantaleoni, M., Peschi, E., Romano, D., and Vitullo, M.: Italian emission inventory 1990-2014 – Informative inventory report 2016, 2016.